Functional analysis of TBC1D1 and TBC1D4 in skeletal muscle

Inaugural-Dissertation

zur Erlangung des Doktorgrades
der Mathematisch-Naturwissenschaftlichen Fakultät
der Heinrich-Heine-Universität Düsseldorf

vorgelegt von

Christian de Wendt
aus Herne

Mülheim an der Ruhr, Juni 2022

aus dem Institut für Klinische Biochemie und Pathobiochemie
des Deutschen Diabetes-Zentrums (DDZ)
Leibniz Zentrum für Diabetes-Forschung
an der Heinrich-Heine-Universität Düsseldorf

Gedruckt mit der Genehmigung der
Mathematisch-Naturwissenschaftlichen Fakultät der
Heinrich-Heine-Universität Düsseldorf

Berichterstatter:

1. Prof. Dr. Hadi Al-Hasani

2. Prof. Dr. Eckhard Lammert

Tag der mündlichen Prüfung: 01.12.2022

Summary

Background and aims

The two closely related RabGTPase-activating proteins (RabGAPs) TBC1D1 and TBC1D4 (AS160) play essential roles in glucose and lipid metabolism in skeletal muscle. TBC1D4, in addition, represents a major factor in adipose tissue insulin sensitivity. In mice, lack of each RabGAP causes severe disturbances in insulin sensitivity of skeletal muscle and adipose tissue and a metabolic switch in energy substrate preference from carbohydrates to lipids *in vivo*. This switch is accompanied by a tissue-specific reduction in glucose transporter 4 (GLUT4) abundance. Both TBC1D1 and TBC1D4 are directly regulated by their upstream kinases AKT- and AMP-dependent protein kinase (AMPK) which are known to be involved in insulin- and exercise-regulated glucose metabolism, respectively.

The aim of this study is to achieve a better understanding of the physiological relevance of the two RabGAPs. For this purpose, *Tbc1d1*- (D1KO), *Tbc1d4*- (D4KO) and double-deficient *Tbc1d1/4* (D1/4KO) mice are studied to address three different topics:

1) Metabolic characterization under high-fat diet (HFD) conditions,
2) The contribution of each RabGAP and their upstream kinase AMPK to exercise- and contraction-mediated glucose metabolism, respectively, and
3) The mechanism of GLUT4 reduction in skeletal muscle of RabGAP deficient mice.

Methods

D1KO mice were crossbred with D4KO and muscle-specific AMPKα_2 kinase-dead (TG) mice to yield triple-deficient mice (TG-D1/4KO) on a genetic C57BL/6J background. Whole-body tolerance towards glucose, insulin and AICAR were assessed by respective tolerance tests in male mice. *In vivo* running performance was measured with a caloric treadmill system. *Ex vivo* contraction- and insulin-stimulated ^{3}H-2-deoxyglucose uptake were determined using isolated *Extensor digitorum longus* (*EDL*) and *Soleus* muscles. Skeletal muscle and liver tissue were analyzed on protein and mRNA levels. *In vivo* electroporation (IVE) method was used to assess the impact of TBC1D1 on GLUT4 abundance by expressing different *Tbc1d1* mutants and Rab proteins in *Tibialis anterior* (TA) muscle of D1KO and C57BL/6J mice which was subsequently analyzed for GLUT4 abundance.

Results

Upon HFD intervention, D4KO and D1/4KO mice demonstrated an impaired glucose and D1/4KO a disturbed insulin tolerance. On the other hand, their sensitivity for AICAR, an exercise-mimetic substance, tended to be improved compared to wildtype (WT) animals.

Inactivation of AMPK resulted in decreased exercise capacity, indicated by a lower treadmill running performance and impaired contraction-induced glucose uptake in *EDL* and *Soleus* muscle compared to wildtype animals. Additional deletion of *Tbc1d1* but not *Tbc1d4* intensified the effects on running performance and contraction-induced glucose uptake. Additional deficiency of *Tbc1d4* (TG-D4KO and TG-D1/4KO) in contrast decreased the ability to clear glucose from the blood resulting in higher plasma glucose levels after fasting-refeeding.
Previously, we and others showed that GLUT4 abundance in glycolytic muscle of *Tbc1d1*-deficient (D1KO) mice was substantially reduced. Expression of wildtype TBC1D1 and its PTB-domain mutant R125W but not the GAP-domain mutant R941K restored GLUT4 levels in *tibialis anterior* (TA) muscle of D1KO mice. Expression of constitutively active TBC1D1 downstream target Rab14 increased GLUT4 expression in TA muscle of C57BL/6J mice.

Conclusion

This work provides new evidence that

1) Deletion of both RabGAPs leads to reduced insulin sensitivity in mice upon HFD treatment, probably caused by their *Tbc1d4*- but not their *Tbc1d1*-deficiency. According to that, D1/4KO mice develop more body fat mass compared to their WT littermates. However, at the same time loss of *Tbc1d4* improves AICAR sensitivity.
2) AMPK deficiency in muscle reduced exercise performance on the treadmill and contraction-induced glucose transport. Additional deletion of *Tbc1d1* but not *Tbc1d4* caused a further decrease in whole body exercise capacity and contraction-stimulated glucose transport into glycolytic *EDL* muscle. Remarkably, skeletal muscle lacking functional AMPK and both RabGAPs still exhibited residual contraction-induced glucose uptake.

   Therefore, this work demonstrates the need for a new signaling pathway independent of AMPK, TBC1D1 and TBC1D4.
3) The absence of the GTPase activating (GAP-)domain of TBC1D1 accounted for the GLUT4 deficit in glycolytic muscles of D1KO mice. In conclusion, the abundance of the glucose transporter must be regulated by Rab proteins that are targeted by TBC1D1. This thesis could exclude RAB8A, RAB14 and RAB12 as possible candidates. Thus, further research is necessary to uncover the full mechanism accounting for GLUT4-deficit in RabGAP-deficient muscles.

Zusammenfassung

Fragestellung

Die zwei nah verwandten RabGTPase-aktivierenden Proteine (RabGAPs) TBC1D1 und TBC1D4 (AS160) spielen eine wichtige Rolle für den Glukose- und Fettstoffwechsel im Skelettmuskel. TBC1D4 repräsentiert zudem einen wichtigen Faktor für die Insulinsensitivität des Fettgewebes. In Mäusen verursacht der Verlust jedes dieser RabGAPs *in vivo* schwere Störungen der Insulinsensitivität in Skelettmuskel und Fettgewebe und einen Wechsel der Energiesubstratpräferenz von Kohlenhydraten zu Fetten. Dieser Wechsel wird von einer gewebespezifischen Reduktion des Glukosetransporters GLUT4 begleitet. Beide Proteine, TBC1D1 und TBC1D4, werden durch die Kinasen AKT und AMP-aktivierte Proteinkinase (AMPK) reguliert, welche bekanntermaßen jeweils in den Insulin- und kontraktionsvermittelten Glukosestoffwechsel involviert sind.

Das Ziel dieser Arbeit ist, ein umfassenderes Verständnis der physiologischen Relevanz der zwei RabGAPs zu erlangen. Zu diesem Zweck wurden *Tbc1d1*- (D1KO), *Tbc1d4*- (D4KO) und doppelt-defiziente *Tbc1d1/4* (D1/4KO) Mäuse untersucht, um drei verschiedene Schwerpunkte zu adressieren:

1) Die metabolische Charakterisierung unter Fütterung einer Hochfettdiät (HFD),
2) Der Beitrag der einzelnen RabGAPs und deren Kinase AMPK zum Bewegungs- und kontraktionsvermittelten Glukosestoffwechsel und
3) Der Mechanismus hinter der Reduktion von GLUT4 im Skelettmuskel RabGAP-defizienter Mäuse.

Methoden

D1KO-Mäuse wurden mit D4KO und muskel-spezifischen AMPKα_2-*kinase-dead* (TG) Mäusen gekreuzt, um Tiere mit einem Defizit an allen drei Proteinen (TG-D1/4KO) auf einem genetischen C57BL/6J-Hintergrund zu erhalten. Die Toleranz gegenüber Glukose, Insulin und AICAR wurde durch entsprechende Toleranztests an männlichen Mäusen bestimmt. Die Laufleistung wurde *in vivo* mit einem kalorimetrischen Laufbandsystem gemessen. Die Kontraktions- und Insulin-induzierte ^{3}H-2-Deoxyglucose-Aufnahme wurden *ex vivo* unter Verwendung isolierter *Extensor digitorum longus* (*EDL*)- und *Soleus*-Muskeln bestimmt. Skelettmuskel- und Lebergewebe wurden auf Protein- und mRNA-Ebene analysiert. Durch *in-vivo*-Elektroporation (IVE) wurde der Einfluss von TBC1D1 auf die Menge an GLUT4 untersucht, indem verschiedene *Tbc1d1*-Mutanten und Rab-Proteine im TA-Muskel von D1KO- und C57BL/6J-Mäusen exprimiert wurden, in dem anschließend GLUT4 quantifiziert wurde.

Ergebnisse

Auf Hochfettdiät zeigten D4KO- und D1/4KO-Mäuse eine verminderte Glukosetoleranz und D1/4KO-Tiere eine gestörte Insulin-Toleranz. Gleichzeitig war ihre Sensitivität für AICAR, eine Substanz, welche Bewegung pharmakologisch imitiert, tendenziell verbessert im Vergleich zu wildtypischen (WT-)Tieren.

Die Inaktivierung von AMPK, führte zu einer verminderten körperlichen Leistungsfähigkeit, welche sich durch eine verringerte Laufleistung auf dem Laufband und eine verminderte kontraktionsinduzierte Glukoseaufnahme in *EDL* und *Soleus*-Muskel im Vergleich zu wildtypischen Tieren bemerkbar machte. Der zusätzliche Verlust von *Tbc1d1*, nicht aber *Tbc1d4*, verstärkte die Effekte auf die Leistungsfähigkeit. Zusätzlicher Verlust von *Tbc1d4* (TG-D4KO und TG-D1/4KO), verminderte dagegen die Fähigkeit, Glukose aus dem Blut zu entfernen, was in erhöhten Plasmaglukosespiegeln nach dem *fasting-refeeding* Experiment resultierte.

Zuvor konnten wir und andere Arbeitsgruppen zeigen, dass die GLUT4-Proteinspiegel in glykolytischen Muskeln von *Tbc1d1*-defizienten (D1KO) Mäusen wesentlich reduziert waren. Die Expression von wildtypischem TBC1D1 und einer Variante mit mutierter PTB-Domäne (R125W), nicht jedoch mit mutierter GAP-Domäne (R941K), stellte die GLUT4-Spiegel im *Tibialis anterior* (TA)-Muskel von D1KO-Mäusen wieder her. Die Expression des konstitutiv aktiven TBC1D1-Zielproteins Rab14 erhöhte die GLUT4-Expression im TA-Muskel von C57BL/6J-Mäusen.

Schlussfolgerungen

Diese Arbeit liefert neue Hinweise darauf, dass

1) Der Verlust von beiden RabGAPs zu einer verminderten Insulinsensitivität in Mäusen auf HFD führt, welche vermutlich durch das Fehlen von *Tbc1d4*, nicht jedoch von *Tbc1d1* verursacht wird. In Übereinstimmung damit, entwickeln D1/4KO Mäuse eine höhere Körperfettmasse verglichen mit ihren WT-Wurfgeschwistern. Gleichzeitig wird durch das Fehlen von *Tbc1d4* die AICAR-Sensitivität verbessert.
2) Der Verlust von AMPK im Muskel vermindert die Laufleistung auf dem Laufband und den kontraktionsinduzierten Glukosetransport. Zusätzlicher Verlust von *Tbc1d1*, nicht aber *Tbc1d4,* verursacht eine weitere Verschlechterung der gesamtkörperlichen Leistungsfähigkeit und des kontraktionsvermittelten Glukosetransports in den glykolytischen *EDL*-Muskel. Bemerkenswerterweise zeigten Skelettmuskeln, denen AMPK und beide RabGAPs fehlten, immer noch eine restliche kontraktionsinduzierte Glukoseaufnahme. Daher zeigt diese Arbeit die Notwendigkeit eines neuen Signalweges auf, der unabhängig von AMPK, TBC1D1 und TBC1D4 funktioniert.

3) Das Fehlen der GTPase aktivierenden (GAP-)Domäne von TBC1D1 verursacht das GLUT4-Defizit in glykolytischen Muskeln von D1KO-Mäusen. Zusammenfassend lässt sich sagen, dass die Häufigkeit des Glukosetransporters durch Rab-Proteine reguliert werden muss, welche als Zielproteine von TBC1D1 fungieren. Diese Arbeit konnte RAB8A, RAB14 und RAB12 als mögliche Kandidaten ausschließen. Daher ist weitere Forschung erforderlich, um den vollständigen Mechanismus aufzudecken, der für das GLUT4-Defizit in RabGAP-defizienten Muskeln verantwortlich ist.

Table of contents

1 Introduction

1.1 *Diabetes mellitus* and insulin resistance

1.1.1 Diabetes mellitus

In the year 2019, 1 in 11 adults between the age of 20 and 79 years was diabetic. This proportion sums up to a total of 463 million people worldwide and their number is continuously growing [1]. Therefore, 10 % of the global health expenditure was spent on diabetes in 2019. If this trend continues, 629 million people (20-79 years) will suffer from diabetes by 2045, resulting in enormous costs for our healthcare systems [2]. Therefore, finding more effective treatment and/or prevention measures for diabetes is of fundamental relevance for both the individual and the whole society.

Diabetes consists of a group of diseases of dysfunctional glucose regulation characterized by hyperglycemia as a result of disturbed insulin secretion or action or both [3]. It can be roughly classified into four categories: Type 1 diabetes (T1D), type 2 diabetes (T2D), gestational diabetes and specific types of diabetes triggered by other causes. Recently, the quest for more precise definitions of diabetes subtypes has emerged in the field [4, 5].

However, in the classical definition the most common forms of diabetes are T1D, which is marked by an absolute insulin deficiency caused by the autoimmune destruction of insulin producing β-cells in the pancreas and T2D which emerges on the background of insulin resistance that leads to a progressive loss of β-cell insulin secretion and affects approximately 87% to 91 % of all diabetes cases in high income countries [2, 3, 6, 7]. T2D is caused by a multifactorial combination of genetic susceptibility and environmental factors that eventually lead to insulin resistance in peripheral tissues and, ultimately, to a failure of insulin secretion by the pancreatic β-cells. The disease progression is highly dependent on the individual genetic predisposition and lifestyle. It is linked to the gradual decline in β-cell mass and function, caused by chronically elevated blood glucose levels (hyperglycemia) and a disturbed lipid metabolism (dyslipidemia) [7]. Hyperglycemia is also known to cause a variety of other pathophysiological complications, such as cardiovascular disease, neuropathy, diabetic retinopathy, and nephropathy. T2D is therefore described to be the leading cause of blindness, chronic kidney disease and amputation worldwide [8].

The risk for T2D is determined by an interaction of genetic and environmental factors. Family history of diabetes, previous gestational diabetes and ethnicity combined with overweight and obesity, older age, unhealthy diet, physical inactivity, and smoking increase the risk. The strongest risk predeterminant among these factors is excess body fat as a result of chronic overnutrition and/or physical inactivity. Higher waist circumference and higher body mass

index (BMI) are therefore associated with a higher risk for T2D [9, 10]. The WHO defines a BMI of ≥ 25 kg/ m² as overweight and a BMI of ≥ 30 kg/ m² as obese. Today, obesity is one of the most relevant public health problems in the world. In industrialized countries, it reaches even epidemic proportions. In general, obesity results from a chronic imbalance between energy intake and energy expenditure which causes several chronic diseases including T2D resulting from insulin resistance [11].

Obesity-linked insulin resistance is likely caused by high amounts of circulating free fatty acids (FFA) and excessive deposition of lipids in non-adipose tissues, mainly skeletal muscle, pancreas, and the liver. There, they can cause insulin resistance by different mechanisms (lipotoxicity). Another hypothesis is that an excess of adipose tissue produces a number of pro-inflammatory cytokines. These adipocyte-derived cytokines cause a state of chronic subclinical inflammation which is linked to insulin resistance and T2D [12].

Although the mechanism by which insulin resistance develops is largely unknown, it seems to result from defects in insulin receptor signaling [13, 14].

However, during the last decade more evidence arose for the genetic component of T2D risk. Having one diabetic parent increases the risk of T2D by 30-40 % compared to the general population. Two diabetic parents increase the risk by 70 %. Persons with siblings suffering from T2D are at the risk of developing diabetes with a 2-3fold risk [8].

1.2 Regulation of glucose homeostasis

1.2.1 Maintenance of whole-body glucose homeostasis

Glucose is the main source of energy for the body. It is distributed among the energy demanding tissues by the blood. To ensure that a sufficient amount of glucose is available to all tissues while avoiding the pathological glycosylation reactions that occur when blood glucose levels rise too high, it has to be kept within a relatively tight range [7]. Therefore, the body developed an ingenious system to ensure its own functioning.

Blood glucose concentrations are mainly regulated by two different hormones, which are secreted from specialized cells of the pancreatic islets (islets of Langerhans) and released into the bloodstream.

One of these hormones is insulin. It controls blood glucose concentrations by stimulating glucose uptake into insulin-responsive tissues such as skeletal muscle, adipose tissue, and the heart. At the same time, insulin causes an inhibition of hepatic glucose production [15]. After a carbohydrate-rich meal, rising blood glucose concentrations trigger the secretion of insulin from pancreatic β-cells into the bloodstream. In skeletal muscle and adipose tissue, the binding of insulin to its receptor at the cell surface accelerates the uptake of glucose from the blood via the facilitative glucose transporter 4 (GLUT4). Upon entry, it is either metabolized

immediately or stored as glycogen or triglycerides for later use. As result of the insulin stimulation, blood glucose levels decrease. During periods of fasting, glucose can be generated from the stored hepatic glycogen and exported into the blood stream in order to raise blood glucose levels. This process, called glycogenolysis, is inhibited by insulin to achieve a reduction in blood glucose levels [16]. Glycogen is generated from surplus glucose for short-term storage in liver and in skeletal muscle. It is a branched polymer of glucose molecules connected to chains by α-1,4-glycosidic linkages and by α-1,6-glycosidic linkages at branching points. These stores are used during fasting or as energy source for skeletal muscle contraction [17].

When blood glucose concentrations are low, the hormone glucagon is released by pancreatic α-cells. It induces the release of glucose from glycogen in hepatocytes into the blood to supply energy for the demanding organs and protect the body from a state of hypoglycemia [7].

During insulin resistance, this regulatory system is imbalanced. Chronic hyperglycemia occurs as result of the inadequate suppression of hepatic glucose output and disturbed glucose uptake of muscle and adipose tissues in response to insulin stimulation [16, 18].

There are a variety of mechanisms known to be involved in the development of insulin resistance [12]. In skeletal muscle of obese individuals, the lipid oxidation is disturbed. It follows that triglycerides, fatty acyl CoA, diacylglycerols (DAG) and ceramides accumulate [19-21], which may disturb insulin signaling through different mechanisms, such as increased serine phosphorylation of insulin receptor and insulin receptor substrate 1 by Protein kinase C (PKC) β and reduced serine phosphorylation of AKT [22, 23].

Additionally, there is evidence that SNAP23, which has been shown to be an essential factor for translocation of GLUT4-storage vesicles (GSVs) to the plasma membrane, is involved in lipid droplet (LD) formation. It was shown that excessive LD formation inhibited the trafficking of GSVs by competing for SNAP23. Overexpression of *Snap23* was able to rescue insulin sensitivity [24].

1.2.2 GLUT4 trafficking

The family of mammalian facilitative glucose transporters (GLUT) is comprised of 14 members. Each transporter consists of 12 transmembrane domains with cytosolic amino and carboxyl termini and transports hexoses or pentoses alongside a concentration gradient [16].

In skeletal muscle and adipose tissue, the predominantly expressed GLUT isoform is the insulin responsive GLUT4. In the basal state, GLUT4 is continuously removed from and recycled back to the plasma membrane, whereas most of the GLUT4 molecules are located within intracellular compartments, called GLUT4-storage vesicles (GSVs) [25, 26]

In response to insulin stimulation, muscle contraction or hypoxia GLUT4 is redistributed from GSVs to the plasma membrane. This process is called GLUT4 translocation. At the same time, studies found that the rate of endocytosis from the plasma membrane may be reduced [26]. In skeletal muscle cells, insulin stimulation and contraction exert additive effects on GLUT4 translocation [27]. GSVs are transported to the plasma membrane along actin filaments of the cytoskeleton that interact with the motor protein motor myosin Va (MyoVa) where they dock and fuse to it [28]. Thus, more GLUT4 transporters become integrated into the cell membrane and facilitate the transport of glucose molecules from the blood stream into the cell.
The retention of GLUT4 transporters in muscle and adipose cells is regulated through clathrin-mediated endocytosis (CME) and a number of clathrin-independent pathways that require organized lipid domains. Being retracted from the membrane and transported in early endosomes back into the cell, GLUT4 becomes redistributed either back to the plasma membrane via recycling endosomes or to late endosomes undergoing subsequent degradation. The half-life of one GLUT4 molecule is approximately 48 h [16, 26].

1.2.3 Regulation of skeletal muscle glucose uptake

Skeletal muscle accounts for ~85 % of peripheral glucose disposal from the blood [29]. In addition to a basal glucose transport rate from the extracellular space into skeletal muscle cell, glucose uptake can be regulated by insulin or skeletal muscle contraction during exercise. Whereas the contraction-induced pathway is only present in skeletal muscle, the insulin-regulated signaling is working in the same way in cells of the white adipose tissue.

In **insulin-stimulated glucose uptake**, the hormone is transported via the bloodstream to the peripheral tissues where it binds to its receptor (IR) at the surface of the cell. Subsequent auto-phosphorylation of the receptor leads to binding and phosphorylation of insulin receptor substrate (IRS) proteins, IRS1 and IRS2. Both activate phosphatidylinositol 3-kinase (PI3K), although activation by IRS1 is sufficient for GLUT4 translocation. PI3K activation leads to stimulation of two separate signaling axes, the activation of the serine/threonine kinase AKT (also known as phosphokinase B) and the Rho-family small GTPase Rac1. Stimulation of both axes results in a rise in GLUT4 translocation [30-32]. While the mechanisms by which Rac1 is acting remain largely unknown, AKT phosphorylates the AKT substrate of 160 kDa (AS160), which is also known as TBC1D4 and its close relative TBC1D1. Under basal conditions, these Rab GTPase activating proteins (Rab-GAPs) inhibit GLUT4 translocation by increasing the intrinsic GTPase activity of their target, the monomeric RabGTPases (Rab: Ras-related proteins in brain). Loaded with GDP, these Rab proteins remain inactive. Upon insulin stimulation, TBC1D1 and TBC1D4 are phosphorylated by their upstream AKT kinase which

may disrupt the recruitment of the RabGAPs from the GLUT4-containing vesicle. Consequently, the GAP activity of the RabGAPs may increase [33-35]. The downstream Rab proteins accumulate in their GTP-bound state in which they facilitate the transport and fusion of the GSVs to the plasma membrane. Thus, GLUT4 translocation and therefore glucose transport rates rise [25].

The mechanisms causing **contraction-induced glucose uptake** into skeletal muscle cells by exercise stimulation are to date still not completely uncovered. Studies reveal evidence for a number of parallel exercise-induced pathways, each of them contributing partially to the glucose disposal into skeletal muscle following muscle contraction [36-40]. However, none of these explanatory approaches has been able to fully elucidate the mechanisms taking place in a contracting/contracted muscle [40, 41].

For the contraction process the muscle consumes energy in form of adenosine triphosphate (ATP) by converting it to adenosine di- or monophosphate (ADP or AMP). The ratios of AMP/ATP and ADP/ATP increase, resulting in an increased activation of AMP-related protein kinase (AMPK). AMPK is an upstream kinase of TBC1D1 and TBC1D4 and causes phosphorylation of both proteins at several residues [42], which finally leads to GLUT4 translocation as described above. Another parameter leading to an increase of glucose uptake is Ca^{2+} signaling. During contraction, Ca^{2+} is released from the sarcoplasmic reticulum causing activation of glucose transport. This pathway seems to depend also on AMPK activation. Until today, it is discussed whether this activation is achieved by an increasing energy demand caused by sarcoplasmic reticulum Ca^{2+}-ATPase (SERCA)-dependent Ca^{2+} re-uptake or the direct phosphorylation of AMPK by calcium/calmodulin-dependent protein kinase kinases (CaMKKs), which are activated by Ca^{2+} release [43]. Consistent with the latter, electroporation of a specific inhibitor for CaMKII, a downstream kinase of CaMKK, into *Tibialis anterior* (TA) muscle, reduced contraction-stimulated glucose uptake by 30 %. However, data from CaMKKα and CaMKKβ knockout mice show that after electrical *in vitro* stimulation both AMPK-Thr172 phosphorylation and glucose uptake are unaltered, which makes a participation of CaMKKs unlikely [41]. Nevertheless, TBC1D1 and TBC1D4 both contain a calmodulin-binding domain (CBD), which at least in case of TBC1D4 does not seem to play a role in GLUT4 translocation [44]. The signaling pathways involving AMPK, are to-date the best-established mechanisms described regarding contraction-induced glucose uptake. Besides, there seem to be several AMPK-independent mechanisms of contraction stimulated glucose transport into skeletal muscle [41].

For instance, the actin cytoskeleton regulating GTPase Rac1 becomes activated by *in vivo* and *ex vivo* contraction as well as by passive mechanical stretching of the muscle independently of AMPK. Its inhibition or knockout results in decreased contraction-induced

glucose uptake [30, 45]. In addition, the actin-based motor protein Myo1c was found to increase contraction- and insulin-induced glucose uptake when expressed *in vivo* in *Tibialis anterior* muscle, whereas a mutation at the catalytic site of Myo1c impaired glucose uptake [46].

During exercise/contraction, nitric oxide synthase (NOS) activity and nitric oxide (NO) production are increased. There is evidence that the inhibition of NOS decreases contraction-stimulated glucose uptake in primarily fast-twitch fiber-containing muscles in rodents [47, 48].

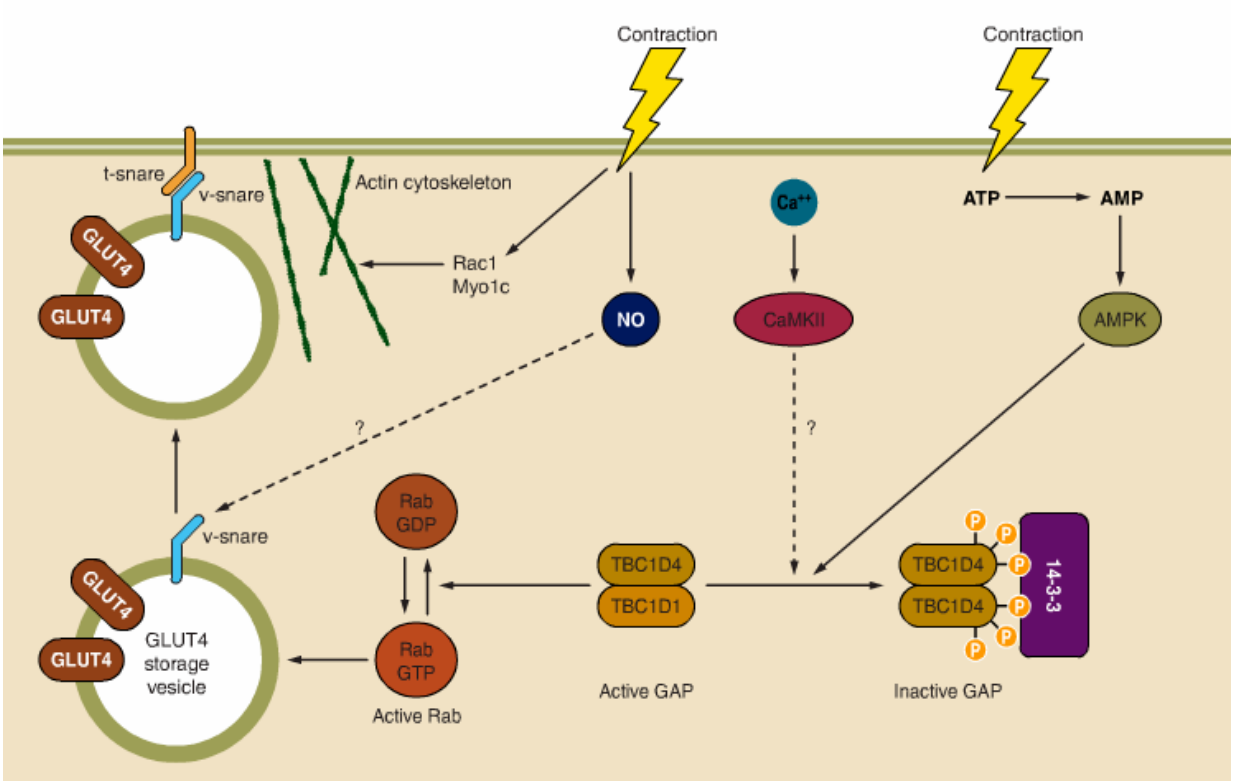

Figure 1.1: Schematic overview of signaling pathways involved in contraction induced GLUT4 translocation to the surface of skeletal muscle cells.
Skeletal muscle contraction leads to conversion of intracellular adenosine triphosphate (ATP) to adenosine monophosphate (AMP). Rising AMP levels activate AMP-related protein kinase (AMPK), which induces the inactivation of Rab GTPase activation proteins (RabGAPs) TBC1D1 and TBC1D4 by phosphorylation. This can also be triggered by rising Ca2+-concentrations leading to an activation of calcium/calmodulin-dependent protein kinase II (CaMKII). Active RabGAPs inhibit translocation of glucose transporter 4(GLUT4)-containing vesicles to the cell surface by catalyzing conversion of Rab-bound GTP to GDP. During muscle contraction their deactivation results in an increased GLUT4 translocation to the membrane, facilitating enhanced glucose uptake. Nitric oxide (NO) and the actin-cytoskeleton regulating proteins Rac1 and Myo1c have been demonstrated to be involved in contraction-induced glucose uptake independently of the AMPK pathway. Dashed lines indicate suggested pathways (modified from Richter and Hargreaves, 2013) [41].

1.3 AMPK function in skeletal muscle

1.3.1 AMPK as energy sensor of the cell

The AMP-activated protein kinase (AMPK) is often referred to as the energy sensor of the cell. It maintains cellular energy stores by regulating anabolic and catabolic pathways to ensure the balance between energy demand and supply [49].

During exercise, ATP consumption increases, resulting in higher AMP/ATP and ADP/ATP ratios caused by the adenylate kinase reaction. This leads to the activation of AMPK. Acute pharmacological activation of AMPK in skeletal muscle has been shown to trigger glucose uptake and fatty acid oxidation and to decrease protein synthesis and the synthase of glycogen [50].

AMPK consists of three subunits, one catalytic α-subunit and two regulatory subunits β and γ. Together they form a heterotrimeric protein complex. Several Isoforms of these subunits have been identified (α1, α2, β1, β2, γ1, γ2, γ3). The activity of the kinase domain is highly dependent on its reversible phosphorylation of α-Thr172. The β subunit acts as a scaffold for the other two subunits and contains a glycogen-binding domain (GBD) that determines the location of the complex to glycogen particles. The γ subunit directly binds adenosine nucleotides, what makes it a sensor for the energy status of the cell. AMPK heterotrimeric subtypes seem to be specialized in function. Studies have shown that the subunit composition has an influence on sensitivity to AMP. The reason for this might also lie in the different cellular localization of the subtypes, since the 12 heterotrimeric combinations of the 7 different subunits seem to be present in a tissue-specific manner, although in skeletal muscle from human and mouse all subunit isoforms can be detected. In mouse skeletal muscle, 5 complexes have been described (α2β2γ1, α2β2γ3, α2β1γ1, α1β2γ1, α1β1γ1). The predominantly expressed form in skeletal muscle is α2β2γ3, which is important for glucose transport, mitochondrial biogenesis, and improved insulin sensitivity [50, 51].

For activation of AMPK, two steps are needed. One is the allosteric binding of AMP or ADP to the γ subunit resulting in conformational changes that promote the second step, the reversible phosphorylation of Thr172 within the catalytic α subunit. These changes in conformation also prevent from dephosphorylation by protein phosphatases, whereas ATP binding to the γ subunit leads to inhibition of AMPK. Thus, increased cellular ratios of ADP/ATP and AMP/ATP cause its activation [52, 53].

In skeletal muscle, α2-containing complexes are predominantly phosphorylated by the upstream kinase LKB1 in response to contraction and pharmacological stimulation. AMPKα1 complexes are likely to be phosphorylated by Ca^{2+}/calmodulin-dependent protein kinase kinase β during long-term low-intensity exercise. The mechanisms leading to GLUT4 translocation and glucose uptake via AMPK are still functional in T2D patients. This makes AMPK a promising potential target for therapeutic drugs in insulin resistant individuals. AMPK

activators can be roughly divided into three categories. AMP analogs bind to the γ subunit at the same site as AMP and lead to the same effect of activation [50]. The most studied compound of this category is AICAR, which is transported into the cell by adenosine transporters and then phosphorylated by adenosine kinase to 5-aminoimidazole-4-carboxamide ribonucleotide (ZMP). [54]. As an AMP analog, ZMP binds to AMPK at the same sites as AMP and causes its activation. The second category comprises substances that influence the cellular AMP/ATP ratio. Prominent representatives of this category are metformin, an inhibitor of mitochondrial respiratory chain complex I, and resveratrol, which inhibits mitochondrial ATP synthase. Both compounds cause a lack of mitochondrial ATP generation leading to AMPK activation due to an increased AMP/ATP ratio. The third category of AMPK activators is the allosteric activators. A described example for these is the compound A-769662, which binds to AMPK in a pocket between the kinase domain of α subunit and the carbohydrate-binding module on the β subunit. By this, it activates AMPK both allosterically and by inhibiting its dephosphorylation on α-Thr172 [55, 56]. AMP analogs as well as compounds altering AMP/ATP ratio are highly interesting as pharmacological tools in examining AMPK function. However, their way of action is too unselective to provide promising candidates for therapeutic use.

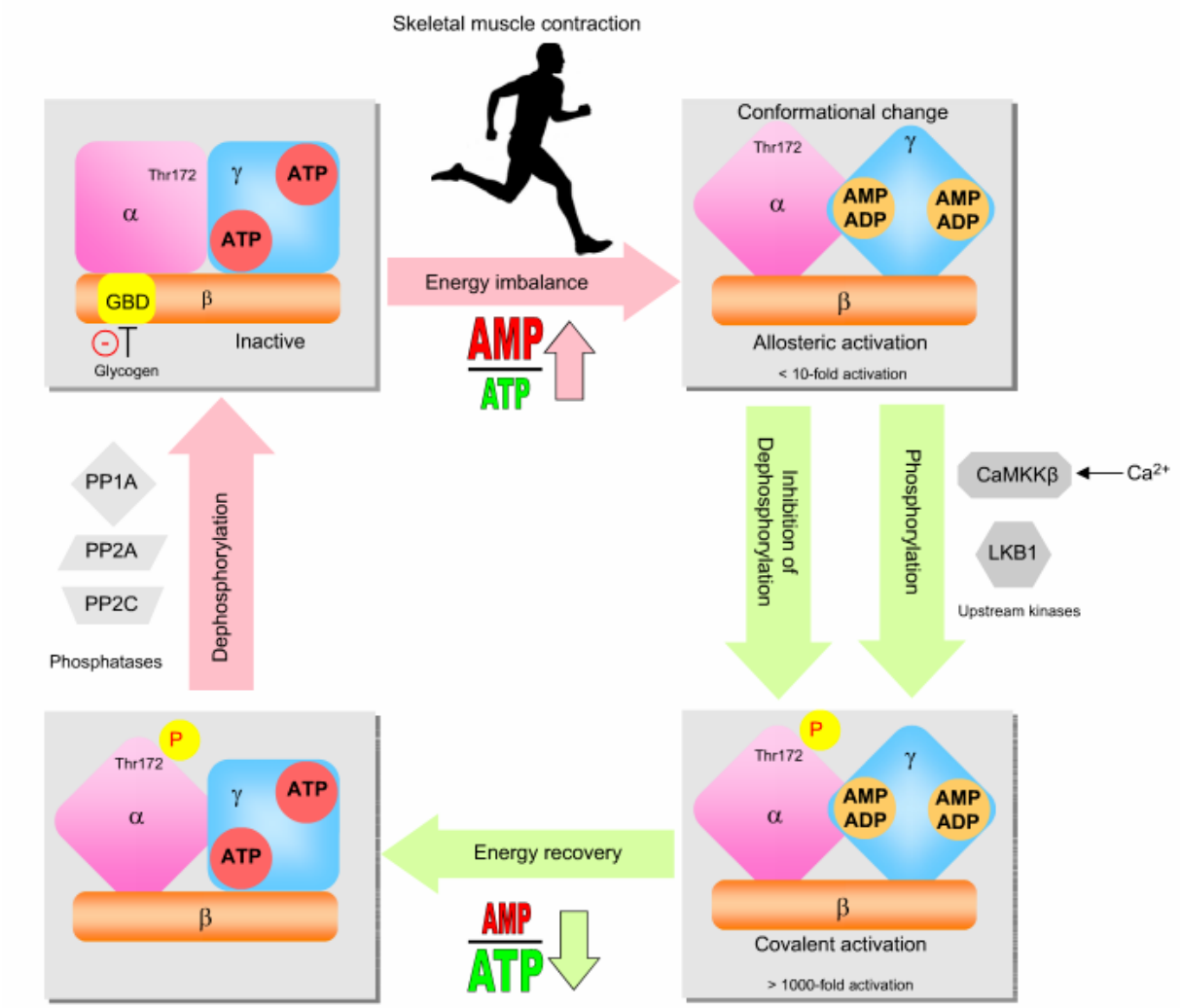

Figure 1.2: Regulation of AMPK in skeletal muscle during exercise.
Skeletal muscle contraction induces an energy imbalance, which leads to rising intracellular AMP/ATP and ADP/ATP ratios. Binding of ADP and AMP to the γ subunit of AMPK causes a conformational change activating it up to 10-fold via an allosteric mechanism. This also promotes phosphorylation of the catalytic α subunit at Threonin172 by upstream kinases liver kinase B1 (LKB1) and calcium/calmodulin-dependent kinase kinase β (CaMKKβ) and protects from dephosphorylation by protein phosphatases. This covalent activation increases AMPK activity 100-fold. Together, the allosteric effect and α-Thr172 phosphorylation cause a >1000-fold activation. When energy is regained after exercise, ATP-binding to AMPK reverses its conformational change enabling dephosphorylation catalyzed by protein phosphatases (PP1A, PP2A, and PP2C). A glycogen binding domain (GBD) at the β subunit inhibits AMPK by attaching the complex to glycogen (modified from Kjøbsted *et al*., 2017) [50].

1.3.2 AMPK-deficient mice

Over the past years, several mouse models deficient for AMPKα1, α2 or even a combination of both subunits have been created [50]. In this thesis, AMPKα2 kinase dead mice on a C57BL/6J background were used for an intercross with *Tbc1d1*- and *Tbc1d4*-decifient animals. These mice express a kinase-dead α2 subunit under control of the muscle creatine kinase (MCK) promoter, that drives transcription in skeletal and heart muscle. For their generation, a rat AMPKα2 cDNA carrying a myc epitope tag at its 5' end was used for in vitro mutagenesis. Lysine 45, which is essential for the binding and hydrolysis of ATP was changed to arginine and cDNA was subcloned into an expression vector which was then used for generation of

AMPK transgenic mice. These were kindly provided by Morris J. Birnbaum and first described in 2001 by Mu *et al*. There, the authors found reduced glycogen levels in gastrocnemius muscle of kinase-dead AMPK-transgenic (TG) mice during fed state. Beyond that, these mice showed higher basal Thr172 phosphorylation, which resulted in an impaired stimulation by *ex vivo* contraction, whereas insulin signaling was not affected. Basal and contraction-stimulated AMPK activity was abrogated in muscles of TG mice. Consistent with this, AICAR and hypoxia, which leads to an intracellular increase of AMP/ATP ratios, were not able to stimulate deoxyglucose uptake into intact *EDL* and *Soleus* muscle of TG mice. Under hypoxic conditions the amount of cell surface GLUT4 remained at basal level. Whole body AICAR tolerance of these mice was reduced and further decreased when mice were older. Assessing contraction-induced glucose uptake in *EDL* muscle, TG mice exhibited a reduction by 40 % compared to WT muscles. However, in contrast to AICAR stimulation, the response was not completely abrogated. This led to the assumption that contraction-mediated increases of glucose transport do not solely depend on AMPK and that contraction and AICAR or hypoxia do not share identical pathways to activate glucose uptake. Voluntary wheel running activity of TG mice was reduced by 20-30 % during active phase [57]. Like in wild-type mice, exercise but not AICAR treatment increased GLUT4 mRNA levels in muscles of TG mice [58].

1.4 Monomeric Rab GTPases

1.4.1 Monomeric Rab GTPases regulate vesicular transport

In eukaryotic cells, the cytoplasm contains a variety of membranous organelles that are that are in mutual exchange by vesicular transport. Therefore, a large diversity of components must be transported via a complex network of interconnected pathways. This process is mainly regulated by Rab GTPases, which are known to be involved in all the critical steps, like budding and scission of vesicles from donor membranes, transport along cytoskeletal components, association and finally fusion to correct target membranes. With more than 60 identified members in humans, Rab GTPases are the largest family of Ras-like GTPases. To regulate vesicular trafficking, they switch between two conformational states. Bound to GTP they are considered to be active, whereas the GDP-bound state is also called “inactive”. The switch between those two stages is supported by two other classes of proteins. The GEFs (guanine nucleotide exchange factors) catalyze the exchange of Rab bound GDP with GTP and therefore serve as “Rab activators”. In contrast to that, the GAPs (GTPase activating proteins) increase the intrinsic hydrolysis activity of Rab proteins leading to their inactivation [59].

1.4.2 The role of monomeric Rab GTPases in GLUT4 trafficking

Glucose homeostasis in the blood is regulated by the rate of gluconeogenesis in the liver and glucose uptake of insulin responsive tissues. Skeletal muscle and adipose tissue play a significant role here. In these tissues, glucose uptake is rate-limited by the number of facilitative glucose transporters present in the plasma membrane that are, upon insulin stimulation, redistributed from intracellular compartments to the plasma membrane (PM) [60]. As described above, this process is regulated by TBC1D1 and TBC1D4 in interaction with several monomeric Rab proteins. *In vitro* studies suggest Rab8A, 8B, 10 and 14 as substrates of TBC1D1 and TBC1D4 [61]. In these studies, silencing of TBC1D1 and TBC1D4 in the L6 rat-muscle cell line led to increased basal cell surface GLUT4, which was restored by simultaneous knockdown of Rab8A and 14, but not 8B and 10. Knockdown of Rab8A and 14 also inhibited the insulin-induced GLUT4 translocation, whereas Rab8B and 10 did not [61].
It is likely, that there are other Rab GTPases involved in GLUT4 trafficking. Recently our lab could demonstrate that knockdown of Rab28 in skeletal muscle diminished basal glucose uptake, while expression of a constitutively active mutant of Rab28 in adipocytes increased it [62].

1.4.3 Monomeric Rab GTPases in autophagy

Besides for GLUT4 translocation, vesicular trafficking and therefore Rab GTPases are also required for the formation of the autophagosome during macroautophagy. This process, shortly called autophagy, is a catabolic mechanism that is evolutionary conserved in all eukaryotes. Its function is, to sequester intracellular macromolecular complexes like organelles, lipids, and proteins in double layered membrane vesicles, called autophagosomes, which determine their content for degradation. Therefore, they fuse with lysosomes to form the autolysosome [63]. Little is known about the regulators controlling membrane trafficking during autophagy. To date, some members of the Rab family have been identified to be involved in these processes. Rab11 for example has been shown to be involved in formation and maturation of the autophagosome when present on the surface of recycling endosomes by binding to TBC1D14 [64]. Recent publications identified the Rab GTPase Rab12 as one candidate involved in autophagy in a big screening of 58 mouse Rab isoforms with Dennd3 as its GEF (guanine nucleotide exchange factor). Rab12-knockdown in mouse embryonic fibroblasts (MEFs) was shown to impair degradation of the amino-acid transporter PAT4 (proton-coupled amino-acid transporter 4) whose accumulation resulted in an increased activity of mTORC1 (mammalian/mechanistic target of rapamycin complex 1), an upstream regulator of autophagy [65, 66]. Furthermore, Rab12 was found to influence degradation of transferrin receptors (TfR) [67]. Unpublished data of our group could show that Rab12 is also

a potent interaction partner increasing its GTP-hydrolysis activity when TBC1D1 is present. The GEF of Rab*8*, called Rabin8*,* has been shown to suppress starvation-induced autophagosome formation in human telomerase-immortalized retinal pigment epithelial (hTERT-RPE) cells and MEF cells [68]. Although this effect was found to be independent of Rab8 and its GTPase activity, Rab8 remains an interesting candidate in the context of autophagy.

1.5 Rab GTPase activating proteins

1.5.1 TBC1D1 and TBC1D4

The most important Rab GTPase activating proteins (RabGAPs) in regulation of GLUT4 trafficking are TBC1D1 (tre-2/USP6, BUB2, cdc16 domain family member 1) and TBC1D4. Both are ubiquitously expressed, but especially in skeletal muscle and white adipose tissue their physiological functions in glucose homeostasis have been extensively studied. TBC1D1 and TBC1D4 are closely related to each other with their GAP domains being 79 % identical and their full-length sequences sharing 47 % identity. Their molecular weight is ~150-160 kDa in SDS-PAGE [69, 70]. While TBC1D1 occurs in all animal species, TBC1D4 can only be found in vertebrates suggesting its evolutionary novelty [71].

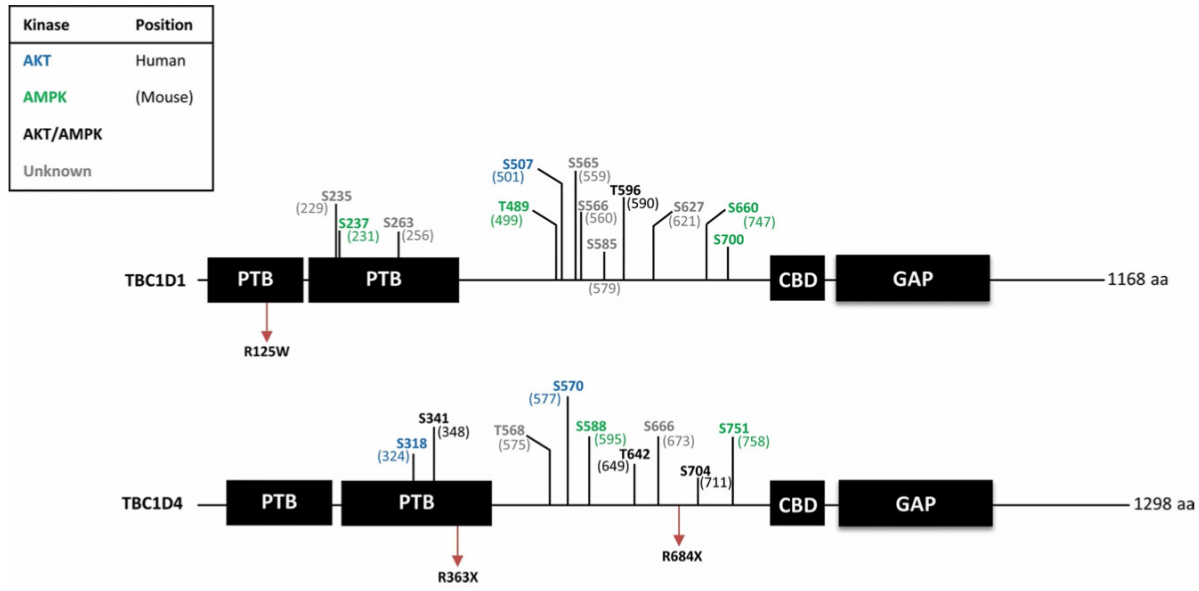

Figure 1.3: Structure of murine TBC1D1 and TBC1D4 with their functional domains and position of known phosphorylation sites.
The amino acid sequence of TBC1D1 and TBC1D4 is ~50% identical. Both proteins contain two amino-terminal PTB domains, a Ca+/ calmodulin-binding domain and a catalytic RabGAP domain. AKT phosphorylation sites are marked in blue, AMPK phosphosites in green. Phosphorylation sites for both AKT and AMPK are shown in black. Phosphosites shown in this figure are the phosphorylation sites in humans. Mouse phosphosites are put in parenthesis. The arrows indicate naturally occurring mutations associated with metabolic traits in humans (modified from Mafakheri, Chadt and Al-Hasani, 2018) [34].

Regarding their functional domains the structure of both RabGAPs is very similar. Both contain two adjacent N-terminal phosphotyrosine-binding (PTB) domains, one calmodulin-binding domain (CBD) and a functional GAP domain near the C-terminus accounting for their family affiliation [69, 70]. By phosphorylation TBC1D1 and TBC1D4 become inactive. Therefore, several serine and threonine residues have been identified being phosphorylated either by their upstream kinases AKT or AMPK. TBC1D1 phosphorylation at Ser231 in mice (Ser237 in humans), Ser660 and Ser700 is triggered by contraction and AICAR but not insulin stimulation in an AMPK-dependent manner. In contrast, Thr590 (Thr596 in humans) can be phosphorylated by contraction, AICAR and insulin stimulation [72-74]. In TBC1D4, Thr649 and Ser673 (Thr642 and Ser666) are phosphorylated only by insulin, but not by exercise. In pre-exercised mouse legs, the levels of phosphorylation after insulin stimulation were further increased at Ser325, Ser348, Ser595, Ser758 (Ser318, Ser341, Ser588 and Ser751 in humans), leading to the conclusion that these are targeted by insulin and contraction. [75-77]. Furthermore, Ser711 can be phosphorylated by contraction and AICAR via AMPK, but also by insulin stimulation, but in an AKT-independent manner [78].

Besides the phosphorylation pattern, a major difference between TBC1D1 and TBC1D4 is their expression profile. While TBC1D1 is highly expressed in glycolytic skeletal muscle, TBC1D4 shows its highest expression in the heart, oxidative muscle, and adipose tissue (Figure 1.4) [79-82].

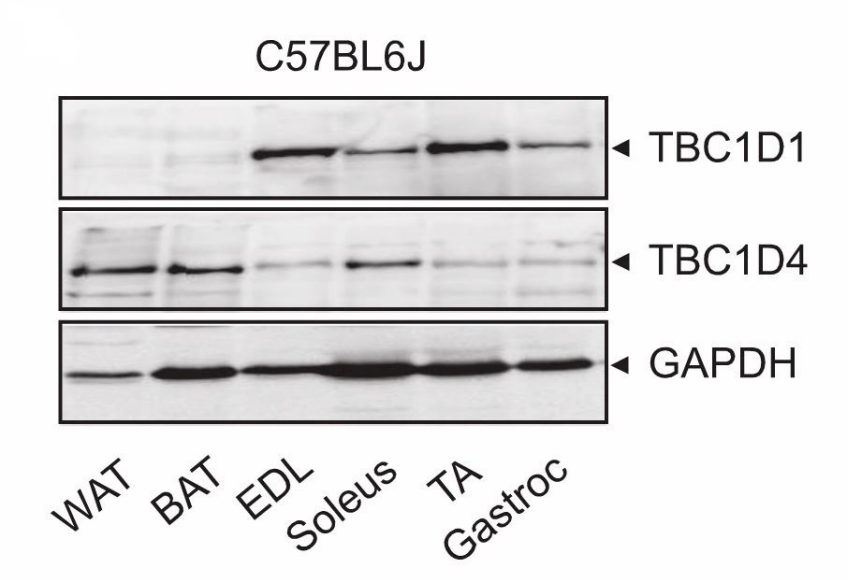

Figure 1.4: TBC1D1 and TBC1D4 protein abundance.
Protein abundance of TBC1D1 and TBC1D4 in white adipose tissue (WAT), brown adipose tissue (BAT), and different skeletal muscle types from C57BL/6J mice analyzed by Western blotting. *EDL*: *Extensor digitorum longus*, TA: *Tibialis anterior*, Gastroc: *Gastrocnemius* (modified from Szekeres *et al*., 2012) [82].

For both RabGAPs, different splice variants have been described, but their respective function

is still unknown. Previous studies revealed two different splice variants of TBC1D1 in adipocytes and skeletal muscle. The shorter one is missing two adjacent exons coding for the amino acids 631-724. There are also two variants of TBC1D4 of which the shorter one is mainly expressed in fat cells and lacks the amino acids 685-739 encoding one single exon [70]. The different expression pattern among different tissues and the presence of different splice variants may be indicative of functional differences of TBC1D1 and TBC1D4 in metabolism.

1.5.2 *Tbc1d1*- and *Tbc1d4*-deficient mice

There have been a several studies investigating the role of TBC1D1 and TBC1D4 in glucose metabolism. For this purpose, mainly knockout mouse models on a C57BL/6 background were used, including single- and even double-deficient mice [79-91].

Taken together, these studies revealed that mice deficient for TBC1D1 (D1KO), TBC1D4 (D4KO) or both proteins (D1/KO) exhibit a disturbed glucose and insulin tolerance, some studies indicate that they compensate for the lack of energy by increasing fatty acid oxidation in skeletal muscle [79], whereas others don't see an effect on fat metabolism [84, 90].

Although both RabGAPs seem to influence glucose homeostasis, there are several hints that they act in different ways and contexts. While TBC1D4 seems to be more important for insulin-induced signaling [84], TBC1D1 might play an important role in AMPK-regulated glucose metabolism. However, its role in exercise-mediated glucose disposal is not uncovered [83, 92].

One major cause for the effects of TBC1D1- and TBC1D4-deficiency on glucose disposal is probably a dramatic decrease in glucose transporter GLUT4 on protein level [79, 83, 84]. According to the pattern in which the examined tissues predominantly express TBC1D1 or TBC1D4, GLUT4 protein content is low in the same tissues of the respective knockout animals. At the same time, mRNA is unchanged [79, 83]. The remaining GLUT4 content is mainly located at the plasma membrane, even at basal state, to maintain basal glucose transport [79, 84]

1.6 Aim of the study

Based on findings about the function of TBC1D1 and TBC1D4 in glucose homeostasis of mice, this study aimed to address several open questions.

- First it was investigated, if high-fat diet (HFD) feeding was able to exacerbate the metabolic phenotype of *Tbc1d1*- and/or *Tbc1d4*-deficient mice, since Rab GAP-deficiency had a protective effect on body fat mass gaining on standard diet (SD).
- The second aim was to find out if and in which proportion TBC1D1 and TBC1D4 contribute to skeletal muscle contraction-induced glucose transport.

- In addition, this work addressed the question, whether contraction or exercise signaling in skeletal muscle require the AMPK-TBC1D1 and/or -TBC1D4 pathway to permit glucose transport.
- Finally, it was assessed if the RabGAP dependent loss of GLUT4 protein content depends on the activation of Rab proteins and if it can be rescued by expressing active or inactive Rab-mutants.

2 Materials

2.1 Mouse strains

Table 2.1: Mouse strains

Strain	Supplier
C57BL/6J	DDZ (German Diabetes-Center, Duesseldorf, Germany)
RCS.B6.SJL-*Nob1.10*	DDZ (German Diabetes-Center, Duesseldorf, Germany)
RCS.B6.SJL-*Nob1.10*-KO-*As160*	DDZ (German Diabetes-Center, Duesseldorf, Germany)
AMPK-DN-RCS.B6.SJL-*Nob1.10*-KO-*As160*	DDZ (German Diabetes-Center, Duesseldorf, Germany)

2.2 Mouse diets

Mice were either fed a standard diet (ssniff, Soest, Germany) or a high-fat diet (Research Diets Inc., New Brunswick, USA).

Table 2.2: Mouse diets

Standard diet		
(Cat. No. V1126 M-Z Extrudat)	**Mass [%]**	**Calories [%]**
Protein	22.1	36
Carbohydrate	53.3	53
Fat	4.5	11
Total calorie content [kcal/g] 3.3		

High-fat diet		
(Cat. No. D12492)	**Mass [%]**	**Calories [%]**
Protein	26.2	20
Carbohydrate	26.3	20
Fat	34.9	60
Total calorie content [kcal/g] 5.2		

2.3 Bacterial strains

Bacterial strains were used for plasmid preparations.

Table 2.3: Bacterial strains

Strain	Supplier
E. coli DH5α	Prof. Dr. Eckhard Lammert (DDZ, Düsseldorf, Germany)

2.4 Antibodies

Table 2.4: Antibodies

Antibody	Supplier
Primary antibodies	
rabbit-anti-GAPDH (14C10)	Cell Signaling Technology (Boston, USA)
rabbit-anti-TBC1D1 (V796)	Cell Signaling Technology (Boston, USA)
rabbit-anti-AS160 (TBC1D4)	Merck Millipore (Darmstadt, Germany)
rabbit-anti-GLUT4	Prof. Dr. Hadi Al-Hasani (DDZ, Duesseldorf, Germany)
rabbit-anti-GLUT1	Merck Millipore (Darmstadt, Germany)
rabbit-anti-AMPKα	Cell Signaling Technology (Boston, USA)
rabbit-anti-phospho-AMPKα (Thr^{172})	Cell Signaling Technology (Boston, USA)
rabbit-anti-Glycogen Synthase	Cell Signaling Technology (Boston, USA)
rabbit-anti-ARK5	Cell Signaling Technology (Boston, USA)
rabbit-anti-SNARK/NUAK2	Cell Signaling Technology (Boston, USA)
mouse-anti-RAB12 (H-11)	Santa Cruz Biotechnology (Dallas, USA)
rabbit-anti-RAB14	Sigma-Aldrich (Saint Louis, USA)
mouse-anti-RAB8	BD Biosciences (Franklin Lakes, USA)
mouse-anti-FLAG M2	Sigma-Aldrich (Saint Louis, USA)
rabbit-anti-GFP	Cell Signaling Technology (Boston, USA)
Secondary antibodies	
goat-anti-rabbit-POD-IgG	Dianova (Hamburg, Germany)
goat-anti-mouse-POD-IgG	Dianova (Hamburg, Germany)
mouse-IgGκ BP-HRP	Santa Cruz Biotechnology (Dallas, USA)

2.5 Plasmids

Table 2.5: Plasmids

Plasmid	Supplier
pEGFP-N1	Clontech (Mountain View, USA)
pcDNA3-*Tbc1d1*-WT	Prof. Dr. Hadi Al-Hasani (DDZ, Duesseldorf, Germany)
pcDNA3-*Tbc1d1*-R125W	Prof. Dr. Hadi Al-Hasani (DDZ, Duesseldorf, Germany)
pcDNA3-*Tbc1d1*-R941K	Prof. Dr. Hadi Al-Hasani (DDZ, Duesseldorf, Germany)
pEGFP-C1-*Rab14*-Q70L	Prof. Dr. Hadi Al-Hasani (DDZ, Duesseldorf, Germany)
pEGFP-C1-*Rab14*-S25N	Prof. Dr. Hadi Al-Hasani (DDZ, Duesseldorf, Germany)
pcDNA3-*Rab8a*-Q67L	Prof. Dr. Hadi Al-Hasani (DDZ, Duesseldorf, Germany)
pcDNA3-*Rab8a*-T22N	Prof. Dr. Hadi Al-Hasani (DDZ, Duesseldorf, Germany)

2.6 Synthetical oligonucleotides

2.6.1 PCR primers for mouse genotyping

All primers were synthesized and supplied by Sigma-Aldrich (Steinheim, Germany).

Table 2.6: PCR primers for mouse genotyping

Primer	Sequence 5' → 3'
Ampk-fwd	CGAGGTCGACGGTATCGATAAGCTTGATATC
Ampk-rev	GAAGGAACCCGTTGGAGGACTGGAGGCGAGG
As160-fwd	AGTAGACTCAGAGTGGTCTTGG
As160 WT-rev	GTCTTCCGACTCCATATTTGC
As160 Geo-rev	GCAGCGCATCGCCTTCTATC
RCS-SJL-fwd	CAACATTCTGAAGGCCTTCTG
RCS-SJL-rev	TCCCTGGCTACAAGCTGAGT
RCS-B6-fwd	GGACAAGCAGCTTTCTTGTTT
RCS-B6-rev	TCCTGGTCCAGAAGCGAG

2.6.2 siRNA oligonucleotides

Table 2.7: siRNA oligonucleotides

siRNA	Supplier	Prod.-No.
ON-TARGETplus Mouse *Rab12* SMARTpool	GE Healthcare (Chalfont St Giles, UK)	L-040865-01-0020
ON-TARGETplus Non-targeting Pool	GE Healthcare (Chalfont St Giles, UK)	D-001810-10-20

2.6.3 SYBR-Green primers

All SYBR-Green primers were supplied by Eurofins Genomics (Ebersberg, Germany). Primer pairs were chosen to be located on two different exons to avoid amplification of genomic DNA.

Table 2.8: SYBR-Green Primers

Primer	Sequence 5' → 3'	Product Size [bp]
Tbc1d1-fwd	ACAGTGTGGGAAAAGATGCT	143
Tbc1d1-rev	AGGTGGAACTGCTCAGCTAG	
Tbc1d4-fwd	CCAACAGTCTTGCCTCAGAG	146
Tbc1d4-rev	GAATGTGTGAGCCCGTCTTC	
Scl2a4-fwd	CAGCGAGTGACTGGAACACT	106
Scl2a4-rev	CAATCACCTTCTGTGGGGCA	
Nuak1-fwd	GGCTCTCCAACCTGTACCAG	139
Nuak1-rev	TAAAGCAAGACACCCAGGGC	
Nuak2-fwd	AGGATCTGCTGCACATACGGA	185
Nuak2-rev	TGGCCGCTCACTGATGTAATC	
Sik1-fwd	GGCACCGAGTCACCAAAACG	194
Sik1-rev	AAGTTTCATGAGCTGGACCTCC	
Sik2-fwd	CGTCGGCCTAGCACCATTG	112
Sik2-rev	GTGGGAGGAGGGTAGATCGC	
Sik3-fwd	AGCTGCTGAAGACGTGGTGT	151
Sik3-rev	GTGCTCCCATCAAACGGCAG	
Gapdh-fwd	CCAGGTTGTCTCCTGCGACT	106
Gapdh-rev	ATACCAGGAAATGAGCTTGACAAAGT	
Rps29-fwd	TGAAGGCAAGATGGGTCAC	127
Rps29-rev	GCACATGTTCAGCCCGTATT	

2.7 Reaction kits, Enzymes, Standards

Table 2.9: Reaction kits, Enzymes, Standards

Kit	Supplier
100 bp DNA Ladder / 1 kb DNA Ladder	Thermo Scientific, Peqlab, Wilmington, MA, USA
10x DreamTaq Green Buffer	Thermo Scientific, Peqlab, Wilmington, MA, USA
5x Phusion HF Buffer	Thermo Scientific, Peqlab, Wilmington, MA, USA
6x Gel Loading Dye	Thermo Scientific, Peqlab, Wilmington, MA, USA
Actrapid® Penfill® human Insulin	Novo Nordisk, Bagsvaerd, Denmark
Amyloglucosidase	Sigma Aldrich, Steinheim, Germany
Complete Protease Inhibitor Cocktail	Roche, Mannheim, Germany
DreamTaq DNA Polymerase 5U/µL	Thermo Scientific, Peqlab, Wilmington, MA, USA
Endotoxin Removal Solution	Sigma Aldrich, Steinheim, Germany
Glucose liquicolor	Human, Wiesbaden, Germany
GoScript© Reverse Transcriptase Kit	Promega, Madison, WI, USA
GoTaq© qPCR Master Mix	Promega, Madison, WI, USA
Hexanucleotide primer	Roche, Manheim, Germany
Hyaluronidase	Sigma Aldrich, Steinheim, Germany
Insulin (Mouse) Ultrasensitive ELISA	DRG Instruments, Marburg, Germany
Invisorb® Genomic DNA Kit II	STRATEC Molecular GmbH, Berlin, Germany
NEFA-HR(2)	Wako Chemicals GmbH, Neuss, Germany
PhosSTOP Phosphatase Inhibitor	Roche, Mannheim, Germany
Phusion High-Fidelity DNA Polymerase 500U	Thermo Scientific, Peqlab, Wilmington, MA, USA
Pierce™ BCA Protein Assay Kit	Thermo Scientific, Pierce, Rockford, IL, USA
Precision Plus Protein Standard Dual Color	Biorad Laboratories, München, Germany
PureLink™ Expi Endotoxin-Free Mega Plasmid Purification Kit	Thermo Scientific, Peqlab, Wilmington, MA, USA
Rothiszint®	Carl Roth, Karlsruhe, Germany
Triglycerides (TRIGS)	Randox Laboratories, Crumlin, UK
TRIzol™ RNA Isolation Reagent	Thermo Scientific, Peqlab, Wilmington, MA, USA
Western Lightning ECL Pro/Ultra	Perkin Elmer, Waltham, MA, USA

2.8 Chemicals

Table 2.10: Chemicals

Chemical	Supplier
2,2,2-Tribromoethanol (Avertin)	Sigma Aldrich, Steinheim, Germany
20 % Glucose solution	B. Braun, Melsungen, Germany

Chemical	Supplier
2-Deoxy-D-glucose	Sigma Aldrich, Steinheim, Germany
5-aminoimidazole-4-carboxamide 1-β-D-ribo-furanoside (AICAR)	Toronto Research Chemicals, North York, ON, Canada
Acetic acid	Carl Roth, Karlsruhe, Germany
Acrylamide (30 %)	Serva, Heidelberg, Germany
Agarose	Biozym Scientific GmbH, Hessisch Oldendorf, Germany
Ammonium persulfate (APS)	MP Biomedicals, Illkirch, France
Bovine serum albumin (BSA) Fraction V	AppliChem, Darmstadt, Germany
Bromophenol blue	Merck, Darmstadt, Germany
Chloroform	AppliChem GmbH, Darmstadt, Germany
D-(+)-Glucose	Sigma Aldrich, Steinheim, Germany
Deoxy-D-Glucose 2-(1,2-3-H(N)	Hartmann Analytic, Braunschweig, Germany
Dimethylsulfoxide (DMSO)	AppliChem, Darmstadt, Germany
Dithiothreitol (DTT)	VWR, Darmstadt, Germany
D-Mannitol	AppliChem GmbH, Darmstadt, Germany
dNTP Set PCR Grade	Roche, Mannheim, Germany
Ethanol absolute	AppliChem GmbH, Darmstadt, Germany
Ethidium bromide	MP Biomedicals, Illkirch, France
Ethylene glycol tetraacetic acid (EGTA)	Serva, Heidelberg, Germany
Ethylenediaminetetraacetic acid (EDTA)	Roth, Karlsruhe, Germany
Isoflurane	Piramal Enterprises, Mumbai, India
Isopropanol	AppliChem GmbH, Darmstadt, Germany
Magnesium chloride ($MgCl_2$)	Roche Diagnostics, Mannheim, Germany
Mannitol, D-[1-14C]-	PerkinElmer, Seer Green, UK
Methanol	Carl Roth, Karlsruhe, Germany
Peptone	Carl Roth, Karlsruhe, Germany
Potassium chloride (KCl)	Merck, Darmstadt, Germany
Skim milk powder	Carl Roth, Karlsruhe, Germany
Sodium chloride (NaCl)	Carl Roth, Karlsruhe, Germany
Sodium dodecyl sulfate (SDS)	Applichem, Darmstadt, Germany
Sodium sulfate (Na_2SO_4)	Merck, Darmstadt, Germany
Tetraethylethylenediamin (TEMED)	Roth, Karlsruhe, Germany
Tris-hydrochloride (Tris-HCl)	Roth, Karlsruhe, Germany
Triton X-100	Sigma Aldrich, Steinheim, Germany
Tween-20	MP Biomedicals, Solon, USA
Yeast extract	Carl Roth, Karlsruhe, Germany
β-Mercaptoethanol (50 mM solution)	Thermo Fisher Scientific, Darmstadt, Germany

2.9 Buffers, solutions, and culture media

Table 2.11: Buffers, solutions, and culture media

Buffer/Solution	Composition
4x Lämmli Sample Buffer	20 % vol Glycerol, 8 % SDS, 10 mM EDTA, 250 mM Tris-HCl, 5 % bromophenol blue solution (2 % bromophenol blue + 4 % SDS in water)
Ampicillin stock solution	100 mg/ml ampicillin in H_2O, sterile filtrated
Electrophoresis Buffer for SDS-PAGE	25 mM Tris-HCl, 192 mM Glycine, 0.1 % (w/v) SDS
Kanamycin stock solution	30 mg/ml kanamycin in H_2O, sterile filtrated
KHB	10 % (v/v) KHB Stock I, 10 % (v/v) KHB Stock II, 80 % (v/v) H_2O
KHB Stock II	2.5 mM $CaCl_2 \cdot 2\ H_2O$, 1.2 mM $MgSO_4 \cdot 7\ H_2O$, 5 mM HEPES
Krebs-Henseleit buffer (KHB) Stock I	118.5 mM NaCl, 4.7 mM KCl, 1.2 mM KH_2PO_4, 25 mM $NaHCO_3$
Lysogeny broth (LB-) agar	1 % peptone, 1 % NaCl, 0.5 % yeast extract, 1.5 % agar
Lysogeny broth (LB-) media	1 % peptone, 1 % NaCl, 0.5 % yeast extract
Protein lysis buffer	20 mM Tris-HCl, 150 mM NaCl, 1 mM EDTA, 1 mM EGTA, 1% Triton X-100
Separation gel buffer for SDS-PAGE	1,5 M Tris-HCl, 0.4 % SDS, pH 8.8
SOC (Super Optimal broth with Catabolite repression)-media	0.5 % yeast extract, 2 % tryptone, 10 mM NaCl, 2.5 mM KCl, 10mM $MgCl_2$, 2 % glucose
Sodium acetate buffer	0.12 M $C_2H_3NaO_2$, 0.48 % CH_3COOH, pH 4.8
Stacking gel buffer for SDS-PAGE	500 mM Tris-HCl, 0.4 % SDS, pH 6.8
Strip-buffer for Western Blots	20% SDS, 1 M Tris-HCl, 0.78 % β-Mercaptoethanol
TAE-buffer	40 mM Tris-acetate, 1mM EDTA, pH 8.0
Transfer buffer for tank blotting	25 mM Tris-HCl, 192 mM Glycine, 20 % Methanol
Wash buffer for Western Blots (TBS-T)	10 mM Tris-HCl, 150 mM NaCl, 0.5 % Tween-20, pH 8.0
Western Blot blocking solution	5 % skimmed milk powder or 5 % BSA, 10 mM Tris-HCl, 150 mM NaCl, 0.5 % Tween-20, pH 8.0

2.10 Devices

Table 2.12: Devices

Device / Instrument	Supplier
CERTOMAT® R benchtop shaker	Sartorius AG, Göttingen, Germany
CERTOMAT® H incubation hood	Sartorius AG, Göttingen, Germany
Chemidoc™ XRS+ System	BioRad Laboratories, München, Germany
Contour XT Glucometer	Bayer, Leverkusen, Germany
Electroporator ECM 830	BTX, Holliston, MA, USA
Eporator	Eppendorf AG, Hamburg, Germany

Device / Instrument	Supplier
Geldoc™ XR+ System	BioRad Laboratories, München, Germany
iMARK™ Microplate Reader	BioRad Laboratories, München, Germany
Muscle Strip Myograph 820MS	DMT, Aarhus, Denmark
Nanodrop 2000	Thermo Scientific, Peqlab, Wilmington, MA, USA
NMR	EchoMRI, Houston, USA
Platinum Tweezertrode 7mm	VWR, Darmstadt, Germany
PowerLab 8/35	ADInstruments, Oxford, UK
Scintillation Counter LS 6000LL	Beckmann, Krefeld, Germany
Shaker CH-4130	INFORS AG, Bottmingen, Switzerland
Sorvall RC-5B Refrigerated Superspeed Centrifuge	Du Pont Instruments, Newtown, CT, USA
StepOnePlus™ Real Time PCR Systems	Applied Biosystems, Foster City, CA, USA
Thermocycler Mastercycler (personal/gradient)	Eppendorf AG, Hamburg, Germany
TissueLyser II	Qiagen, Hilden, Germany
Uniprep Gyrator	UniEquip, München, Germany

2.11 Software and Online-Tools

Table 2.13: Software

Software	Supplier
NanoDrop 2000/2000c	Thermo Scientific, Peqlab, Wilmington, MA, USA
PhenoMaster	TSE Systems, Bad Homburg, Germany
LabChart Pro v7.3.8	ADInstruments, Oxford, UK
StepOne Software 2.1/2.3	Thermo Scientific, Peqlab, Wilmington, MA, USA
Image Lab 4.0.1	BioRad Laboratories, München, Germany
GraphPad Prism 9.3.1	GraphPad Software, San Diego, CA, USA

3 Methods

3.1 Animals

3.1.1 Animal housing and colony maintenance

Mice were housed in groups of 2-6 animals in Makrolon cages (Type III, EBECO, Castrop-Rauxel, Germany) according to general guidelines of animal protection. Environmental temperature was kept constantly at 22 °C, while simulating a 12-hour day-night-cycle (lights on at 6 a.m.). After weaning in week 3, experimental animals were either fed a standard chow diet (SD) containing 22.1% (wt/wt) protein (30 cal%), 4.5% fat (11 cal%), and 53.3% carbohydrates (53 cal%) containing 3.3 kcal/g energy (Ssniff, Soest, Germany, Table 2.2: Mouse diets) or a high-fat diet (HFD) containing 60 % calories from fat (Research Diets Inc., Table 2.2: Mouse diets). Mice had *ad libitum* access to food and water.
All experiments were approved by the Ethics Committee of the State Office for Nature, Environment and Consumer Protection (States of Brandenburg and North Rhine-Westphalia, Germany) under the file names 84-02.04.2012.A057, 84-02.04.2012.A296, 84-02.04.2013.A010, 84-02.04.2013.A352 and 84-02.04.2015.A442.

3.1.2 Breeding of *Tbc1d1*-/*Tbc1d4*-deficient mice

Recombinant congenic RCS.B6.SJL-*Nob1.10*$^{SJL/SJL}$ mice, which carry a naturally occurring mutation in the *Tbc1d1* gene, were previously crossbred with heterozygous *Tbc1d4* (*As160*) knockout mice (kindly provided by Prof. Johannes Loffing, University of Zürich, Switzerland). An intercross of the resulting F1 offspring was carried out (Diploma thesis Anja Immisch, 2012) to obtain wildtype control animals (WT, RCS.B6.SJL-*Nob1.10*$^{B6/B6}$-*As160*$^{+/+}$), *Tbc1d1*-deficient mice (D1KO, RCS.B6.SJL-*Nob1.10*$^{SJL/SJL}$-*As160*$^{+/+}$), *Tbc1d4* knockout mice (D4KO, RCS.B6.SJL-*Nob1.10*$^{B6/B6}$-*As160*$^{-/-}$) and animals lacking both RabGAPs (D1/4KO, RCS.B6.SJL-*Nob1.10*$^{SJL/SJL}$-*As160*$^{-/-}$).

3.1.3 Breeding of kinase-dead AMPKα_2, *Tbc1d1*-/*Tbc1d4*-deficient mice

Transgenic mice overexpressing a kinase-dead α_2-subunit of the AMPK enzyme (AMPK-DN), as previously described [57], were received as a kind gift from Morris J. Birnbaum from University of Pennsylvania, Philadelphia, USA and crossbred with RabGAP-deficient animals

(3.1.2) to obtain the five experimental genotypes: Wildtype (WT, AMPK$\alpha_2^{+/+}$-RCS.B6.SJL-*Nob1.10*$^{B6/B6}$-*As160*$^{+/+}$), *Ampk*-transgenic mice (TG, AMPK$\alpha_2^{Tg/+}$-RCS.B6.SJL-*Nob1.10*$^{B6/B6}$-*As160*$^{+/+}$), *Ampk*-transgenic, *Tbc1d1*-deficient mice (TG-D1KO, AMPK$\alpha_2^{Tg/+}$-RCS.B6.SJL-*Nob1.10*$^{SJL/SJL}$-*As160*$^{+/+}$), *Ampk*-transgenic, *Tbc1d4* knockout mice (TG-D4KO, AMPK$\alpha_2^{Tg/+}$-RCS.B6.SJL-*Nob1.10*$^{B6/B6}$-*As160*$^{-/-}$) and *Ampk*-transgenic, *Tbc1d1*- and *Tbc1d4*- double-deficient mice (TG-D1/4KO, AMPK$\alpha_2^{Tg/+}$-RCS.B6.SJL-*Nob1.10*$^{SJL/SJL}$-*As160*$^{-/-}$).

3.1.4 Genotyping

Genomic DNA was isolated from mouse tail-tips using the Invisorb® Genomic DNA Kit II (Table 2.9: Reaction kits, Enzymes, Standards) following the manufacturer's instructions. Genotyping was carried out by PCR with primer oligonucleotides for mouse genotyping (Table 2.6: PCR primers for mouse genotyping) and subsequent agarose gel analysis of the amplified PCR fragments with ethidium bromide staining.

3.1.5 Nuclear magnetic resonance (NMR-) spectroscopy

The body composition of mice was measured using nuclear magnetic resonance (NMR-) spectroscopy. This method is based on the principle that nuclei of atoms exposed to a magnetic field absorb electromagnetic radiation and re-emit it at a specific resonance frequency that depends on the strength of the magnetic field and the magnetic properties of the isotopes. In a first step the nuclear spins of a sample are aligned by the application of a constant magnetic field. In a second step the electromagnetic radiation is applied in form of a radio frequency pulse. This leads to the perturbation of the alignment of the nuclear spins. The frequency required for perturbation depends on the static magnetic field and the nuclei of observation. Based on this frequency, the proportion of the respective tissues can be calculated.

For this thesis, a special mouse NMR instrument was used (Table 2.12: Devices). This enables the user to measure fat mass, lean mass, and free fluids. *Tbc1d1*- (D1KO), *Tbc1d4*- (D4KO) and double-deficient (D1/4KO) mice were raised on a HFD (Table 2.2: Mouse diets) after weaning and their body weight and body composition was measured every three weeks until week 21 of life. Body weight was determined using a scale and fat mass and lean mass were measured using NMR. For further analysis the mean of two repeated measurements was taken.

3.1.6 Intraperitoneal glucose tolerance test (i.p.GTT)

For intraperitoneal glucose tolerance test, 12-week-old male *Tbc1d1*- (D1KO), *Tbc1d4*- (D4KO) or double-deficient (D1/4KO) as well as wildtype mice (WT), were kept on a high-fat diet (HFD) and fasted for 16 h overnight prior to the experiment.

For further experiments 19-28-week-old muscle specific kinase-dead AMPKα_2 mice (TG) and mice additionally deficient for either *Tbc1d1* (TG-D1KO), *Tbc1d4* (TG-D4KO) or both RabGAPs (TG-D1/4KO) and their wildtype littermates (WT) were kept on standard chow diet (SD) and fasted 6h from 8 am to 2 pm.

After fasting, all mice were injected a sterile glucose solution (2 g/kg body weight, 20% solution) intraperitoneally and blood glucose levels were measured before and 15, 30, 60, 120 (and 240) minutes after the injection with a glucometer (Table 2.12: Devices). Blood for the measurement and for later determination of plasma insulin levels was collected from the tail tip. After 120 minutes (240 minutes respectively) blood glucose levels had returned to basal state.

3.1.7 Intraperitoneal insulin tolerance test (i.p.ITT)

For insulin tolerance test (i.p.ITT) nonfasted 16-week-old male D1KO, D4KO and D1/4KO mice on a high fat diet (HFD) were injected intraperitoneally with insulin (1 IU/kg body weight) and blood glucose levels were measured before and 15, 30 and 60 minutes after the injection with a glucometer (Table 2.12: Devices).

3.1.8 Intraperitoneal AICAR tolerance test (i.p.ATT)

For 5-aminoimidazole-4-carboxamide ribonucleotide (AICAR) tolerance test (i.p.ATT) non-fasted 14-week-old male D1KO, D4KO and D1/4KO mice on a high-fat diet (HFD) or 20-29-week-old TG, TG-D1KO, TG-D4KO and TG-D1/4KO mice on a SD were injected intraperitoneally with AICAR (0.25 g/kg body weight; Table 2.10: Chemicals) which is an activator of the AMP-activated protein kinase (AMPK) and blood glucose levels were measured before and 15, 30, 60 min (and 120 min for kinase-dead AMPKα_2 mice) after the injection with a glucometer (Table 2.12: Devices).

3.1.9 Fasting / Refeeding

For fasting-refeeding experiments, 21-30-week-old male TG, TG-D1KO, TG-D4KO and TG-D1/4KO mice on a SD were fasted for 16 h overnight (starting at 4 p.m.), followed by 1 hour of *ad libitum* refeeding with the respective diet. Blood glucose was measured from the tail-tip after fasting and again after refeeding using a glucometer (Table 2.12: Devices). For further analysis of insulin, triglycerides and free fatty acids in plasma, blood samples were collected.

3.1.10 *In vivo* acute running performance

One day before performing the exercise test, mice were familiarized with a calorimetric treadmill system (TSE Systems, Bad Homburg, Germany) at low speed (15 cm * s^{-1}, 5° incline) for 5 min. Acute exercise testing consisted of a run to exhaustion starting at 15 cm * s^{-1} (5° incline) for the first 2 min, then continuously increasing speed by 5 cm * s^{-1} every 2 min. By gently pushing them with a paper towel, mice were motivated to run. Time to exhaustion was defined as the time when mice were no longer able to maintain their normal running position and had frequent contact with the grid at the rear of the treadmill. Maximum O_2 consumption (VO_{2max}; ml * min^{-1} * $kg^{-0.75}$) and respiratory exchange ratio (RER; VCO_2 * VO_2^{-1}) were determined with the help of the PhenoMaster software (Table 2.13: Software).

3.1.11 *In vivo* electrotransfection (IVE)

Male C57BL6/J and D1KO mice were used for the expression of *Rab8a*- and *Rab14*-mutant constructs with mammalian expression vectors (Table 2.5: Plasmids) in *Tibialis anterior* (TA) muscle. C57BL/6J mice were used for the knockdown of *Rab12* with siRNA technology in *EDL* and *Soleus* muscle. All mice were narcotized using isoflurane inhalation anesthesia. This was carried out by means of an isoflurane pump at 5% by volume of isoflurane and an O_2 flow of 500 ml/min in an anesthesia chamber. Once the animals went limp, they were taken out of the chamber and their hind limbs were shaved using an electric hair clipper. To increase accessibility of the muscle cells to the transfected nucleic acids, 15 Units Hyaluronidase diluted in 30 µl sterile saline were injected into respective muscles. During subsequent incubation, mice were allowed to wake again. After 1 hour, animals were anesthetized for a second time to inject siRNA oligonucleotides (4 µg/30 µl saline) or plasmid-DNA (30 µg/30 µl saline) into *EDL* and *Soleus* or *TA* muscle, respectively. After injection, muscles were electroporated by

eight electric pulses of 20 ms each and a frequency of 1 Hz delivered by a Tweezertrode electrode (Table 2.12: Devices) connected to an ECM 830 Electroporator (Table 2.12: Devices). After one week, mice were sacrificed, and respective muscles were taken for further analysis.

3.2 Biochemical methods

3.2.1 Preparation of cleared protein extracts from tissues

For protein lysates, skeletal muscle and liver tissue were taken from sacrificed mice, snap-frozen in liquid nitrogen and stored at -80 °C until further processing. To prepare the lysates 30 mg of frozen tissue was powdered using a mortar cooled down with liquid nitrogen. All subsequent steps were conducted on ice. The powder was mixed with 600 µl protein lysis buffer (Table 2.11: Buffers, solutions, and culture media) containing protease and phosphatase inhibitor cocktail (Table 2.9: Reaction kits, Enzymes, Standards). Subsequently, it was homogenized for 4 min at 25 Hz using steel beads and a TissueLyser II (Table 2.12: Devices) and homogenates were centrifuged for 10 min at 20,000 x g at 4 °C. The supernatant was transferred to a fresh Eppendorf tube and its protein concentration determined via BCA assay kit (Table 2.9: Reaction kits, Enzymes, Standards).

3.2.2 Determination of protein concentration

Protein concentration of skeletal muscle and liver lysates was determined with the bicinchoninic acid (BCA) method using the Pierce™ BCA Protein Assay Kit (Table 2.9: Reaction kits, Enzymes, Standards). This method is based on the biuret reaction in which peptides containing three or more amino acid residues form a colored chelate complex with copper ions in an alkaline environment and therefore reduce Cu^{2+} to Cu^{+}. In a second step, two molecules of bicinchoninic acid together with one copper ion form an intense purple-colored chelate complex which exhibits a strong linear absorbance at 562 nm with increasing protein concentrations.

Protein lysates were diluted 1:20 with MQ water and applied in duplicates to a 96-well plate. The assay was conducted according to the manufacturer's instructions. To calculate protein concentrations, a BSA standard was used at defined concentrations. For long-term storage, lysates were kept at -80 °C.

3.2.3 SDS-PAGE

Sodium dodecyl sulfate polyacrylamide gel electrophoresis (SDS-PAGE) was conducted based on the method developed by Ulrich K. Laemmli [93]. Muscle lysates were prepared in 4 x Laemmli sample buffer (Table 2.11: Buffers, solutions, and culture media) and heated at 95 °C for 5 min (for detection of GLUT4 protein, lysates were incubated using the same buffer conditions for 30 min at RT). A final concentration of 20 or 40 µg of total protein was loaded on self-cast SDS-gels containing varying concentrations of polyacrylamide (Table 2.10: Chemicals). For determination of protein size, a protein standard was used (Table 2.9: Reaction kits, Enzymes, Standards).

3.2.4 Western Blot analysis

After SDS-PAGE, proteins were transferred to nitrocellulose or polyvinylidene difluoride (PVDF) membranes at 200 mA for protein specific durations using wet tank blotting. Subsequently, membranes were incubated for 1 hour in blocking solution (Table 2.11: Buffers, solutions, and culture media) and probed with primary and secondary antibodies diluted in blocking buffer containing either 5 % skimmed milk powder or 5 % bovine serum albumin (BSA) (Table 2.11: Buffers, solutions, and culture media). Incubation with primary antibodies was carried out either for 1 hour at room temperature (RT) or overnight at 4 °C. Secondary antibodies were incubated for 1 hour at RT. In between antibody incubations, membranes were washed 3 times for 5 min with washing buffer (Table 2.11: Buffers, solutions, and culture media). Detection of proteins was carried out with chemiluminescence (Table 2.9: Reaction kits, Enzymes, Standards) using a digital imaging system (Table 2.12: Devices).

Table 3.1: Blotting conditions for different target proteins

Target protein	Dilution buffer	Transfer conditions
GAPDH	1:2,500 in 5 % skimmed milk	1-2 h or overnight
TBC1D1	1:1,000 in 5 % skimmed milk	overnight
AS160 (TBC1D4)	1:1,000 in 5 % skimmed milk	overnight
GLUT4	1:1,000 in 5 % skimmed milk	overnight
GLUT1	1:1,000 in 5 % skimmed milk	overnight
AMPKα	1:1,000 in 5 % BSA	2 h

Target protein	Dilution buffer	Transfer conditions
phospho-AMPKα (Thr^{172})	1:1,000 in 5 % BSA	2 h
Glycogen Synthase	1:1,000 in 5 % BSA	overnight
ARK5	1:1,000 in 5 % skimmed milk	2 h
SNARK/NUAK2	1:1,000 in 5 % skimmed milk	overnight
RAB12 (H-11)	1:500 in 5 % skimmed milk	1 h
RAB14	1:1,000 in 5 % skimmed milk	1 h
RAB8	1:2,000 in 5 % skimmed milk	1 h
FLAG	1:1,000 in 5 % skimmed milk	1 h
GFP	1:1,000 in 5 % skimmed milk	1 h

3.2.5 Determination of triglyceride and glycogen content in tissue or plasma samples

Homogenized tissue (40 mg; liver and gastrocnemius muscle) and plasma samples were analyzed using the Triglycerides (TRIGS) assay kit (Table 2.9: Reaction kits, Enzymes, Standards) according to the manufacturer's guidelines.

Glycogen content was determined using the amyloglucosidase method [94]. Therefore, tissue homogenates were incubated with 30% potassium hydroxide (wt/vol) at 100 °C for 30 min. Glycogen was precipitated with acetic acid and ethanol. Then, samples were incubated for 3 h at 37 °C with an assay buffer containing sodium acetate and amyloglucosidase for breaking down glycogen to glucose molecules. The latter was measured enzymatically with a glucose oxidase-based colorimetric Glucose liquicolor kit (Table 2.9: Reaction kits, Enzymes, Standards) according to the manufacturer's instructions.

3.2.6 Determination of Insulin and NEFAs in mouse plasma

Plasma insulin content was determined with ELISA (Table 2.9: Reaction kits, Enzymes, Standards) according to the manual. Non-esterified fatty acids (NEFA) in plasma were measured by an enzymatic colorimetric assay (Table 2.9: Reaction kits, Enzymes, Standards) according to the manufacturer`s instructions.

3.2.7 Measurement of *ex vivo* glucose uptake via ^{3}H-DOG-transport in contracted skeletal muscle

Glucose uptake was assessed by the accumulation of [^{3}H]2-deoxyglucose (Hartmann Analytic; Braunschweig, Germany) in intact *EDL* and *Soleus* muscle with the use of [^{14}C]mannitol (PerkinElmer, Waltham, MA) as an extracellular marker. Mice were anesthetized by intraperitoneal injection of 500 mg/kg Avertin [2,2,2-tribromoethanol] and intact *Extensor digitorum longus* (*EDL*) and *Soleus* muscles were isolated from tendon to tendon putting silk loops on each tendon. Animals were then sacrificed by cervical dislocation under anesthesia. Isolated muscles were mounted in a Muscle Strip Myograph chamber (DMT, Table 2.12: Devices) and incubated for 15 min in pre-oxygenated (95% oxygen/5% carbon dioxide) Krebs-Henseleit buffer (KHB; Table 2.11: Buffers, solutions, and culture media) supplemented with 8 mmol/L pyruvate and 15 mmol/L mannitol. All incubation steps were conducted under continuous gassing (95% oxygen/5% carbon dioxide) at 30°C. After recovery, a basal mechanical tension was applied (2-3 mN to *EDL*, 4-5 mN to *Soleus* muscle) and muscles were again incubated for 30 min. Then, muscles were electrically stimulated to contract with 300 ms trains of 0.1 ms pulses at 160 Hz every second in the presence of 1 mmol/l [^{3}H]2-deoxy-glucose and 19 mmol/l [^{14}C]mannitol. After 10 min of stimulation and additional 10 min of radioactive incubation muscles were immediately frozen in liquid nitrogen and stored at -20°C. Cleared protein lysates were used to determine incorporated radioactivity by scintillation counting. [^{14}C]mannitol counts were used to correct for the extracellular space.

Contraction force was measured via the force transducer of the myograph and a PowerLab 8/35 data acquisition system (ADInstruments, Table 2.12: Devices) Analysis of maximum contraction force (Forcemax) and Time for Half-Capacity was carried out with the software LabChart (ADInstruments, Table 2.13: Software).

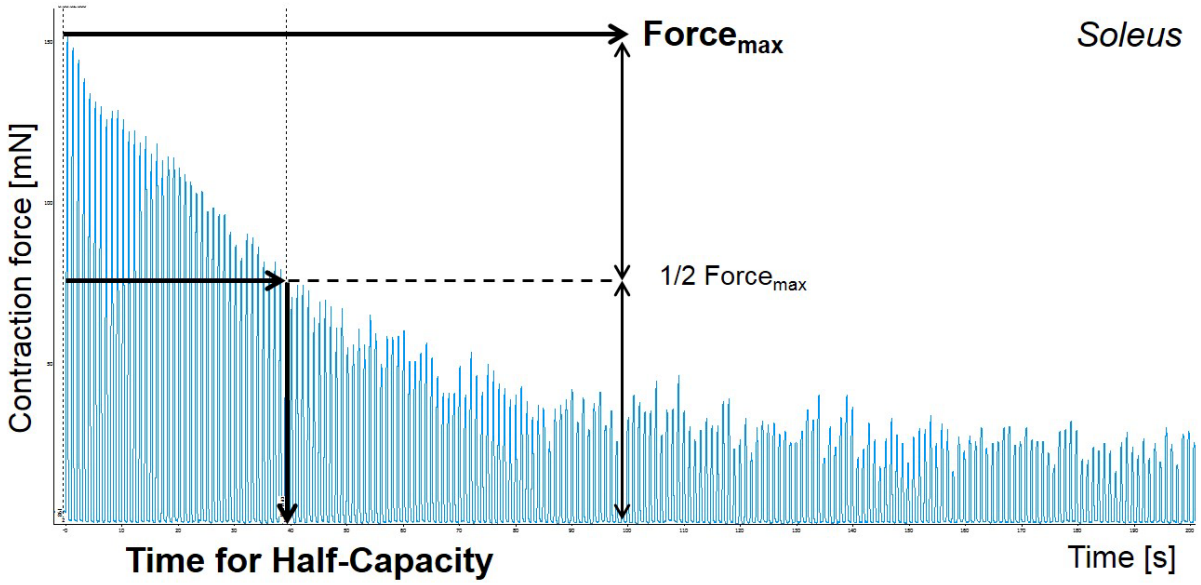

Figure 3.1: Analysis of skeletal muscle contraction performance.
Maximum contraction force (Force$_{max}$) and the time until force has decreased to half-maximal level (Time for Half-Capacity) were analyzed for *EDL* and *Soleus* muscle in LabChart (ADInstruments, Table 2.13: Software).

3.3 Molecular biological methods

3.3.1 Transformation of *E.coli*

Transformation is a method to introduce exogenous genetic material into bacterial cells. It is used in this case for the amplification of mammalian expression vectors in *Escherichia coli* (*E. coli*) bacteria. Therefore, cells from the DH5α-strain, that had previously been made electrocompetent, were treated with an electric pulse (1700 V) for several milliseconds to introduce the plasmid.

Plasmid solutions were pre-diluted to obtain a concentration between 100 and 300 ng/µl. Then 1 µl was added to 30 µl freshly thawed bacteria on ice. The solution was transferred to a pre-cooled cuvette and treated with the electroporator (Table 2.12: Devices). Immediately after electroporation, 1 ml of SOC (Super Optimal broth with Catabolite repression; Table 2.11: Buffers, solutions, and culture media) medium was added and the solution was transferred to a new reaction tube. After 1 hour of incubation at 37 °C under constant shaking, 10 µl of the suspension were plated on a LB culture plate containing either 100 µg/ml ampicillin or 30 µg/ml kanamycin as antibiotic, depending on the resistance provided by the transformed plasmid. The antibiotic ensures that only transformed cells build colonies on the culture plates after incubation at 37 °C overnight.

3.3.2 Cultivation of *Escherichia coli* bacteria

Cultivation after transformation was done from one single picked colony over day in 3-5 ml liquid lysogeny broth (LB, Table 2.11: Buffers, solutions, and culture media) medium supplemented with the respective antibiotic at 37 °C under constant shaking (220 rpm, benchtop shaker, Table 2.12: Devices). Pre-cultures were used to inoculate overnight cultures of 0.5-1 liter medium that were again cultured overnight in a shaker (Table 2.12: Devices) at 37 °C.

3.3.3 Isolation of endotoxin-free plasmid DNA from *E.coli*

The isolation of up to 5 mg of plasmid-DNA from 0.5-1 liter overnight bacterial culture was conducted with the help of PureLinkTM Expi Endotoxin-Free Mega Plasmid Purification Kit (Table 2.9: Reaction kits, Enzymes, Standards) according to the manufacturer's instructions. Therefore, 0.5-1 l of overnight culture of bacteria containing the plasmid construct of interest, were prepared and cells harvested by centrifugation at 4,000 x g for 15 min and 4 °C. The supernatant LB medium was discarded, and the pellet resuspended in 50 ml of Resuspension buffer containing RNase A by vortexing and pipetting until suspension was homogenous. To lyse bacteria, 50 ml of Lysis buffer were added, suspension was mixed by inverting it several times and the mixture was incubated for 5 min at RT. Afterwards, proteins, cellular debris, genomic DNA, and detergent forms were precipitated using 50 ml of Precipitation buffer containing 3.1 M potassium acetate to neutralize the alkaline solution. The lysate was clarified from solid precipitates by passing it over a vacuum-assisted filtration cartridge, which was subsequently washed with 50 ml of Wash buffer. To remove bacterial endotoxins being harmful to the tissue in *in vivo* applications, 12.5 ml of Endotoxin Removal buffer were mixed with the clarified lysate by inverting the bottle 10 times. A DNA-binding cartridge was equilibrated with 100 ml of Equilibration buffer and loaded with the cleared lysate. With the help of an applied vacuum, the lysate was passed through the cartridge. During this step, the negatively charged phosphates of the DNA backbone interacted with the positive charges on the resin surface, which led to the binding of the DNA to the matrix of the cartridge. After washing the cartridge twice with 175 ml of washing buffer, it was attached to a clean bottle and DNA was eluted with 50 ml of endotoxin-free Elution buffer interrupted by 1 min of incubation after half of the volume allowing DNA to detach from the cartridge. The precipitation of DNA was done by adding 0.7 volume isopropanol per volume eluate. After centrifugation at 13,000 x g for 30 min at 4 °C, supernatant was discarded and DNA pellet was washed with 5 ml 70% Ethanol absolute followed by another centrifugation step at 13,000 x g for 10 min at 4 °C. Supernatant was discarded and the pellet was air-dried for 10 min, before it was resuspended in 500 µl of

nuclease-free water. DNA concentration was determined in the Nanodrop at 260 nm and solution was stored at 4 °C.

3.3.4 Isolation of genomic DNA from murine tail tips

To determine the genotypes of experimental animals, approximately 0.3 cm of their tail tip was collected after weaning in a 1.5 ml reaction tube and genomic DNA was isolated using the Invisorb® Genomic DNA Kit II (Table 2.9: Reaction kits, Enzymes, Standards). Therefore, mouse tail tips were lysed in 200 µl Lysis Buffer G containing 10 µl Proteinase K at least for 2-3 h (or overnight) at 1,200 rpm and 60 °C in a thermomixer. Samples were then centrifuged at 16,000 x g for 1 min and supernatant was transferred to a new 1.5 ml reaction tube. Afterwards, 450 µl of Binding Buffer G, containing DNA binding silica particles, were added and the solution was briefly vortexed and incubated for 5 min at RT. In a centrifugation step for 30 sec at 16,000 x g silica particles bound to the DNA were spinned down and the fluid supernatant was discarded. The pellet was washed three times by resuspending it in 650 µl Wash Buffer with the help of a Uniprep Gyrator (Table 2.12: Devices) and spinning it down at 16,000 x g for 30 sec. After the last washing, supernatant was removed, and the pellet was dried at 60 °C for 10 min in a thermomixer to completely evaporate the residual ethanol from the Wash Buffer. For elution of the DNA from the silica particles, 200 µl pre-warmed Elution Buffer were added and samples were vortexed and incubated at 60 °C for 3 min. Subsequently, silica particles were spinned down at 16,000 x g for 2 min and the DNA-containing supernatant (150 µl) was transferred to a new reaction tube and stored at 4 °C.

3.3.5 Determination of DNA and RNA concentration

Concentration measurements of DNA and RNA were carried out with the help of a Nanodrop 2000 Spectrophotometer (Table 2.12: Devices). Therefore, the optical density (OD) of the nucleic acid containing samples was measured at wavelength of 260 nm. The concentration of nucleic acids can be calculated from the absorbance using the following formula:

$$c = (A * \varepsilon)/b$$

c = nucleic acid concentration in ng/µl
A = absorbance in AU
ε = wavelength-dependent extinction coefficient in ng-cm/µl
b = path length in cm

To assess the purity of samples, the ratio of the absorbance at 260 nm and 280 nm was used. For DNA, a ratio of ~1.8 and for RNA a ratio of ~2.0 is considered to be pure. Significantly lower ratios may indicate the presence of phenol, protein, or other contaminants.

3.3.6 Genotyping of experimental mice

Mouse genotypes were determined by polymerase chain reaction (PCR) using isolated genomic DNA at a concentration of 10 ng/µl and primer oligonucleotides for the specific genes (Table 2.6: PCR primers for mouse genotyping). Size of the amplified fragments was analyzed with agarose gel-electrophoresis using ethidium bromide staining according to standard lab procedures.

3.3.7 RNA isolation from mouse tissue

For the isolation of RNA, frozen mouse tissue was mortared in a mortar pre-cooled with liquid nitrogen. 30 mg of the powder were homogenized in 500 µl Trizol (Table 2.9: Reaction kits, Enzymes, Standards) together with a steal bead in a TissueLyser II (Table 2.12: Devices) for 5 min at 25 Hz. After 5 min incubation at RT, solid tissue fragments were spun down by centrifugation at 12,000 x g for 10 min at 4 °C and supernatants were transferred to a new reaction tube. Then, 100 µl Chloroform (Table 2.10: Chemicals) were added and the tube was inverted several times for 15 sec and incubated 2-3 min at RT. Another centrifugation step at 12,000 x g for 15 min at 4 °C was conducted to separate the protein containing organic phase from the upper aqueous phase containing the RNA. The latter was carefully taken using a pipette and transferred to a new 1.5 ml reaction tube. RNA was precipitated by adding 250 µl Isopropanol and samples were incubated for 10 min at RT. After centrifugation at 12,000 x g for 10 min at 4 °C, supernatant was discarded carefully, and the RNA pellet was washed with 500 µl 75 % ethanol abs. and centrifuged at 7,500 x g for 5 min at 4 °C. Again, supernatant was discarded, and the pellet was air-dried for approximately 30 min at RT. Afterwards, RNA was diluted in 15-30 µl nuclease-free water dependent on tissue and size of the pellet and therefore incubated in a thermomixer for 10 min at 60 °C and 300 rpm. RNA concentration was measured with the help of a Nanodrop 2000 (Table 2.12: Devices, 3.3.5) and samples were stored at -80 °C.

3.3.8 cDNA-synthesis

For the synthesis of complementary DNA (cDNA) that was subsequently employed for gene expression analysis, an amount of 2 µg of total RNA (3.3.7) was used for reverse transcription. This was carried out with the help of the GoScript™ Reverse Transcriptase Kit (Table 2.9: Reaction kits, Enzymes, Standards). In a first step, RNA was mixed with random hexanucleotide primers (Table 2.9: Reaction kits, Enzymes, Standards) and a dNTP mix. This solution was then incubated for 5 min at 65 °C to allow the primers to anneal to the RNA templates. Afterwards, another master mixture was prepared, containing $MgCl_2$, the reverse transcriptase and a reaction buffer. This was added to the RNA mix and incubated in a thermocycler (Table 2.12: Devices) according to the protocol in Table 3.2. For expression analysis by real-time quantitative polymerase chain reaction (qPCR, 3.3.9), cDNA was diluted 1:40 in nuclease free water.

Table 3.2: Thermocycler protocol for cDNA synthesis

Stage	Temperature	Duration
Lid heating	37 °C	∞
Annealing	25 °C	5 min
Synthesis	42 °C	60 min
Reverse transcriptase inactivation	70 °C	15 min
Hold	4 °C	∞

3.3.9 Quantitative real-time polymerase chain reaction (qPCR)

Quantitative real-time PCR is a very sensitive method facilitating the detection of even small amounts of DNA by amplification of a target gene from cDNA. The amount of amplified product can be simultaneously monitored during a series of temperature changes repeated in in a specific number of cycles. After each cycle, amplified DNA can be measured by fluorescence intensity of the DNA-intercalating SYBR-Green dye. One cycle consists of three successive steps of denaturation, annealing and elongation. During the denaturation phase, samples are heated to 95 °C resulting in a separation of the two complementary strands of cDNA. In the second step, temperature is lowered to 60 °C allowing specific binding of the primers to the DNA. The third step, called elongation phase, provides the optimal working temperature for the DNA polymerase, an enzyme catalyzing the polymerization of the PCR-product out of single deoxyribonucleotides (dNTPs).

The experiment was performed using self-designed SYBR-Green PCR primer-oligonucleotides (Table 2.8: SYBR-Green Primers). Whenever possible, primer pairs were chosen to be located on two different exons to avoid amplification of genomic DNA. Data were normalized to the housekeeping genes *Gapdh* (gastrocnemius muscle) or *Rps29* (liver), respectively and analyzed according to the ΔCt method [95]. The assembly of the samples for qPCR was done as follows (Table 3.3: Composition of qPCR samples).

Table 3.3: Composition of qPCR samples

Component	Volume
2x GoTaq qPCR Master Mix	5 µl
Forward primer (1 µM)	0.5 µl
Reverse primer (1 µM)	0.5 µl
cDNA (1:40)	4 µl
Total	10 µl

The procedure was carried out according to the temperature protocol in **Table 3.4**.

Table 3.4: qPCR cycling protocol

Stage	Temperature	Duration	Repeats
Lid heating	105 °C	∞	-
Hot start	95 °C	2 min	-
Denaturation	95 °C	15 s	40 x
Annealing/Elongation	60 °C	60 s	

3.4 Statistical analysis

Unless otherwise stated, data are reported as means ± SEM. Significant differences were determined by one-way or two-way ANOVA with Dunnet correction for comparison of genotype specific differences and Sidak correction for treatment specific differences. For comparison of two groups, paired, two-tailed Students *t* test was used, as indicated in the figure legends. *P* values <0.05 were considered statistically significant. All data were analyzed using GraphPad Prism 7.0.3 software (Table 2.13: Software).

4 Results

4.1 Metabolic characterization of *Tbc1d1*- and *Tbc1d4*-deficient mice on a high-fat diet (HFD)

The aim of this study was to clarify the specific metabolic role of each of the two closely related RabGAPs TBC1D1 and TBC1D4. Therefore, different physiological and biochemical parameters were determined in *Tbc1d1*- (D1KO), *Tbc1d4*-deficient (D4KO) and *Tbc1d1/Tbc1d4*-deficient mice (D1/4KO). As a challenge, mice were fed a high fat diet (HFD) with 60% kcal from fat starting after weaning at week 3 of life.

4.1.1 Development of body composition in *Tbc1d1*- and *Tbc1d4*-deficient mice on a high-fat diet (HFD)

To investigate the impact of a RabGAP deficiency on body weight and composition, mice were fed a HFD after weaning and measured every 3 weeks on a scale and analyzed by nuclear magnetic resonance (NMR-)spectroscopy.

In week 3 of life wild-type (WT) mice had a body weight of 11.57 ± 0.62 g (n = 24) which doubled by week 6 to 23.74 ± 0.32 g (n = 23) and then increased slightly by 3-4 g every 3 weeks up to a final body weight of 42.21 ± 1.43 g (n = 21) in week 21 (Figure 4.1A). Compared to WT, body weight of D1KO and D4KO animals was not changed. Double-deficient D1/4KO mice exhibited body weights like that of WT animals until week 15 of life. In week 18, their mean value was significantly increased by 3.59 g compared to WT mice, whereas in week 21 there was still a difference of 3.65 g, which failed to reach significance (P = 0.0598).

The body fat mass of WT mice developed from 1.19 ± 0.07 g (n = 24) in week 3 to 13.29 ± 1.31 g (n = 21) in week 21 (Figure 4.1B). Compared to this, fat mass of D1KO and D4KO mice was unchanged throughout the whole experiment. In contrast, D1/4KO mice had 3.61 g more body fat on average in week 18 and week 21 of life.

Lean mass was in the beginning of the experiment 10.26 ± 0.54 g (n = 24) for WT animals (Figure 4.1C). Afterwards, it increased up to 20.90 ± 0.21 g (n = 23), whereas it rose slightly during the following measurements to a final value of 27.95 ± 0.40 g (n = 21). The initial lean mass of D1KO mice was increased on average by 1.62 g compared to WT animals in week 3. In the following weeks, the difference was not present anymore. D4KO and D1/4KO mice showed no difference in lean mass compared to WT animals.

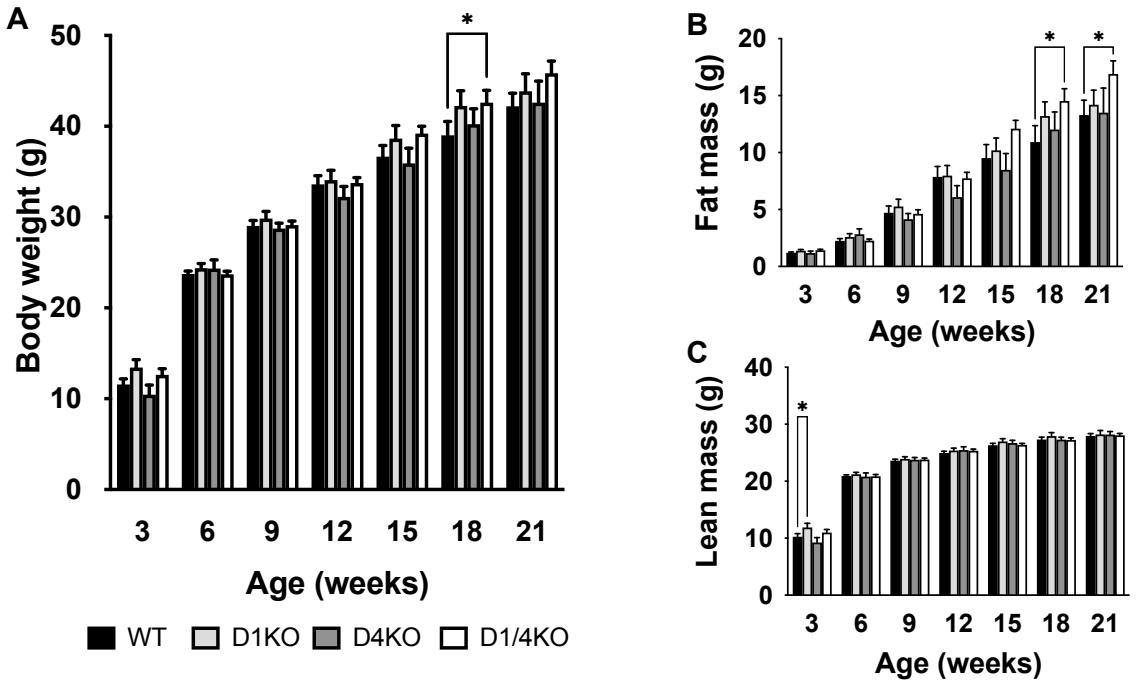

Figure 4.1: Body weight and body composition of male RabGAP-deficient D1KO, D4KO and D1/4KO mice on a HFD.
Body weight in grams (A), fat mass (B) and lean mass (C) of *Tbc1d1*- (D1KO), *Tbc1d4*-deficient (D4KO) and double-deficient *Tbc1d1/Tbc1d4*-deficient (D1/4KO) mice in comparison to wildtype (WT) animals was measured in week 3, 6, 9, 12, 15, 18 and 21 of life. Data are presented as mean ± SEM (n = 10-26). *P < 0.05, WT vs. D1KO, D4KO, D1/4KO (two-way ANOVA with Dunnett correction).

4.1.2 Glucose, insulin and AICAR tolerance in D1KO, D4KO and D1/4KO mice on a HFD

4.1.2.1 Glucose tolerance

An intraperitoneal glucose tolerance test (i.p.GTT) was performed to test whole-body glucose disposal of mice on a HFD *in vivo* (3.1.6). The intraperitoneal application of glucose led to a rapid resorption into the blood bypassing the activation of incretin hormones in the gut that would further stimulate insulin secretion. Besides blood glucose (BG), plasma insulin (PI) concentration was measured in collected blood samples at different time points (basal and 15, 30, 60, 120 and 240 minutes after injection).

Before the experiment, mice were fasted for 16 hours. After the fasting period, D4KO and D1/4KO mice showed reduced blood glucose compared to WT and D1KO mice (Figure 4.2; D4KO and D1/4KO vs. WT: 85.6 ± 2.9 and 87.3 ± 2.9 vs. 111.1 ± 6.4 mg/dl, P<0.01). 16h-fasting BG remained unaltered in D1KO mice (109.3 ± 5.59 mg/dl) compared to the WT controls.

To enable comparison between the different genotypes, the time courses of measured BG and plasma insulin values were normalized to basal levels for each genotype.

During the first 30 min after glucose injection, BG of WT mice rose to 460.3 % of basal level. In the following 210 min it constantly decreased until it was almost back to the basal level (102.7 %, Figure 4.2B). D1KO mice did not show any alterations in BG levels compared to WT controls. However, BG of D4KO was increased 30 min and 60 min after glucose injection compared to WT (D4KO vs. WT, 30 min: 538.9 ± 26.8 vs. 460.3 ± 28.9, $P<0.05$; 60 min: 492.5 ± 35.9 vs. 392.7 ± 28.3 %, $P<0.01$). D1/4KO mice had elevated BG 15 min, 30 min and 60 min after the injection (D1/4KO vs. WT, 15 min: 448.7 ± 30.7 vs. 355.4 ± 28.4, $P<0.01$; 30 min: 600.6 ± 21.4 vs. 460.3 ± 28.9, $P<0.0001$; 60 min: 562.0 ± 24.7 vs. 392.7 ± 28.3 %, $P<0.0001$). This was also reflected by an increased area under the curve (AUC) from D1/4KO mice (Figure 4.2B; D1/4KO vs. WT: 78548.0 ± 2969.7 vs. 61551.8 ± 4220.7 a.u., $P<0.01$).

Plasma insulin in WT mice after 16 hours of fasting was 1.1 µg/l (Figure 4.2C). After glucose injection, it increased slowly up to 234.4 % of basal concentration in 240 min (Figure 4.2D). In D1KO and D4KO mice plasma insulin concentrations were not different in course of the experiment compared to WT mice. D1/4KO mice had significantly increased plasma insulin levels 60 min and 120 min after glucose injection (D1/4KO vs. WT, 60 min: 835.7 ± 175.6 vs. 171.2 ± 38.4, $P<0.05$; 120 min: 944.0 ± 250.7 vs. 214.2 ± 60.3 %, $P<0.01$). This was also reflected by the AUC, which tended to be increased compared to WT mice (Figure 4.2D).

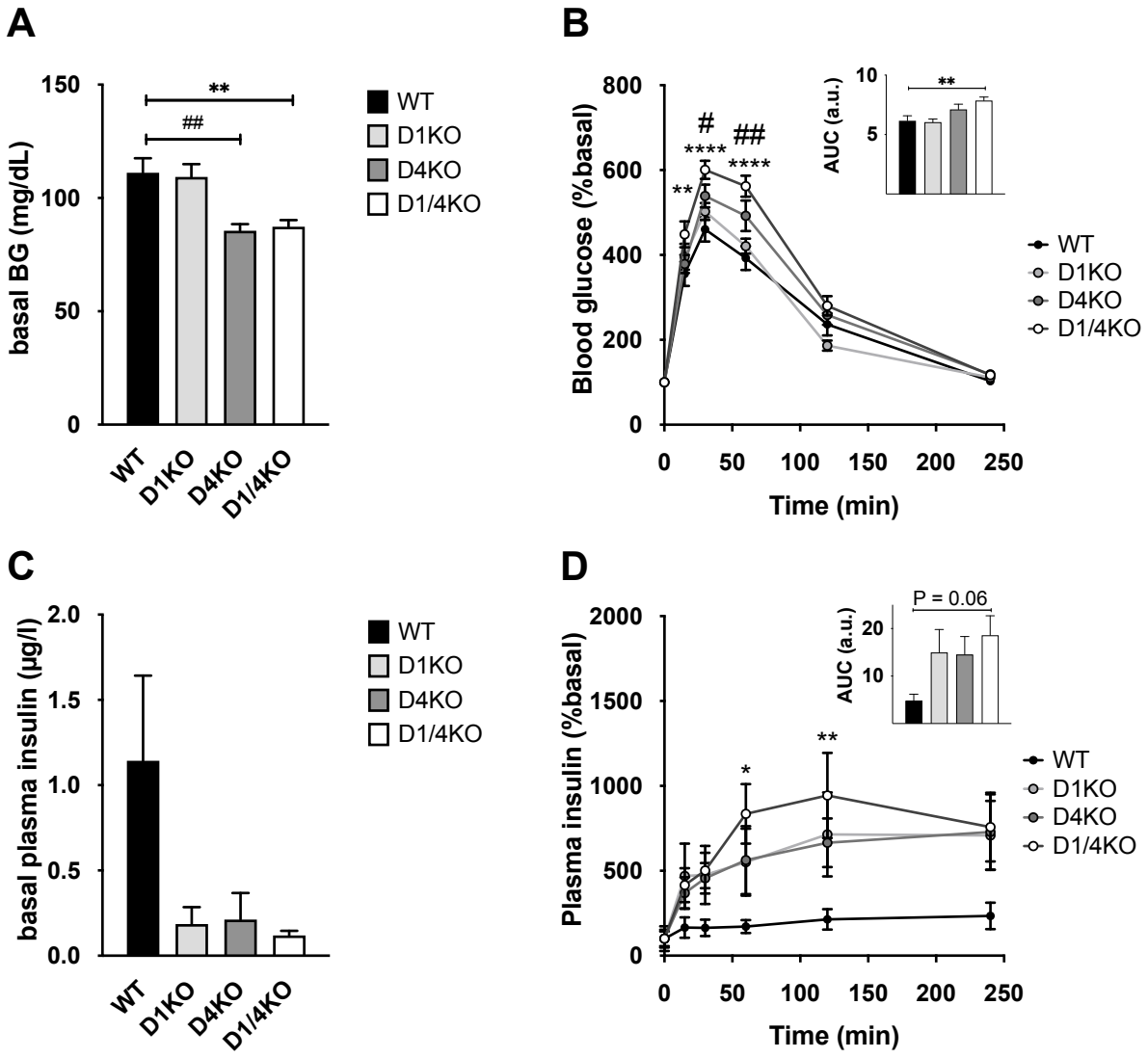

Figure 4.2: Intraperitoneal glucose tolerance test (i.p.GTT) of WT, D1KO, D4KO and D1/4KO mice.
Male *Tbc1d1*- (D1KO), *Tbc1d4*-deficient (D4KO) and double-deficient *Tbc1d1/Tbc1d4*-deficient (D1/4KO) mice aged 12 weeks were subjected to intraperitoneal tolerance test for glucose (i.p.GTT) after 16 hours fasting and compared to wildtype (WT) controls. A: Basal blood glucose levels after 16 hours of fasting (n = 9-13) B: Relative blood glucose concentrations before and 15, 30, 60, 120 and 240 min after intraperitoneal injection of glucose (2 mg/kg BW) and area under the curve (AUC; n = 9-13). C: Basal plasma insulin concentrations after 16 hours of fasting (n = 2-5). D: Relative plasma insulin concentrations during i.p.GTT and AUC (n = 5-6). Data are presented as mean ± SEM. #P < 0.05, ##P < 0.01 WT vs. D4KO; *P < 0.05, **P < 0.01, ****P < 0.0001 WT vs. D1/4KO (A-D: one-way ANOVA with Dunnett correction; B, D: two-way ANOVA with Dunnett correction).

4.1.2.2 Insulin tolerance

Chronic intake of high-caloric food leads to a reduction in insulin sensitivity. Thus, mice were tested for insulin tolerance under HFD conditions to reveal differences based on their genotype.

Therefore, 16 weeks old, random fed mice were exposed to an intraperitoneal injection of 1 IU/kg body weight (BW) insulin and BG levels were measured before and 15, 30 and 60 min after the injection.

The mean basal BG in WT animals was 202.9 mg/dl (Figure 4.3A). Compared to this, BG levels of D1KO and D4KO mice tended to be lower but were not significantly changed (196.6 and 183.2 mg/dl, respectively). In D1/4KO mice basal BG was reduced by 42.3 mg/dl (D1/4KO vs. WT: 160.5 ± 5.5 vs. 202.9 ± 13.2 mg/dl; P<0.01).

To compare the course of BG during the test between the different genotypes, all values were normalized to basal BG and expressed as % of basal. After insulin injection, the BG of WT mice declined over time. After 15 min it reached 63.1 % of the basal value, after 30 min 47.8 % and after 60 min 35.3 %. Compared to that, single knockout mice showed no differences in BG concentrations. In D1/4KO mice the decrease of BG over time was limited compared to WT animals (Figure 4.3B; D1/4KO vs. WT: 15 min: 80.5 ± 2.7 vs. 63.1 ± 6.6, P<0.01; 30 min: 62.3 ± 3.7 vs. 47.8 ± 2.1, P<0.05; 60 min: 52.8 ± 2.6 vs. 35.3 ± 3.2 %, P<0.01). These results were also reflected by the AUC (Figure 4.3B; D1/4KO vs. WT: 4151.7 ± 139.6 vs. 3302.0 ± 174.3; P<0.01).

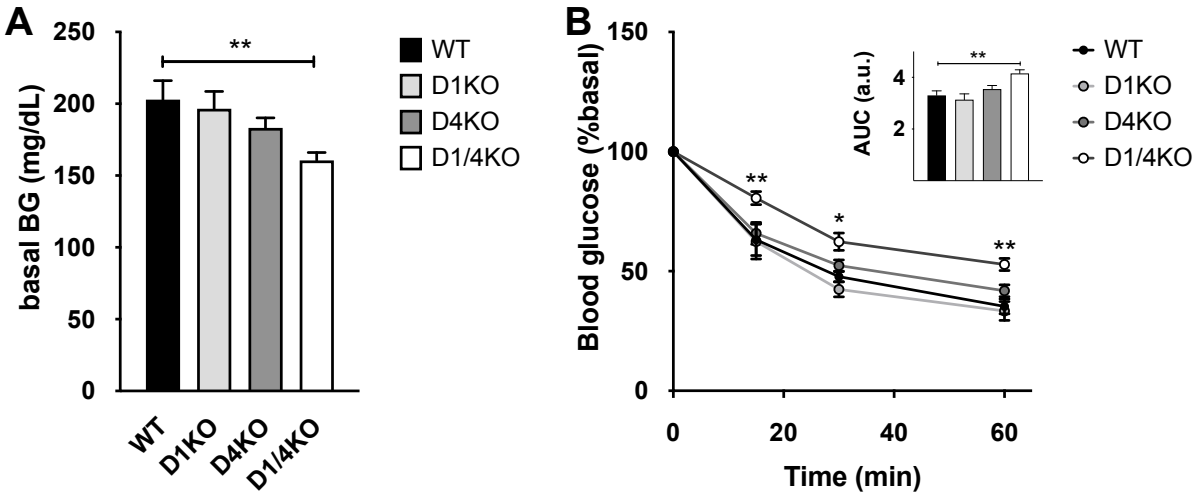

Figure 4.3: Intraperitoneal insulin tolerance test (i.p.ITT) of WT, D1KO, D4KO and D1/4KO mice.
Male *Tbc1d1*- (D1KO), *Tbc1d4*-deficient (D4KO) and double-deficient *Tbc1d1/Tbc1d4*-deficient (D1/4KO) mice aged 16 weeks were subjected to intraperitoneal tolerance test for insulin (i.p.ITT) and compared to wildtype (WT) controls. A: Random fed blood glucose (BG), B: Blood glucose concentrations before and 15, 30, 60 min after intraperitoneal injection of insulin (1 IU/kg) and area under the curve (AUC). Data are presented as mean ± SEM (n = 8-15). *P < 0.05, **P < 0.01, WT vs. D1/4KO (A, B: one-way ANOVA with Dunnett correction; B: two-way ANOVA with Dunnett correction)

4.1.2.3 AICAR tolerance

To test whether one of the RabGAPs has a predominant function in AICAR-regulated glucose disposal over the other, an intraperitoneal AICAR tolerance test was performed with D1KO, D4KO and D1/4KO mice and respective control littermates on a HFD (3.1.8).

Basal blood glucose prior to the injection of 250 mg/kg BW AICAR in random fed WT mice was 201.4 mg/dl (Figure 4.4A). In D1KO mice equal values were measured (190.1 ± 9.0 mg/dl). D4KO and D1/4KO mice both had lower blood glucose concentrations compared to WT animals (Figure 4.4A; D4KO and D1/4KO vs. WT: 165.3 ± 7.6 and 168.0 ± 7.9 vs. 201.4 ± 9.6 mg/dl; P<0.05).

The BG values over time were again expressed as % of basal to facilitate better comparison of the different courses among the genotypes (Figure 4.4B). In WT mice, BG concentrations slightly decreased during the first 15 min after AICAR injection to 91.1 % of basal BG. After 30 min, the concentration reached exactly 50.0 % and after 60 min it was 41.8 %.

Tbc1d1-deficient mice tended to have higher BG values throughout the experiment and a higher AUC (D1KO vs. WT: 4478.3 ± 232.9 vs. 3867.4 ± 148.7 a.u.; P=0.06), which failed to reach significance. In D4KO mice BG concentrations were decreased 30 and 60 min after AICAR injection (D4KO vs. WT, 30 min: 36.0 ± 3.0 vs. 50.0 ± 3.5, P<0.05; 60 min: 24.8 ± 2.2 vs. 41.8 ± 1.7 %, P<0.01). This difference is also evident in the AUC (D4KO vs. WT: 3141.1 ± 174.5 vs. 3867.4 ± 148.7 a.u., P<0.05). D1/4KO displayed a reduced BG concentration 15 min after AICAR injection (D1/4KO vs. WT, 15 min: 77.6 ± 4.0 vs. 91.1 ± 6.0 %; P<0.05). After 30 and 60 min the difference was not significant anymore. The AUC of D1/4KO mice was unaltered.

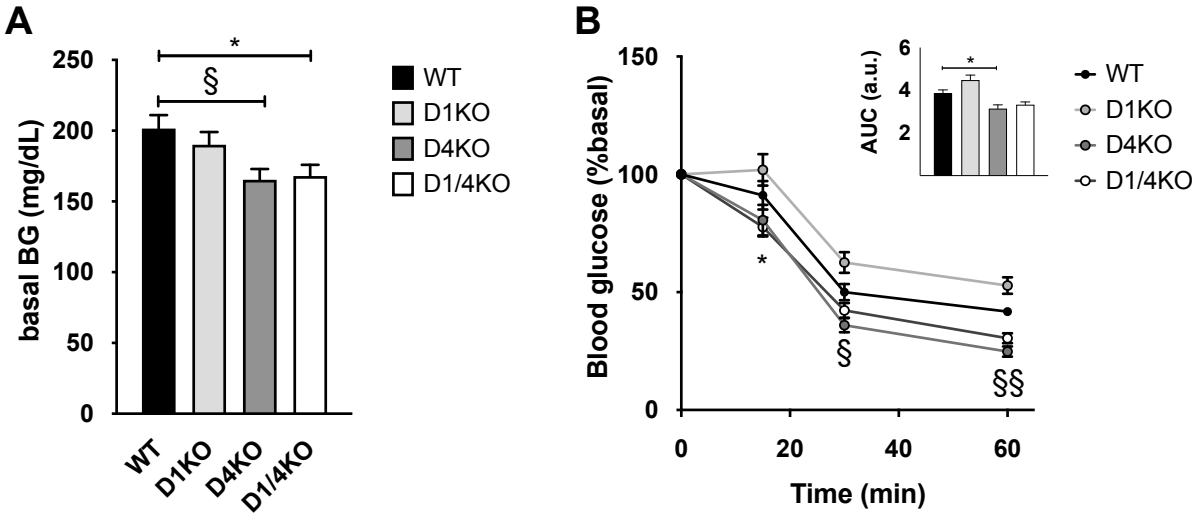

Figure 4.4: Intraperitoneal AICAR tolerance test (i.p.ATT) of WT, D1KO, D4KO and D1/4KO mice.
Male *Tbc1d1*- (D1KO), *Tbc1d4*-deficient (D4KO) and double-deficient *Tbc1d1/Tbc1d4*-deficient (D1/4KO) mice aged 14 weeks were subjected to intraperitoneal tolerance test for AICAR (i.p.ATT) and compared to wildtype (WT) controls. A: Random fed blood glucose (BG), B: Blood glucose concentrations before and 15, 30, 60 min after intraperitoneal injection of AICAR (250 mg/kg BW) and area under the curve (AUC). Data are presented as mean ± SEM (n = 9-11). §P < 0.05, §§P < 0.01 WT vs. D4KO; *P < 0.05 WT vs. D1/4KO (A, B: one-way ANOVA with Dunnett correction; B: two-way ANOVA with Dunnett correction)

4.1.3 Storage of energy supplying substrates in skeletal muscle and liver of RabGAP deficient mice on a HFD

To investigate the impact of HFD feeding on the storage of energy supplying substrates, glycogen and triglyceride content were analyzed from quadriceps muscle and liver of D1KO, D4KO and D1/4KO mice and compared to WT controls.

Control mice had a mean glycogen concentration of 0.55 ± 0.05 µg/mg (n = 12) in skeletal muscle (Figure 4.5A) and 24.75 ± 3.17 µg/mg (n = 18) in liver tissue (Figure 4.5B). In RabGAP-deficient mice, this was unaltered. Triglyceride content was also similar compared to controls in muscle (Figure 4.5C; WT: 7.69 ± 1.07 µg/mg; n = 12) as well as in liver (Figure 4.5D; WT: 7.43 ± 1.23 µg/mg; n = 19).

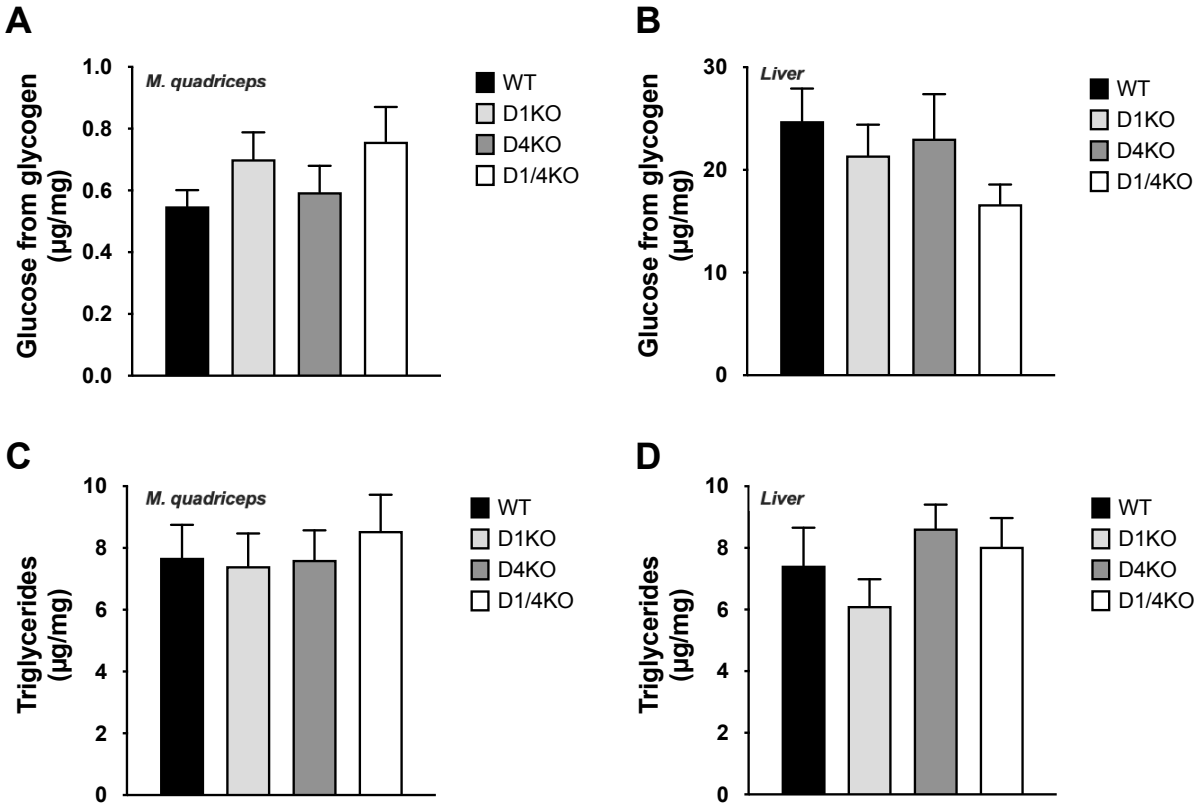

Figure 4.5: Glycogen and triglyceride content in *Musculus quadriceps* and liver of WT, D1KO, D4KO and D1/4KO mice.
Tissues from male *Tbc1d1*- (D1KO), *Tbc1d4*-deficient (D4KO) and double-deficient *Tbc1d1/Tbc1d4*-deficient (D1/4KO) mice were analyzed for glycogen (A, B) and triglyceride content (C, D) and compared to wildtype (WT) controls. A: Glycogen content in *M. quadriceps* (n = 12), B: Hepatic glycogen content (n = 13-18), C: Triglyceride content in *M. quadriceps* (n = 12), D: Triglycerides in liver (n = 13-18). Data are presented as mean ± SEM (one-way ANOVA with Dunnett correction)

The following experiments were conducted with D1KO, D4KO and D1/4KO mice fed a SD.

4.2 Contribution of TBC1D1 and TBC1D4 to contraction-induced glucose uptake

4.2.1 *Ex vivo* contraction-induced glucose uptake in *EDL* and *Soleus* of D1KO, D4KO and D1/4KO mice

During AICAR tolerance test, D1KO mice tend to show a decreased AICAR tolerance (AUC: P=0.06) whereas D4KO animals respond even more sensitive to the injected exercise mimetic than WT controls (Figure 4.4). This observation hints towards different metabolic roles of the two RabGAPs in whole-body glucose homeostasis regarding AMPK- and/or exercise-related glucose disposal. The main organ of the body responsible for AMPK-regulated glucose uptake is the skeletal muscle. To investigate, whether a difference between TBC1D1 and TBC1D4 function is measurable in contracted skeletal muscles, glycolytic *EDL* and oxidative *Soleus* muscles from standard chow diet (SD) fed animals were stimulated to contract by electric pulses in an *ex vivo* setting and subsequent glucose transport into the muscles was measured (3.2.7).

Figure 4.6 shows, that contraction increased glucose uptake of all genotypes in *EDL* and *Soleus* muscle.

In *EDL* from WT mice glucose uptake after contraction was about 2.5 times higher than without contraction (Figure 4.6A). Compared to this, transport rates in D1KO *EDL* muscles were strongly impaired after contraction, although not blunted (D1KO vs. WT, contracted: 2.80 ± 0.12 vs. 4.45 ± 0.27 nmol/mg/20 min; P<0.0001; basal: 1.13 ± 0.11 vs. 1.78 ± 0.19 nmol/mg/20 min; P=0.140). Glucose uptake into *EDL* muscles of D4KO mice was unchanged compared to WT in contracted and basal state (D4KO vs. WT, contracted: 4.64 ± 0.42 vs. 4.45 ± 0.27; P=0.923; basal: 2.00 ± 0.20 vs. 1.78 ± 0.19 nmol/mg/20 min; P=0.879). In D1/4KO mice a reduction of glucose transport was detected in contracted and even in basal state, without contraction (D1/4KO vs. WT, contracted: 2.00 ± 0.15 vs. 4.45 ± 0.27; P<0.0001 basal: 0.94 ± 0.10 vs. 1.78 ± 0.19 nmol/mg/20 min; P<0.05).

In *Soleus* muscle, basal glucose uptake rates are the same in all groups (D1KO, D4KO and D1/4KO vs. WT: 2.40 ± 0.20, 2.51 ± 0.18 and 1.84 ± 0.16 vs. 2.38 ± 0.37 nmol/mg/20 min). Contraction increases transport rates of WT muscles by about 1.74 times. At the same time, muscles lacking one of the RabGAPs, show similar glucose transport rates as the WT (D1KO and D4KO vs. WT: 4.22 ± 0.32 and 4.51 ± 0.27 vs. 4.14 ± 0.34 nmol/mg/20 min). Contraction-induced glucose transport into D1/4KO muscles is reduced by almost one third (Figure 4.6B; D1/4KO vs. WT: 2.86 ± 0.28 vs. 4.14 ± 0.34 nmol/mg/20 min; P<0.05). Still, contraction slightly increases glucose transport into *Soleus* muscle of D1/4KO mice (Figure 4.6B; basal vs. contracted: 1,84 ± 0.16 vs. 2.86 ± 0.28 nmol/mg/20 min; P<0.05).

The results show a muscle-type specific, RabGAP-dependent effect on glucose uptake.

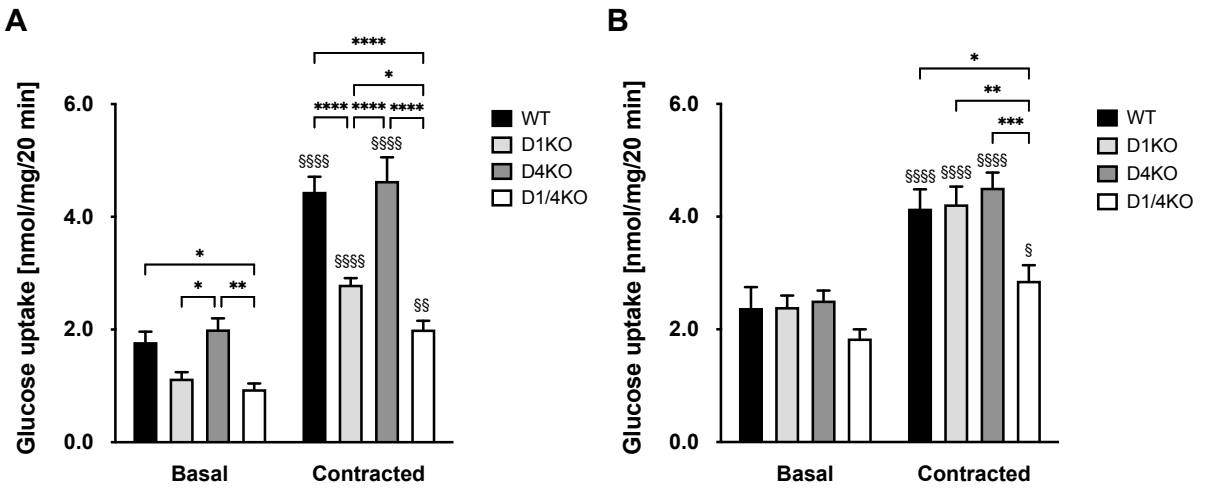

Figure 4.6: Contraction-induced glucose uptake in *EDL*(A) and *Soleus*(B) muscle of RabGAP-deficient mice. Skeletal muscles from 12-16-weeks old male *Tbc1d1*- (D1KO), *Tbc1d4*-deficient (D4KO) and double-deficient *Tbc1d1/Tbc1d4*-deficient (D1/4KO) mice were isolated and assayed for contraction-induced [^{3}H]-deoxyglucose uptake. *EDL* (A; n = 8-9) and *Soleus* muscle (B; n = 8-10). Data are presented as mean ± SEM. *P < 0.05, **P < 0.01, ***P < 0.001, ****P < 0.0001, WT vs. D1KO vs. D4KO vs. D1/4KO (two-way ANOVA with Tuckey correction). §P < 0.05, §§P < 0.01, §§§§P < 0.0001, basal vs. contracted (two-way ANOVA with Sidak correction)

4.2.2 *Ex vivo* contraction force generation of *EDL* and *Soleus* muscle

During *ex vivo* contraction of *EDL* and *Soleus* muscle the maximum force production ($Force_{max}$) and the Time for Half-Capacity were measured as described in 3.2.7 (Figure 4.7).

The strongest contractive force ($Force_{max}$) achieved by *EDL* muscle of WT mice was 75.8 ± 17.5 mN (n = 8). Muscles of D1KO, D4KO and D1/4KO mice did not show significantly different values (Figure 4.7A). $Force_{max}$ of *Soleus* muscle was 39.6 ± 13.1 mN (n = 5). In D1KO mice this was significantly increased (D1KO vs. WT: 128 ± 41.3 vs. 39.6 ± 13.1 mN; P<0.05) Muscles of D4KO and D1/4KO mice showed not difference compared to WT (Figure 4.7B). Time for Half-Capacity in *EDL* muscle of WT mice was 11.8 ± 1.8 s (n= 8) and did not change in muscles of D1KO, D4KO and D1/4KO mice (Figure 4.7C). In *Soleus* muscle Time for Half-Capacity was 21.3 ± 4.5 s (n = 5) in WT mice. D1KO and D4KO mice were not significantly different, although *Soleus* muscles of D4KO mice tended to have increased values (D4KO vs. WT: 31.6 ± 1.2 vs. 21.3 ± 4.5 s; P=0.06). D1/4KO mice had a longer Time for Half-Capacity compared to WT (D1/4KO vs. WT: 32.3 ± 1.3 vs. 21.3 ± 4.5 s; P<0.05) (Figure 4.7D).

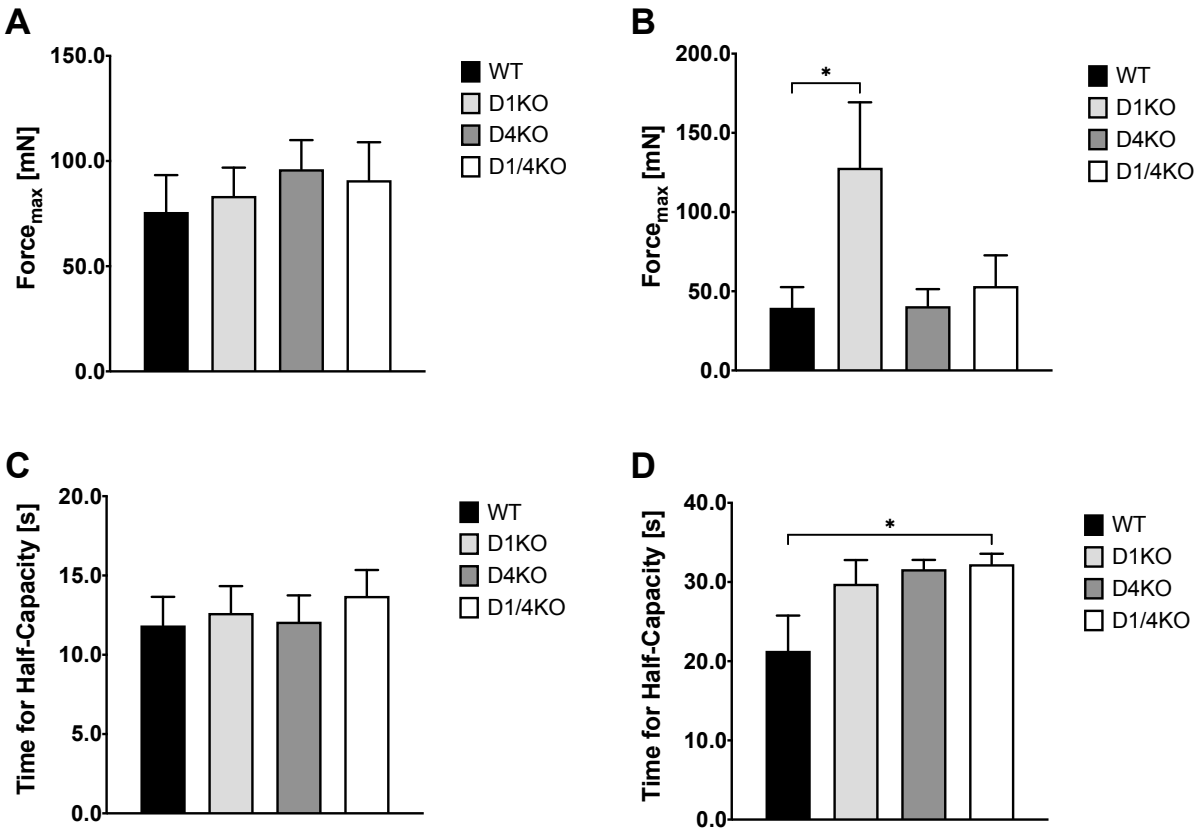

Figure 4.7: Contraction Force$_{max}$ and Time for Half-Capacity of *EDL* (A, C) and *Soleus* (B, D) muscle from RabGAP-deficient mice.
Skeletal muscles from 12-16-weeks old male *Tbc1d1*- (D1KO), *Tbc1d4*-deficient (D4KO) and double-deficient *Tbc1d1/Tbc1d4*-deficient (D1/4KO) mice were isolated and assayed for maximum contraction force (Force$_{max}$) and Time for Half-Capacity of *EDL* (A; n = 8-9) and *Soleus* muscle (B; n = 3-7). Data are presented as mean ± SEM. *P < 0.05, WT vs. D1KO, D4KO or D1/4KO (one-way ANOVA with Dunnett correction).

4.2.3 Combined stimulation of glucose uptake by *ex vivo* contraction and insulin in *EDL* and *Soleus* muscle of D1/4KO mice

The availability of GLUT4 transporter in WT and D1/4KO mice is different. To find out, if the abundance of GLUT4 is the rate limiting factor for contraction-stimulated glucose uptake, *EDL* and *Soleus* muscle of D1/4KO mice and WT controls were stimulated by *ex vivo* contraction, insulin, or both. The intention was to achieve the maximum possible stimulation of GLUT4 translocation with both stimuli. Subsequently glucose uptake was measured.

In *EDL* muscle of WT mice, stimulation either by insulin or contraction caused a doubling of glucose transport rates compared to basal (insulin and contraction vs. basal: 10.8 ± 0.7 and 10.7 ± 0.8 vs. 5.0 ± 0.2 nmol/mg/20 min; P <0.0001). Combined stimulation with insulin + contraction resulted in a further increase in glucose uptake compared to single stimulation (14.4 ± 0.6 nmol/mg/20 min; P < 0.001).

In *EDL* of D1/4KO mice, insulin alone failed to significantly increase glucose uptake (Figure 4.8). Contraction and combined stimulation with insulin + contraction resulted in doubled glucose transport rates compared to basal state (contraction and insulin + contraction vs.

basal: 8.0 ± 0.7 and 8.5 ± 1.2 vs. 3.8 ± 0.4 nmol/mg/20 min; P < 0.001). There was no difference between contraction- and insulin + contraction-induced glucose uptake. Compared to WT, glucose transport in *EDL* muscle of D1/4KO mice was impaired in all stimulated muscles (Figure 4.8).

In *Soleus* muscles of WT mice stimulation with insulin or contraction alone increased glucose transport rates compared to basal state (insulin and contraction vs. basal: 17.98 ± 1.24 and 14.83 ± 0.93 vs. 9.35 ± 0.43 nmol/mg/20 min; P < 0.0001) (Figure 4.8B). Combined stimulation with insulin and contraction further increased glucose transport rates compared to single stimulation with contraction (insulin + contraction vs. contraction: 20.87 ± 1.06 vs. 14.83 ± 0.93 nmol/mg/20 min; P < 0.0001) but not compared to insulin. In *Soleus* muscle of D1/4KO mice insulin and contraction stimulated glucose transport were not different compared to basal state. Insulin + contraction stimulation increased glucose transport rates compared to basal (insulin + contraction vs. basal: 13.40 ± 1.87 vs. 8.87 ± 0.70 nmol/mg/20 min; P < 0.05). However, compared to WT, glucose transport rates in *Soleus* of D4KO mice after combined stimulation with insulin and contraction were significantly reduced (WT vs. D1/KO: 20.87 ± 1.06 vs. 13.40 ± 1.87 nmol/mg/20 min; P < 0.001).

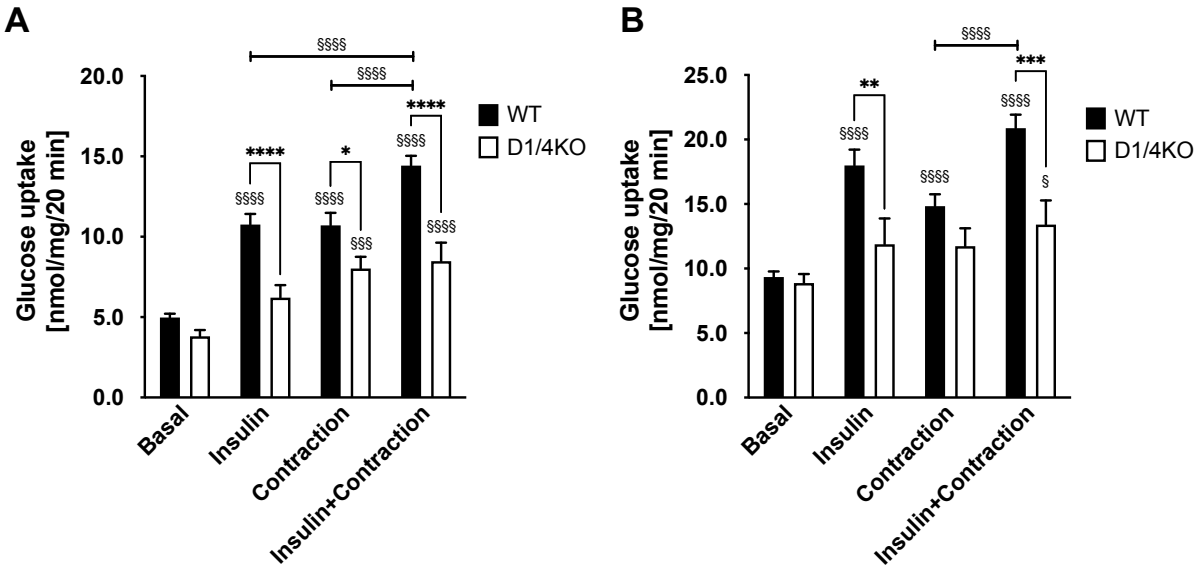

Figure 4.8: Contraction- and insulin-induced glucose uptake in *EDL* (A) and *Soleus* (B) muscle of D1/4KO mice.

Skeletal muscles from male *Tbc1d1/Tbc1d4* double-deficient (D1/4KO) mice were isolated and assayed for contraction-, insulin- and contraction + insulin-indced [^{3}H]-deoxyglucose uptake. *EDL* (A; n = 6-42) and *Soleus* muscle (B; n = 7-42). Data are presented as mean ± SEM. *P < 0.05, **P < 0.01, ***P < 0.001, ****P < 0.0001, WT vs. D1/4KO (two-way ANOVA with Sidak correction). §P < 0.05, §§§P < 0.001, §§§§P < 0.0001, basal vs. insulin vs. contraction + insulin (two-way ANOVA with Tuckey correction).

4.3 The role of TBC1D1 and TBC1D4 in AMPK-dependent glucose metabolism in skeletal muscle

4.3.1 Protein abundance in gastrocnemius muscle of AMPKα$_2$-transgenic *Tbc1d1*- and/or *Tbc1d4*-deficient mice

TBC1D1 and TBC1D4 both are substrates of AMPK which is known to be activated by skeletal muscle contraction. To address the question, if one of them plays a predominant role in exercise-regulated glucose homeostasis, RabGAP-deficient mice (D1KO, D4KO and D1/4KO) were crossbred with muscle-specific kinase-dead AMPKα$_2$ (TG) mice to generate AMPKα$_2$-transgenic *Tbc1d1*-deficient (TG-D1KO), *Tbc1d4*-deficient (TG-D4KO) and double RabGAP-deficient (TG-D1/4KO) mice.

Western blot analysis of TBC1D1, TBC1D4, AMPK, GLUT4 and GLUT1 protein was performed to evaluate the protein abundance of the newly generated mouse model after crossbreeding kinase-dead AMPKα$_2$ (TG) mice with RabGAP-deficient mice (D1KO, D4KO and D1/4KO) (3.2.4).

It could be confirmed that WT, TG and TG-D4KO mice were expressing TBC1D1, but TG-D1KO and TG-D1/4KO mice were not. Furthermore WT, TG and TG-D1KO mice expressed TBC1D4, whereas TG-D4KO and TG-D1/4KO mice were lacking the protein (Figure 4.9A). Overexpression of the *myc*-tagged kinase-dead α$_2$-subunit is in the blot indicated by a slightly higher molecular weight and a 4-5-fold stronger AMPK signal in the transgenic (TG, TG-D1KO, TG-D4KO, TG-D1/4KO) muscles compared to WT (Figure 4.9A, B).

Consistent with previously published results from D1KO and D1/4KO mice [79], GLUT4 expression was reduced in *gastrocnemius* muscle of TG-D1KO and TG-D1/4KO mice by one third compared to WT, TG and TG-D4KO (Figure 4.9A, C). GLUT1 content was unaltered among all the analyzed genotypes (Figure 4.9A, D).

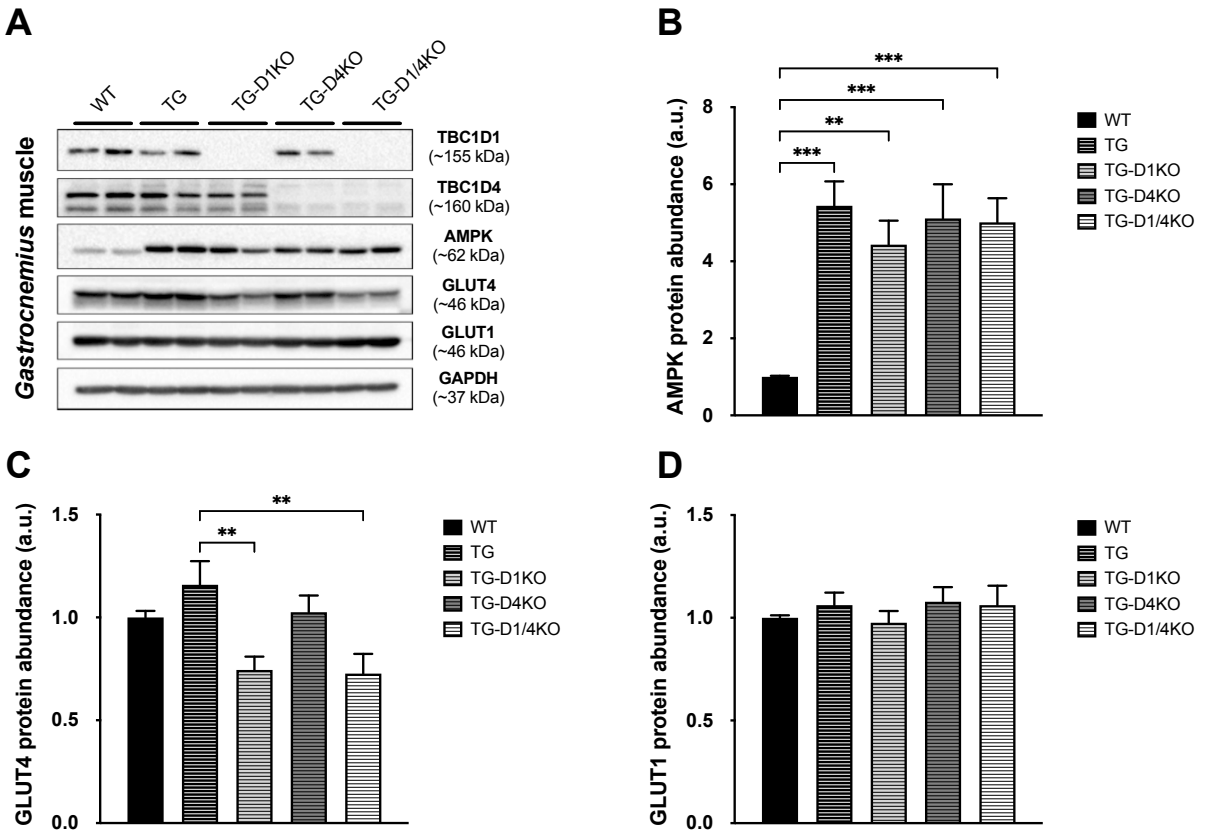

Figure 4.9: Expression of glucose transporters in *gastrocnemius* muscle of TG and RabGAP-deficient mice. A: Representative Western Blots for TBC1D1, TBC1D4, AMPK, GLUT4 and GLUT1 abundance of male AMPKα_2-transgenic (TG) and AMPKα_2-transgenic *Tbc1d1*- (TG-D1KO), *Tbc1d4*-deficient (TG-D4KO) and double-deficient *Tbc1d1/Tbc1d4*-deficient (TG-D1/4KO) mice in comparison to WT controls shown in reference to GAPDH as loading control. B-D: Western Blot quantification of protein abundance using antibodies for AMPK (B), GLUT4 (C) and GLUT1 (D). Data are presented as mean ± SEM (n = 7-9). **P < 0.01, ***P < 0.001 TG vs. WT, TG-D1KO, TG-D4KO, TG-D1/4KO (one-way ANOVA with Dunnett correction).

4.3.2 AICAR tolerance of AMPKα_2-transgenic *Tbc1d1*- and/or *Tbc1d4*-deficient mice

To test the effect of combined absence of AMPKα_2-function and the RabGAPs TBC1D1 and/or TBC1D4 on whole-body glucose disposal, an intraperitoneal AICAR tolerance test (i.p.ATT) (Figure 4.10) was performed (3.1.8). Earlier results from RabGAP-deficient mice showed an improved AICAR sensitivity for D4KO and D1/4KO mice (Figure 4.4). D1KO animals tended to have an impaired AICAR tolerance.

Although basal blood glucose concentrations were not significantly changed (Figure 4.10A), values were normalized to basal concentrations to allow a better comparison of the different courses.

During i.p.ATT the blood glucose (BG) concentrations of WT mice decreased from 100 % to 86.4 % 15 min after AICAR injection, 53.2 % after 30 min and 55.9 % after 60 min. AMPK-transgenic (TG) mice showed significantly higher BG values 60 min after the injection (Figure 4.10B; TG vs. WT: 80.6 ± 9.9 vs. 55.9 ± 6.2 %, P < 0.05). Throughout the experiment BG

concentrations of TG mice were elevated compared to WT controls but the difference failed to reach significance. The BG values of TG-D1KO mice tended to increase compared to TG mice, whereas TG-D4KO animals tended to have lower BG concentrations, which was significant 15 min after AICAR injection (TG-D4KO vs. TG: 73.5 ± 3.6 vs. 86.4 ± 4.7 %, $P < 0.05$). TG-D1/4KO showed no differences compared to TG animals.

No significant changes in the area under the curve (AUC) could be observed for in samples of these mice (Figure 4.10B).

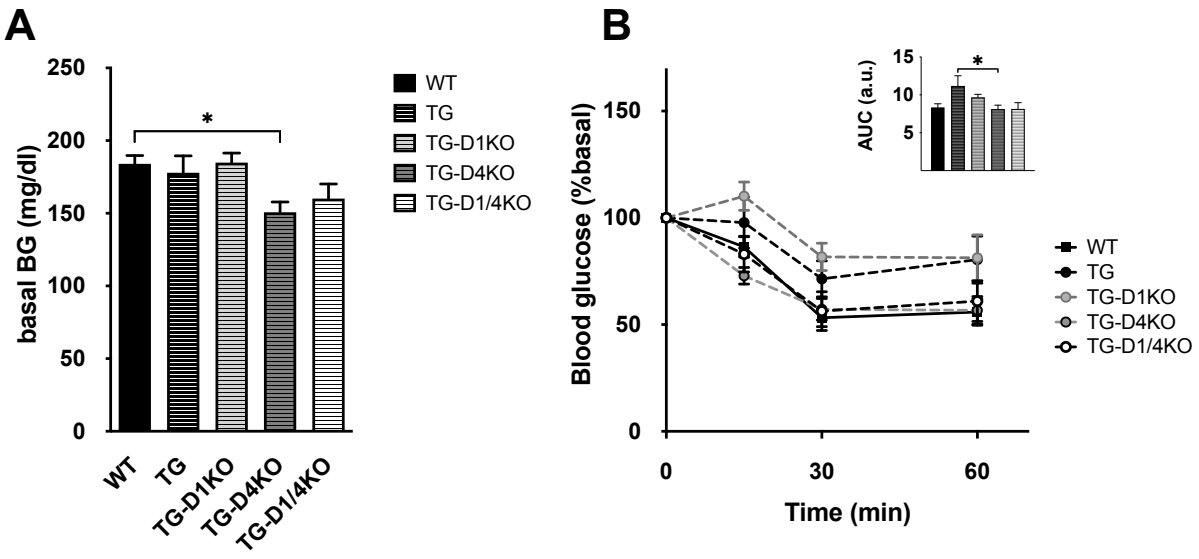

Figure 4.10: Intraperitoneal AICAR tolerance test (i.p.ATT) of WT, TG, TG-D1KO, TG-D4KO and TG-D1/4KO mice.
Male AMPKα_2-transgenic (TG) and AMPKα_2-transgenic *Tbc1d1*- (TG-D1KO), *Tbc1d4*-deficient (TG-D4KO) and double-deficient *Tbc1d1/Tbc1d4*-deficient (TG-D1/4KO) mice in comparison to WT controls aged 20–30 weeks were subjected to intraperitoneal tolerance tests for AICAR (ATT). A: Random fed blood glucose levels. B: Blood glucose concentrations before and 15, 30 and 60 min after intraperitoneal injection of AICAR (250 mg/kg) and AUC. Data are presented as mean ± SEM (n = 7-10). *P < 0.05, WT vs. TG vs. TG-D1KO vs. TG-D4KO (one-way ANOVA with Tuckey correction).

4.3.1 Fasting – refeeding

To test the effect of combined absence of AMPKα_2-function and the RabGAPs TBC1D1 and/or TBC1D4 on whole body glucose disposal, a fasting-refeeding experiment (3.1.9) was conducted. BG levels and the respective plasma insulin concentrations were measured after 16 hours of fasting and again after 1 hour of *ad libitum* refeeding (Figure 4.11A, B). Besides, plasma triglycerides (TG's; Figure 4.11C) and non-esterified fatty acids ("free fatty acids", FFA's; Figure 4.11D) were measured to obtain a comprehensive picture of energy metabolism during the experiment.

After the fasting period (0 min), BG levels were around 100 mg/dl in mice of all genotypes. There were no genotype-related differences in BG and plasma insulin. After 1 hour of refeeding

(60 min), BG concentration of WT mice increased to a level of 221.4 mg/dl. Values of TG mice were unaltered compared to WT and TG-D1KO mice showed no differences in comparison to TG mice. In contrast, TG-D4KO and TG-D1/4KO mice reached significantly higher BG levels compared to TG animals, while plasma insulin concentrations were unchanged (Figure 4.11A, B; TG vs. TG-D4KO vs. TG-D1/4KO: 206.8 ± 22.9 vs. 293.8 ± 46.5 vs. 368.7 ± 72.9 mg/dl, $P < 0.0001$).

Figure 4.11C shows the respective plasma triglyceride concentrations. Triglycerides in WT mice were similar after fasting (0.77 mmol/l) and after refeeding (0.73 mmol/l). In contrast to that, triglyceride concentrations in plasma of TG mice were increased after 16 h of fasting compared to WT animals (WT vs. TG: 0.77 ± 0.25 vs. 1.32 ± 0.57 mmol/l, $P < 0.05$). No difference was detected after 1 h of refeeding. In relation to TG triglyceride levels, there was again a decrease in plasma triglycerides due to the RabGAP-deficiency in fasted TG-D1/4KO animals (Figure 4.11C; TG vs. TG-D1/4KO: 1.32 ± 0.57 vs. 0.84 ± 0.21 mmol/l, $P < 0.05$).

The mean FFA concentration in plasma of WT mice after 16 h of fasting was 1.47 mmol/l and after refeeding it was reduced to 0.48 mmol/l (Figure 4.11D; $P < 0.0001$). TG mice showed higher plasma FFA concentrations than WT after fasting (WT vs. TG: 1.47 ± 0.28 vs. 1.85 ± 0.09 mmol/l, $P < 0.01$), whereas TG-D1KO mice had decreased values compared to TG animals (TG vs. TG-D1KO: 1.85 ± 0.09 vs. 1.39 ± 0.41 mmol/l, $P < 0.001$). TG-D4KO and TG-D1/4KO mice did not differ from TG animals.

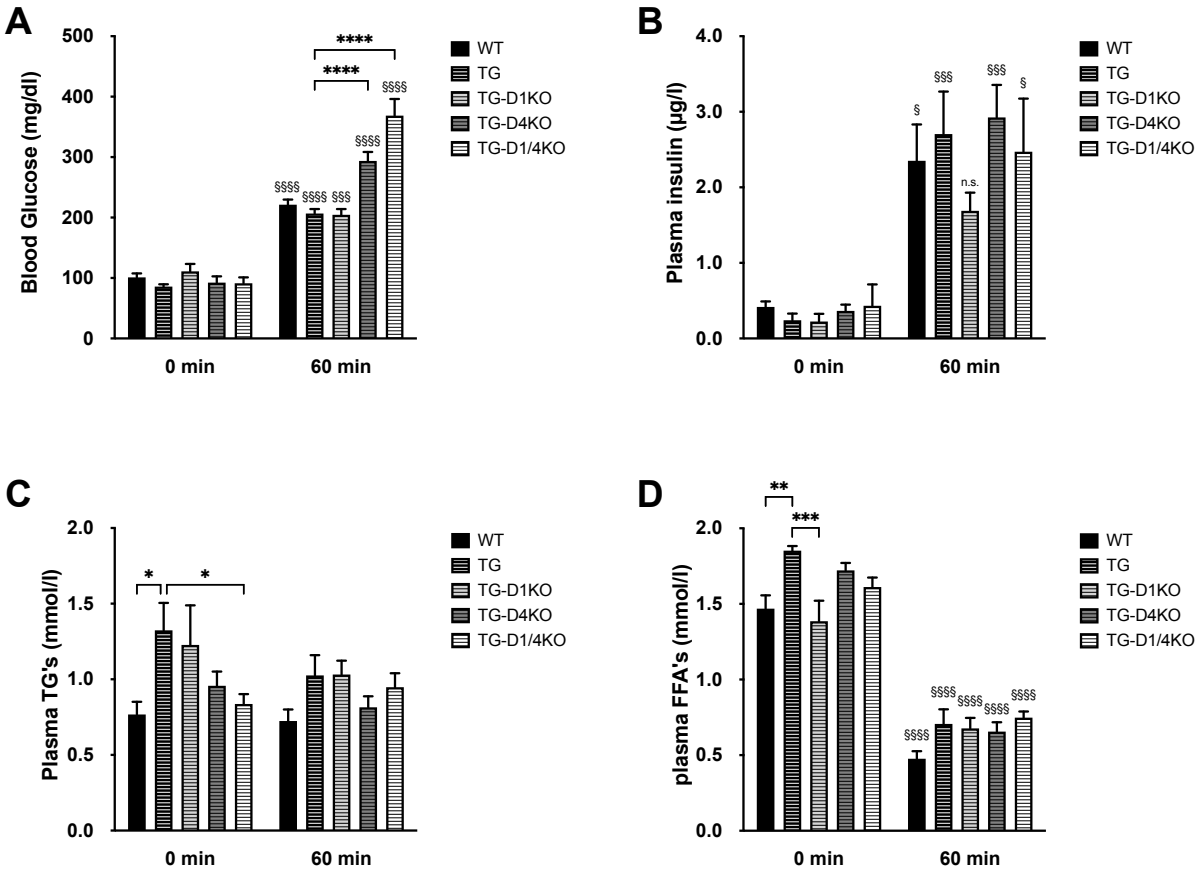

Figure 4.11: 16 h fasting – 1 h refeeding of TG, TG-D1KO, TG-D4KO and TG-D1/4KO mice.
Male AMPKα_2-transgenic (TG) and AMPKα_2-transgenic *Tbc1d1*- (TG-D1KO), *Tbc1d4*-deficient (TG-D4KO) and double-deficient *Tbc1d1/Tbc1d4*-deficient (TG-D1/4KO) mice in comparison to WT controls were 16 hours fasted and refed for 1 hour. After refeeding, plasma was tested for glucose (A; n = 7-10), insulin (B; n = 4-10), triglycerides (C; n = 9-12) and free fatty acids (D; n = 9-11). Data are presented as mean ± SEM. *P < 0.05, **P < 0.01, ***P < 0.001, ****P < 0.0001; TG vs. WT, TG-D1KO, TG-D4KO, TG-D1/4KO (two-way ANOVA with Dunnett correction). §P < 0.05, §§§P < 0.001, §§§§P < 0.0001; 0 min vs. 60 min (Mixed-effects analysis with Sidak correction).

4.3.2 Glucose tolerance of AMPKα$_2$-transgenic *Tbc1d1*- and/or *Tbc1d4*-deficient mice

To validate the results of the fasting-refeeding experiment in a more controlled and detailed way, an intraperitoneal Glucose tolerance test (i.p.GTT) was performed (Figure 4.12; 3.1.6). Although basal blood glucose concentrations were not significantly changed, values were normalized to basal concentrations to allow a better comparison of the different courses.

During i.p.GTT, blood glucose levels of WT mice reached 250.9 % of the basal value after 15 min and 265.7 % after 30 min. Afterwards, they went down again to 133.3 % at minute 120. TG mice showed no significant difference compared to WT animals after intraperitoneal glucose injection (Figure 4.12B). Compared to TG animals, values of TG-D1KO and TG-D4KO mice were also unchanged. However, TG-D1/4KO mice showed significantly increased blood

glucose levels after 15 min (Figure 4.12B; TG-D1/4KO vs. TG: 315.4 ± 27.1 vs. 260.8 ± 13.2 %, P<0.05), but this was not reflected by the area under the curve (AUC) (Figure 4.12B).
The plasma insulin concentrations did not significantly differ after 6 hours of fasting (Figure 4.12C). The plasma insulin excursion 15 min after glucose injection was significantly lower in TG mice compared to WT (TG vs. WT: 146.6 ± 21.1 vs. 328.0 ± 126.2 %, P<0.01). Between TG, TG-D1KO, TG-D4KO and TG-D1/4KO mice, no differences could be measured, neither in the excursion of plasma insulin nor in the AUC (Figure 4.12D).

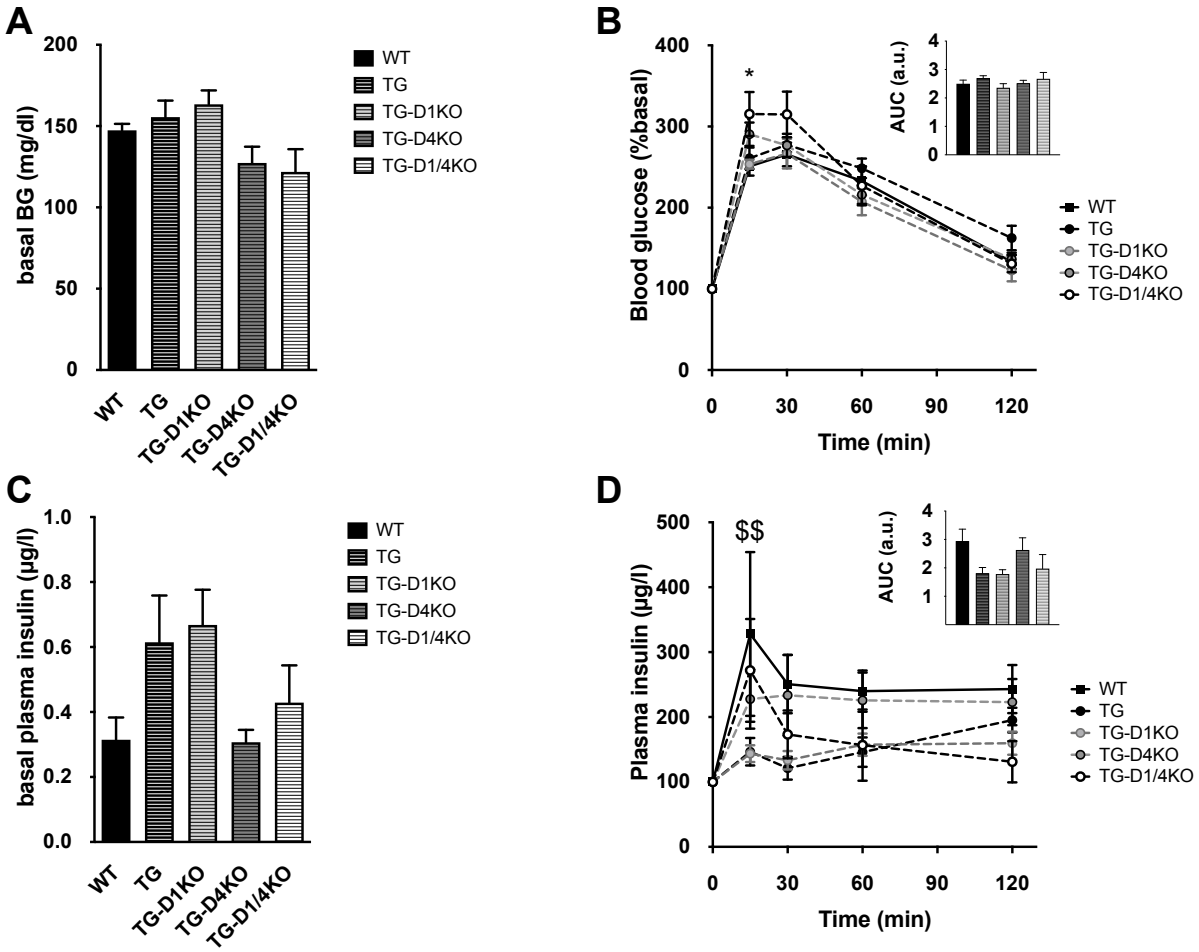

Figure 4.12: Intraperitoneal glucose tolerance test (i.p.GTT) of WT, TG, TG-D1KO, TG-D4KO and TG-D1/4KO mice.
Male 19–29 weeks old AMPKα_2-transgenic (TG) and AMPKα_2-transgenic *Tbc1d1*- (TG-D1KO), *Tbc1d4*-deficient (TG-D4KO) and double-deficient *Tbc1d1/Tbc1d4*-deficient (TG-D1/4KO) mice in comparison to WT controls were subjected to an intraperitoneal tolerance test for glucose (i.p.GTT). A: Basal blood glucose levels after 6 h fasting. B: Relative blood glucose concentrations (% of basal) before and 15, 30, 60 and 120 min after intraperitoneal injection of glucose (2 mg/kg) and area under the curve (AUC). C: Basal plasma insulin concentrations after 6 h fasting. D: Relative plasma insulin concentrations during i.p.GTT and AUC. Data are presented as mean ± SEM (n = 6-11). $$P < 0.01, WT vs. TG; *P < 0.05, TG vs. TG-D1/4KO (B, D: two-way ANOVA with Dunnett correction; A, D: one-way ANOVA with Dunnett correction).

4.3.3 *In vivo* running exercise performance

To test the proportion of participation of the two different RabGAPs in relation to AMPK-independent exercise performance, mice were forced to run on a treadmill, completing an acute running protocol until exhaustion (3.1.10). In Figure 4.13A, the time to exhaustion, which means the time, at which animals were not able to keep running anymore, is plotted.

WT mice managed to run for 12.47 min until exhaustion. TG mice stayed on the treadmill for 8.85 min, 3.62 min less than WT animals. The additional lack of TBC1D1 in TG-D1KO mice caused another reduction by about 3.44 min. Combined deficiency of AMPKα_2 and TBC1D4 did not significantly affect running capacity of the animals (10.13 min) compared to TG mice, whereas TG-D1/4KO mice showed an intermediate phenotype of 7.34 min until exhaustion.

The VO_2max is a measure of oxidative capacity and therefore endurance capacity. It was decreased in TG mice (36.11 ml/min/kg$^{0.75}$) compared to WT (41.77 ml/min/kg$^{0.75}$; Figure 4.13B). Further RabGAP deficiency had no influence on maximal oxygen consumption, since VO_2max values of TG-D1KO, TG-D4KO and TG-D1/4KO mice did not differ from TG.

Another parameter, measured during the acute running test, was the respiratory exchange ratio (RER). This value represents the ratio of produced carbon dioxide (CO_2) to consumed oxygen (O_2). It indicates which fuel source is metabolized to supply energy to the body. The average RER during the experiment was between 0.77 and 0.79 and did not differ among animals of the different genotypes (Figure 4.13C).

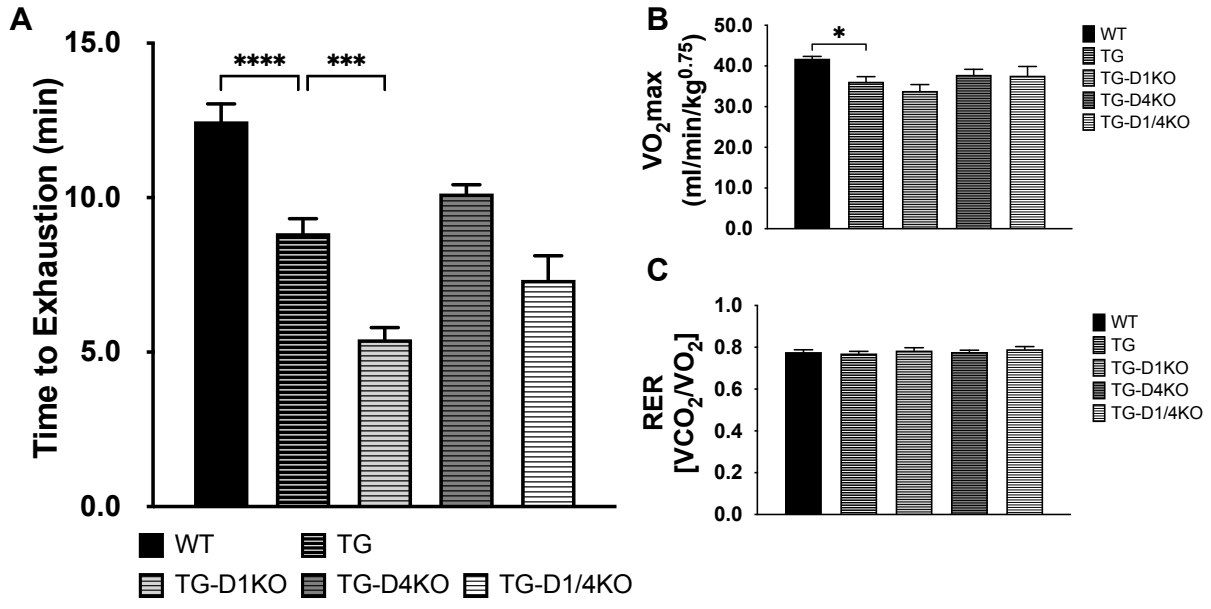

Figure 4.13: *In vivo* acute running performance of WT, TG, TG-D1KO, TG-D4KO and TG-D1/4KO mice.
Male AMPKα_2-transgenic (TG) and AMPKα_2-transgenic *Tbc1d1*- (TG-D1KO), *Tbc1d4*-deficient (TG-D4KO) and double-deficient *Tbc1d1/Tbc1d4*-deficient (TG-D1/4KO) mice in comparison to WT controls were forced to run on a caloric treadmill with increasing speed until exhaustion. The time mice managed to run on the treadmill (A; n = 6-10), VO_2max (B; n = 3-8) and Respiratory exchange ratio (RER; C; n = 6-10) were measured. Data are presented as mean ± SEM. *P < 0.05, ***P < 0.001, ****P < 0.0001, TG vs. WT, TG-D1KO, TG-D4KO, TG-D1/4KO (one-way ANOVA with Dunnett correction).

4.3.4 *Ex vivo* contraction-induced glucose uptake in isolated skeletal muscles

Since skeletal muscle is the major energy-consuming organ during exercise, the reduced running capacity in TG and TG-D1KO mice raises the question if skeletal muscle accounts for this effect. To address this question, *EDL* and *Soleus* muscle were dissected, and *ex vivo* contracted by electrical stimulation. Subsequently, uptake of tritiated 2-deoxy-D-glucose was measured (3.2.7).

In Figure 4.14A and B the contraction-stimulated glucose transport in RabGAP-deficient *EDL* (A) and *Soleus* (B) muscle with inactivated AMPKα_2 is displayed. In both types of muscle, the inactivation of AMPKα_2 caused a severe reduction in contraction-stimulated glucose transport by about one third compared to WT muscles. However, stimulation increased glucose transport.

In *EDL* muscle (Figure 4.14A) further absence of TBC1D1 caused a severely reduced glucose transport following muscle contraction. This effect could also be observed in TG-D1/4KO muscles. Glucose transport rates in *EDL* of TG-D4KO mice did not differ from TG.

In *Soleus* muscle (Figure 4.14B) contraction failed to stimulate glucose transport when functional AMPKα_2 and both RabGAPs where absent (TG-D1/4KO). Compared to TG muscles no difference was measured in glucose transport rates of stimulated TG-D1KO, TG-D4KO and TG-D1/4KO mice.

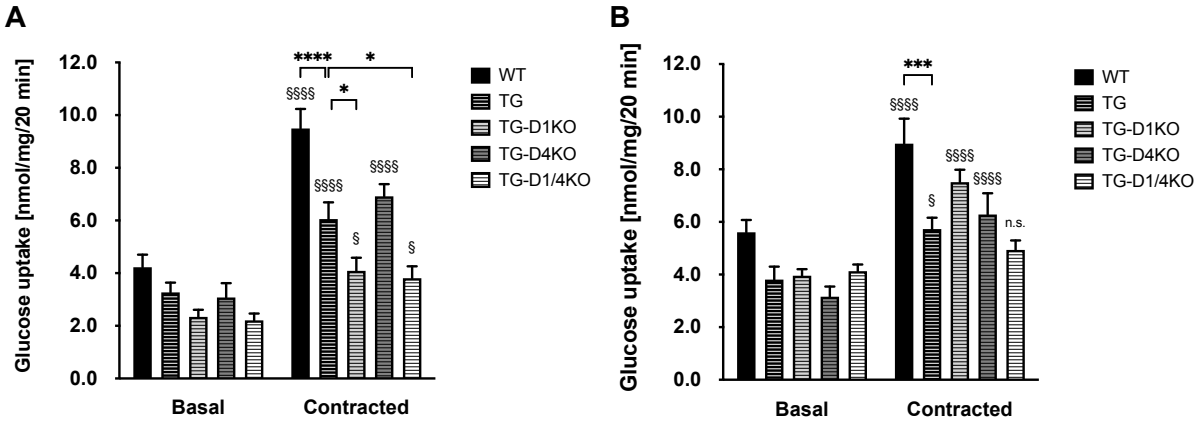

Figure 4.14: Contraction induced glucose uptake in *EDL* and *Soleus* muscle of AMPKα_2-transgenic and RabGAP-deficient mice.
Skeletal muscles from male AMPKα2-transgenic (TG) and AMPKα2-transgenic *Tbc1d1*- (TG-D1KO), *Tbc1d4*-deficient (TG-D4KO) and double-deficient *Tbc1d1/Tbc1d4*-deficient (TG-D1/4KO) mice in comparison to WT controls were isolated and assayed for contraction-induced [^{3}H]-deoxyglucose uptake. *EDL* (A; n = 9-11) and *Soleus* muscle (B; n = 7-10) from WT, TG and TG-D1KO, TG-D4KO or double-deficient TG-D1/4KO mice. Data are presented as mean ± SEM. *P < 0.05, ***P < 0.001, ****P < 0.0001, TG vs. WT, TG-D1KO, TG-D4KO, TG-D1/4KO (Two-way ANOVA with Dunnett correction). §P < 0.05, §§§§P < 0.0001, basal vs. contracted (two-way ANOVA with Sidak correction)

After contraction, *EDL* and *Soleus* muscle of WT mice showed an increased AMPKα phosphorylation at Threonin 172 (Thr^{172}) (Figure 4.15A, B). This was completely abrogated in mice that were transgenic for AMPKα_2.

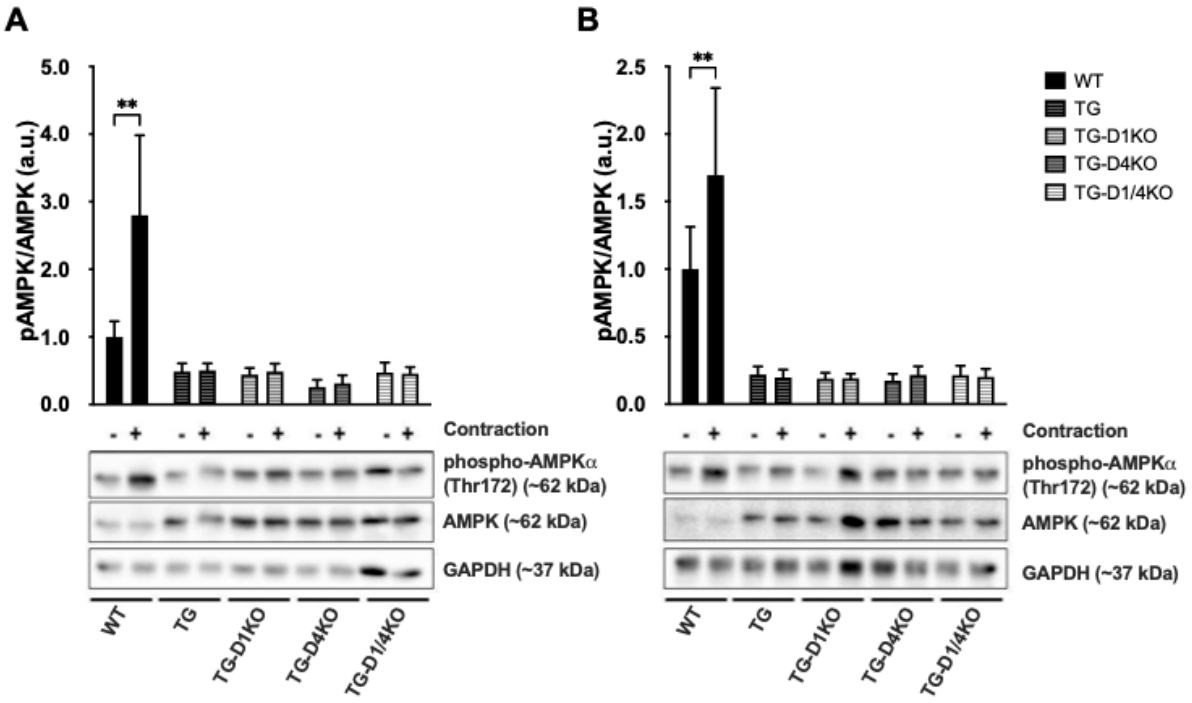

Figure 4.15: AMPKα-Thr^{172} phosphorylation after *ex vivo* contraction of *EDL* and *Soleus* muscle of WT, TG, TG-D1KO, TG-D4KO and TG-D1/4KO mice.
EDL (A; n = 5-8) and *Soleus* (B; n = 6-8) muscle from AMPKα$_2$-transgenic (TG) and AMPKα$_2$-transgenic *Tbc1d1*-(TG-D1KO), *Tbc1d4*-deficient (TG-D4KO) and double-deficient *Tbc1d1/Tbc1d4*-deficient (TG-D1/4KO) mice in comparison to WT controls were contracted *ex vivo* in a myograph chamber for 10 min, snap frozen and blotted for AMPKα-Thr^{172} phosphorylation and normalized to total AMPKα protein amount. Data are presented as mean ± SEM. **P < 0.01, basal vs. contracted (two-way ANOVA with Sidak correction)

4.3.5 GLUT4 protein abundance in *EDL* and *Soleus* muscle

It was shown before that GLUT4 transporter protein content is reduced in *gastrocnemius* muscle of D1KO and D1/4KO mice by about 25% (Figure 4.9C). Our group has published in 2015, that a knockout of TBC1D1 is associated to a reduction of GLUT4 transporter in glycolytic muscle types [79]. In accordance with that, the deletion of TBC1D4 is accompanied by a reduced GLUT4 abundance in oxidative muscle and white adipose tissue. This pattern could also be observed in mice that were crossbred with the AMPKα$_2$-transgenic (TG) mouse strain using western blot technique (3.2.4). In the TG mice the GLUT4 abundance was not changed, neither in glycolytic *EDL* (Figure 4.16A), nor in oxidative *Soleus* muscle (Figure 4.16B). However, in *EDL* of mice lacking TBC1D1 (TG-D1KO, TG-D1/4KO) the amount of GLUT4 was decreased by 30% or 21% compared to TG. In *Soleus* muscle, a reduction by 32% and 39% occurred in muscles of TG-D4KO and TG-D1/4KO animals respectively.

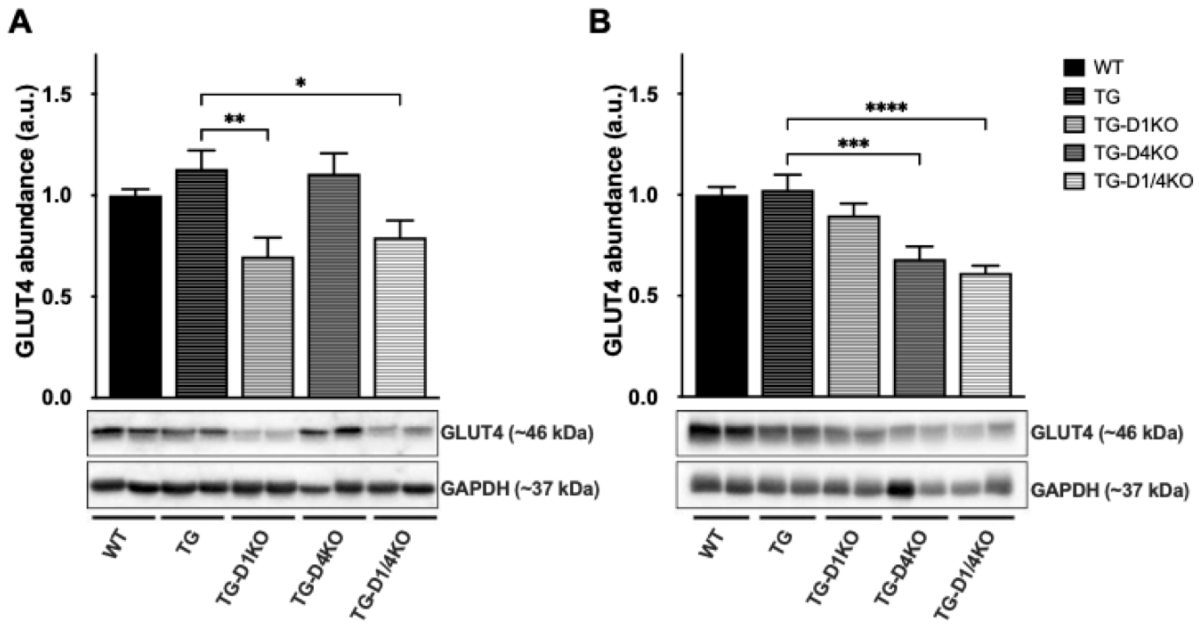

Figure 4.16: GLUT4 protein abundance in *EDL* and *Soleus* muscle of WT, TG, TG-D1KO, TG-D4KO and TG-D1/4KO mice.
GLUT4 protein abundance of *EDL* (A) and *Soleus* muscle (B) from male AMPKα2-transgenic (TG) and AMPKα2-transgenic *Tbc1d1*- (TG-D1KO), *Tbc1d4*-deficient (TG-D4KO) and double-deficient *Tbc1d1/Tbc1d4*-deficient (TG-D1/4KO) mice in comparison to WT controls in reference to GAPDH. Data are presented as mean ± SEM, (n = 8) *P < 0.05, **P < 0.01, ***P < 0.001, ****P < 0.0001, TG vs. WT, TG-D1KO, TG-D4KO, TG-D1/4KO (one-way ANOVA with Dunnett correction).

4.3.6 Glycogen and Triglyceride content in *gastrocnemius* muscle and liver from TG, TG-D1KO, TG-D4KO and TG-D1/4KO mice.

Changes in glucose transport may have an impact on the storage of energy-rich substrates in skeletal muscle and liver. A lack of these substrates could cause the observed impairment in running capacity of TG-D1KO mice. To check this hypothesis, glycogen, and triglyceride content of *gastrocnemius* muscle, which has a mixed fiber type composition, and of liver tissue, were analyzed (3.2.5).

There were no significant differences in glycogen or triglyceride content of gastrocnemius muscle among the different genotypes compared to TG tissues (Figure 4.17A). In liver, glucose from glycogen was decreased in samples of TG-D4KO and TG-D1/4KO mice. Triglyceride content was increased in liver of TG-D1/4KO animals.

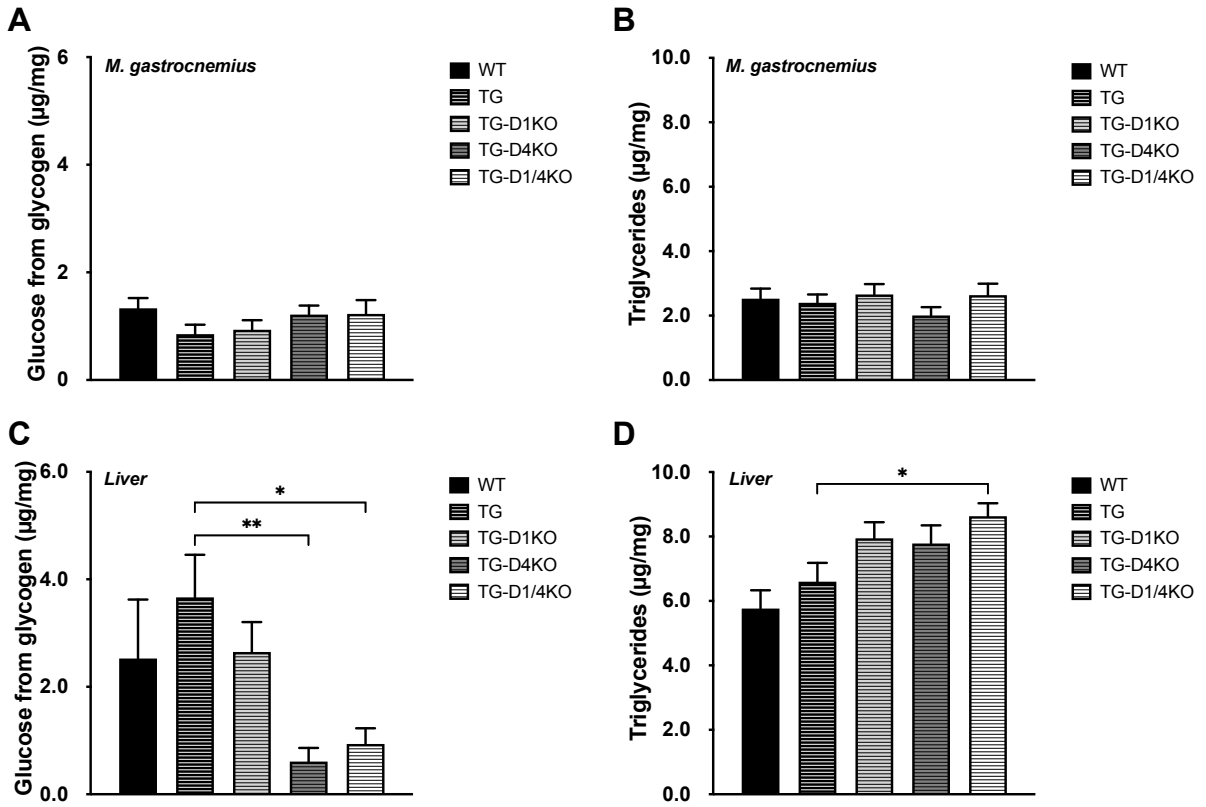

Figure 4.17: Glycogen and triglyceride content in *gastrocnemius* muscle (A, B) and liver (C, D).
Tissues from male 4 h fasted AMPKα_2-transgenic (TG) and AMPKα_2-transgenic *Tbc1d1*- (TG-D1KO), *Tbc1d4*-deficient (TG-D4KO) and double-deficient *Tbc1d1/Tbc1d4*-deficient (TG-D1/4KO) mice in comparison to WT controls were analyzed for glycogen and triglyceride concentrations. Glycogen (A) and triglyceride content (B) of *gastrocnemius* muscle (n = 15-17) and hepatic glycogen (C; n = 10–12) and triglyceride content (D; n = 15–17). Data are presented as mean ± SEM. *P < 0.05, **P < 0.01, TG vs. WT, TG-D1KO, TG-D4KO, TG-D1/4KO (one-way ANOVA with Dunnett correction).

4.3.7 Glycogen Synthase protein abundance in *gastrocnemius* muscle and liver

In addition to glycogen content, the expression of glycogen synthase was analyzed, which is the key enzyme in glycogenesis. Male mice were dissected after 4 hours of fasting and gastrocnemius muscle and liver tissue were taken and analyzed by Western Blotting (3.2.4). Figure 4.18 shows the quantification of the results of the Western Blot. In *gastrocnemius* muscle (Figure 4.18A) no changes among the analyzed genotypes could be detected. In liver samples of TG-D1/4KO mice GS protein abundance was increased by ~2.5-fold compared to TG samples.

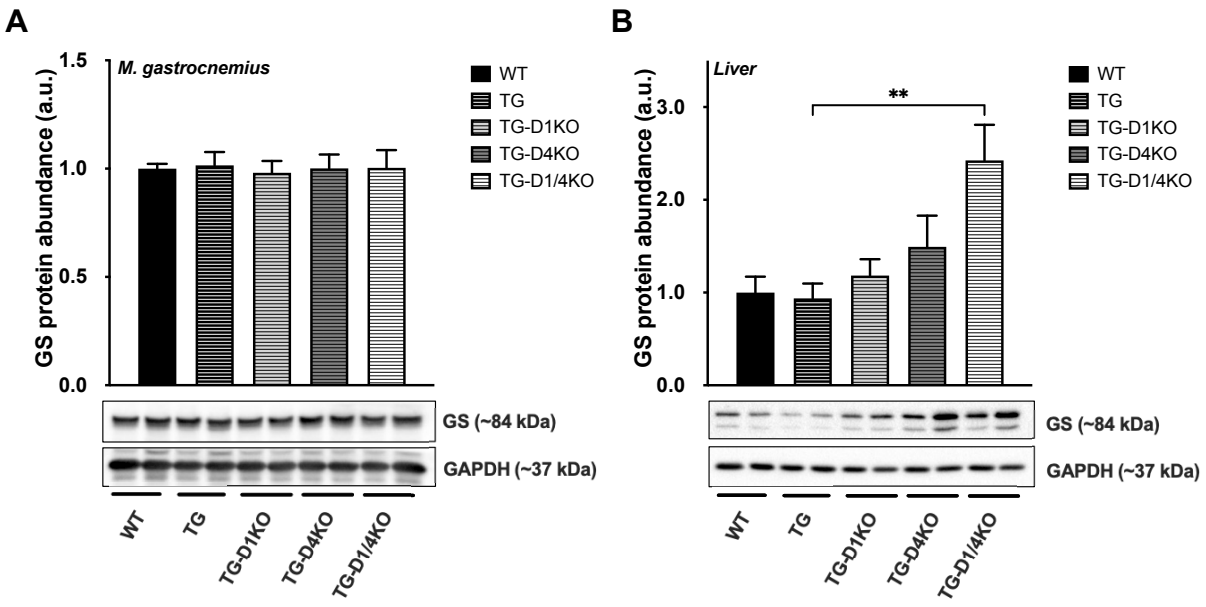

Figure 4.18: Glycogen Synthase protein abundance in *gastocnemius* muscle and liver.
Western Blot quantification of GS protein abundance in *gastrocnemius* muscle (A) and liver tissue (B) of AMPKα2-transgenic (TG) and AMPKα2-transgenic *Tbc1d1*- (TG-D1KO), *Tbc1d4*-deficient (TG-D4KO) and double-deficient *Tbc1d1/Tbc1d4*-deficient (TG-D1/4KO) mice in comparison to WT controls shown in reference to GAPDH as loading control. Data are presented as mean ± SEM (n = 7-8). **P < 0.01, TG vs. WT, TG-D1KO, TG-D4KO, TG-D1/4KO (one-way ANOVA with Dunnett correction).

4.3.8 Gene expression of AMPK-related kinases in *gastrocnemius* muscle and liver

Transgenic expression of kinase-dead AMPKα$_2$ in skeletal muscle and heart leads to decreased exercise capacity (Figure 4.13) and contraction-stimulated glucose transport into skeletal muscle (Figure 4.14). However, even without functional AMPKα$_2$ and its downstream targets TBC1D1 and TBC1D4, *ex vivo* contraction is still able to stimulate the uptake of glucose into *EDL* and *Soleus* muscle. To find possible candidates compensating for the lack of functional AMPK, relative gene expression of several AMPK-related kinases was measured by quantitative real-time PCR (qPCR) (3.3.9) in *gastrocnemius* muscle and liver of TG, TG-D1KO, TG-D4KO and TG-D1/4KO mice.

In both tissues, the mRNA expression of *Tbc1d1* and *Tbc1d4* was completely abrogated in the respective knockout animals (Figure 4.19A, C). Interestingly, the expression of the GLUT4-coding gene *Scl2a4* was reduced in skeletal muscle from TG-D1/4KO mice and showed a strong tendency to be decreased in TG-D1KO mice (95% confidence interval (CI) of difference: -0.001922 to 0.3418; Figure 4.19A). In the liver, where the *Scl2a4*-expression was generally low, a significant reduction due to kinase-dead AMPKα$_2$ could be observed (Figure 4.19C).

Among the AMPK-related kinases, gene expression levels of *Nuak1*, *Nuak2* and *Sik1*, *Sik2*, and *Sik3* were tested in both tissues. In *gastrocnemius* muscle, the gene *Nuak1* encoding for ARK5, was significantly up regulated in TG mice compared to WT, whereas the other kinases

were unaltered (Figure 4.19B). In liver, no changes in gene expression of the analyzed candidates were detected (Figure 4.19D).

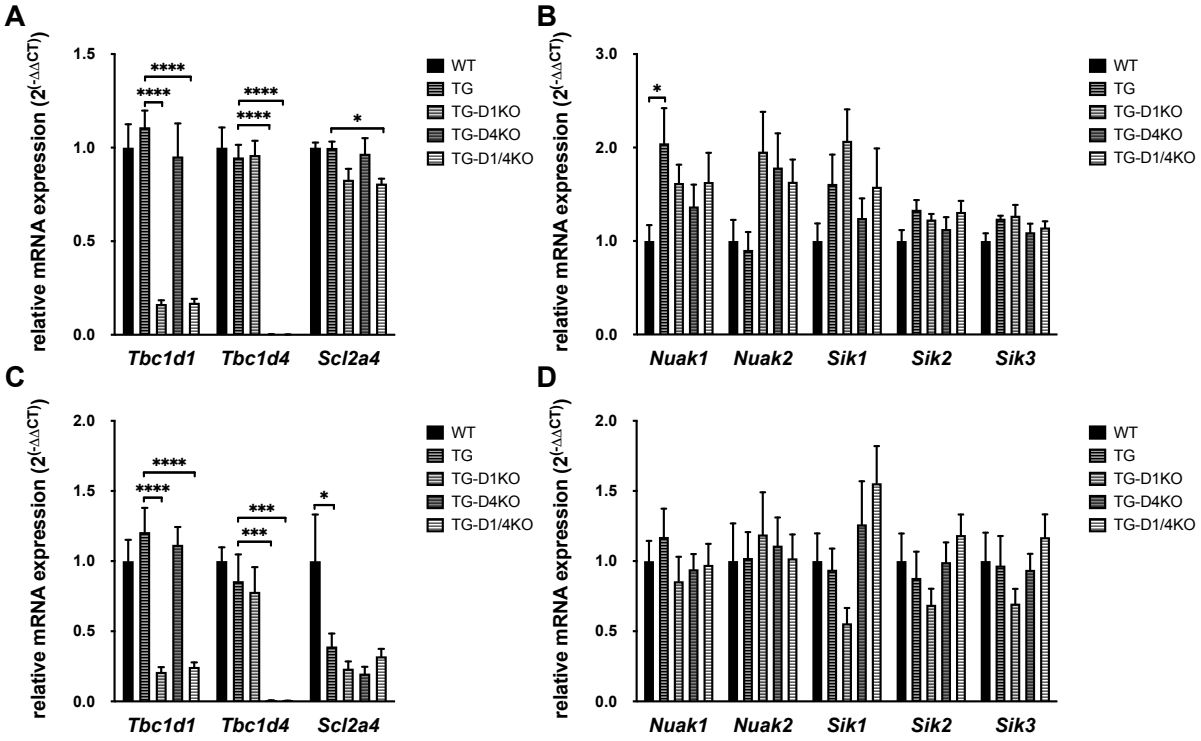

Figure 4.19: Relative gene expression of AMPK-related kinases in *gastrocnemius* muscle (A, B) and liver (C, D).
Expression of *Tbc1d1*, *Tbc1d4* and *Scl2a4* (A, C) and various AMPK-related kinases (B, D) were analyzed by quantitative real-time polymerase chain reaction (qPCR) in *gastrocnemius* muscle of AMPKα2-transgenic (TG) and AMPKα2-transgenic *Tbc1d1*- (TG-D1KO), *Tbc1d4*-deficient (TG-D4KO) and double-deficient *Tbc1d1/Tbc1d4*-deficient (TG-D1/4KO) mice in comparison to WT controls in relation to *Gapdh* and in liver tissue related to *Rps29*. Data are presented as mean of relative gene expression ($2^{-\Delta\Delta CT}$) ± SEM (n = 6-10). *P < 0.05, ***P < 0.001, ****P < 0.0001; TG vs. WT, TG-D1KO, TG-D4KO, TG-D1/4KO (one-way ANOVA with Dunnett correction).

4.3.9 ARK5/NUAK1 and SNARK/NUAK2 protein abundance in *gastrocnemius* muscle of TG, TG-D1KO, TG-D4KO and TG-D1/4KO mice

On mRNA level, the expression of the AMPK-related kinase *Nuak1* coding for the ARK5 protein was up regulated in *gastrocnemius* muscle of TG mice compared to WT animals. To further investigate, if ARK5 might be regulated due to a compensatory mechanism replacing AMPK-function, protein abundance was determined via Western Blot analysis.

The overall amount of ARK5 protein showed strong variations between the genotypes. It was not significantly altered in TG mice compared to WT animals (Figure 4.20) and there were no differences in ARK5 abundance between TG and TG-D1KO, TG-D4KO and TG-D1/4KO muscles.

The data from qPCR also revealed an increased expression of *Nuak2,* which codes for the AMPK-related kinase SNARK/NUAK2. However, Western Blot analysis revealed, that protein expression was unchanged in *gastrocnemius* muscle of TG muscles compared to WT and TG-D1KO, TG-D4KO and TG-D1/4KO mice compared to TG animals (Figure 4.20B).

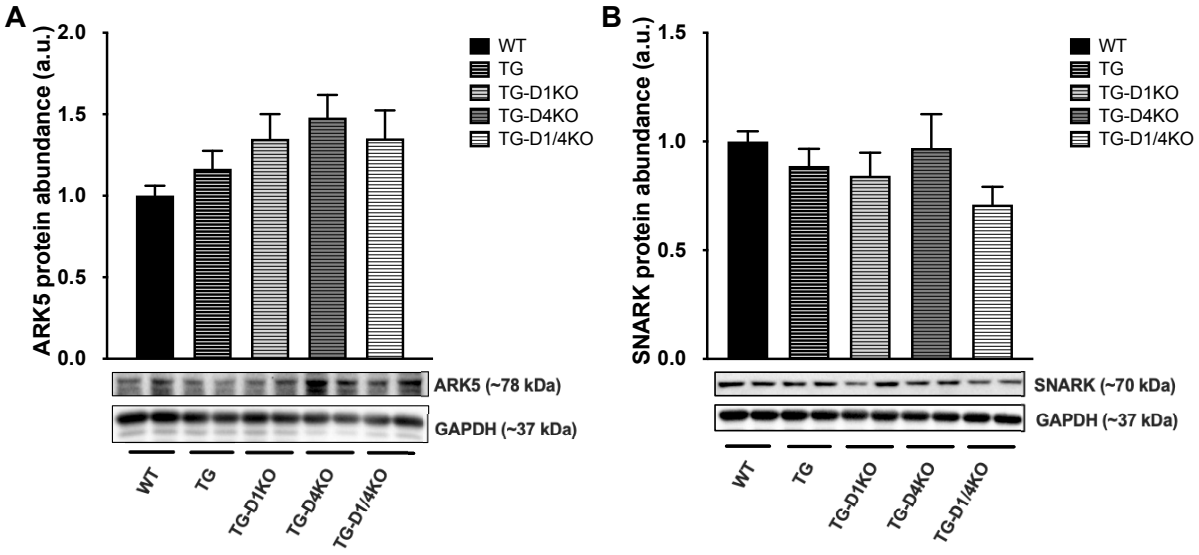

Figure 4.20: ARK5/NUAK1 and SNARK/NUAK2 protein abundance in *gastocnemius* muscle.
Western Blot quantification of ARK5/NUAK1 (A) and SNARK/NUAK2 (B) protein abundance in *gastrocnemius* muscle of AMPKα2-transgenic (TG) and AMPKα2-transgenic *Tbc1d1*- (TG-D1KO), *Tbc1d4*-deficient (TG-D4KO) and double-deficient *Tbc1d1/Tbc1d4*-deficient (TG-D1/4KO) mice in comparison to WT controls shown in reference to GAPDH as loading control. Data are presented as mean ± SEM (n = 8).

4.4 GLUT4-degradation in *Tbc1d1/Tbc1d4*-deficient mice

In kinase-dead AMPKα_2 and RabGAP-deficient mice, the abundance of GLUT4 protein in skeletal muscle is reduced by ~20% (Figure 4.9C and Figure 4.16A, B). This effect can be referred to their RabGAP-deficiency as it has been described in D1KO, D4KO and D1/4KO mice with functional AMPK [79].

To find out which functional domain of the TBC1D1 molecule can influence GLUT4 transporter abundance, *Tibialis anterior* (TA) muscles of D1KO mice were transfected with different *Tbc1d1* mutant constructs by *in vivo* electrotransfection (IVE). This technique makes it possible to observe the impact of the transfected product under *in vivo* conditions.

4.4.1 Expression of the *Tbc1d1* mutants R941K and R125W in TA muscle of D1KO mice

The R941K-mutant of *Tbc1d1* is based on an amino acid exchange of Arginine (R) to Lysine (K) at position 941. This mutation leads to an inactivation of the GAP-activity of the protein [96]. Another mutation of *Tbc1d1* that was described before, is the exchange of Arginine (R) to Tryptophan (W) at position 125 (R125W) which is located in the N-terminal phosphotyrosine-binding (PTB) domain. To test whether the GAP activity or the PTB-domain of TBC1D1 accounts for the reduction of GLUT4 transporter, both mutants were expressed in TA muscles of *Tbc1d1*-deficient mice (D1KO) by IVE (3.1.11). The abundance of GLUT4 transporter and TBC1D1 was measured one week after the transfection with Western Blotting (3.2.4).

First, the effect of the *Tbc1d1*-R941K mutant was tested. The transfection of *Tbc1d1*-WT led to a strong expression of TBC1D1 in the D1KO muscle (Figure 4.21A, B). Also, the mutant was well expressed, but compared to the wild-type *Tbc1d1,* the protein abundance was only ~50 %. GLUT4 levels in D1KO muscles expressing *Tc1d1*-WT were increased by ~50 % compared to muscles transfected with empty *pEGFP*-Vector (Figure 4.21A, C). In contrast to this, expression of the R941K-mutant did not lead to a significant alteration in GLUT4 abundance compared to the *pEGFP*-transfected controls. Compared to *Tbc1d1*-WT transfected muscles, GLUT4 content was lower in *Tbc1d1*-R941K treated muscles.

Figure 4.22 shows the TBC1D1 and GLUT4 abundance of TA muscles from D1KO mice after IVE with *Tbc1d1*-R125W mutant. The expression of TBC1D1 was ~45 % of the amount after transfection with *Tbc1d1*-WT (Figure 4.22A, B). GLUT4 abundance after IVE with *Tbc1d1*-R125W increased by ~50 %, similar to GLUT4 content after transfection with *Tbc1d1*-WT Figure 4.22A, C).

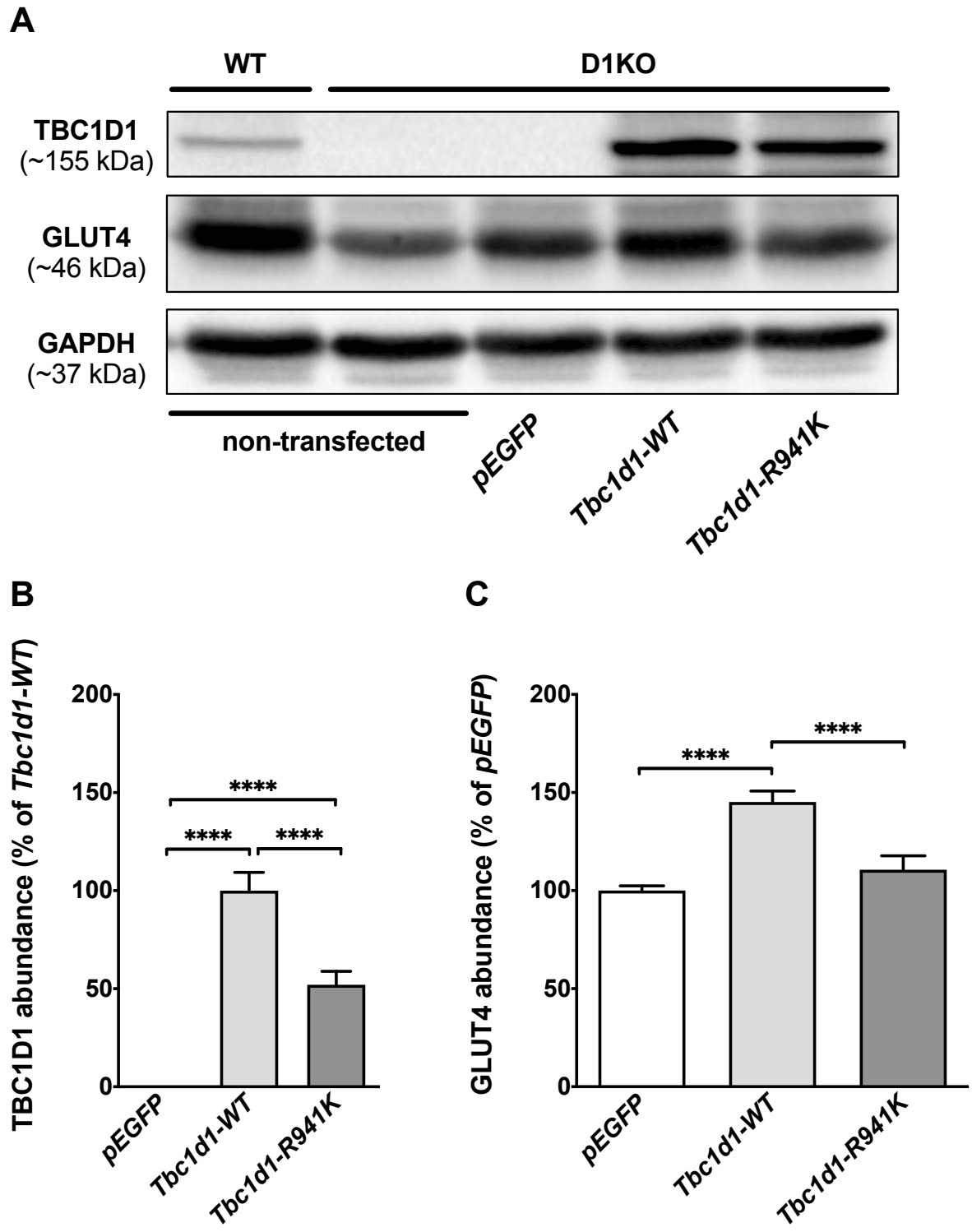

Figure 4.21: Expression of *Tbc1d1*-R941K mutant in TA muscle of D1KO mice via IVE.
A: Representative Western Blots of TBC1D1, GLUT4 and GAPDH in non-transfected TA muscle of wild-type (WT) and *Tbc1d1*-deficient (D1KO) mice as well as muscle of D1KO mice after IVE, transfected with pcDNA3-FLAG Vector containing *Tbc1d1*-WT (n = 14), *Tbc1d1*-R941K (n = 10) or pEGFP-Vector (n = 30) as control. B, C: Western Blot quantification of TBC1D1 (B) and GLUT4 (C) protein abundance in TA muscle of D1KO mice after IVE. Data are presented as mean ± SEM. ****P < 0.0001, pEGFP vs. *Tbc1d1-WT* vs. *Tbc1d1-R941K* (one-way ANOVA with Tuckey correction).

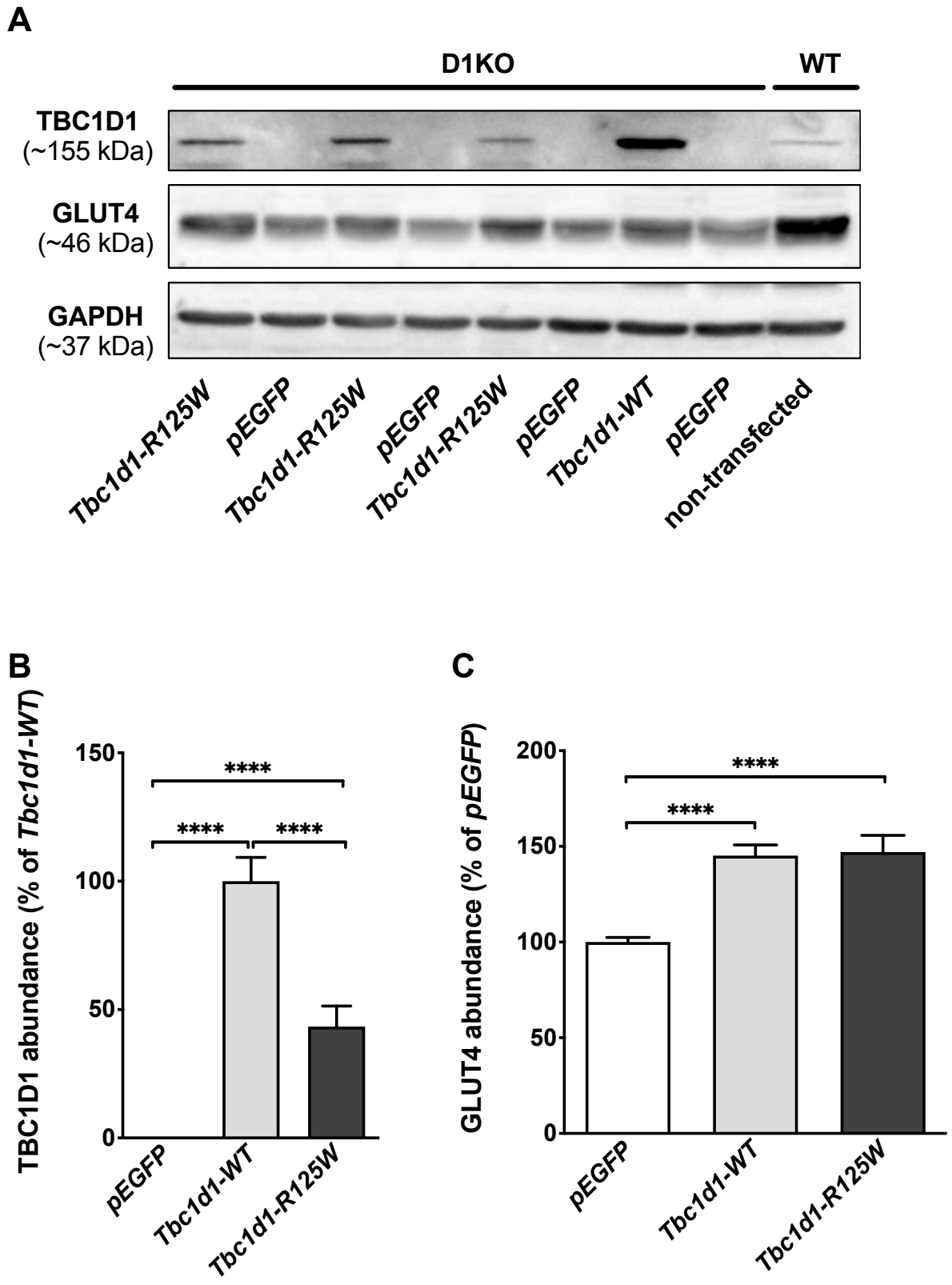

Figure 4.22: Expression of *Tbc1d1*-R125W mutant in TA muscle of D1KO mice via IVE.
A: Representative Western Blots of TBC1D1, GLUT4 and GAPDH in non-transfected TA muscle of wild-type (WT) and *Tbc1d1*-deficient (D1KO) mice as well as muscle of D1KO mice after IVE, transfected with pcDNA3-FLAG vector containing *Tbc1d1*-WT (n = 14), *Tbc1d1*-R125W (n = 6) or pEGFP-Vector (n = 30) as control. B, C: Western Blot quantification of TBC1D1 (B) and GLUT4 (C) protein abundance in TA muscle of D1KO mice after IVE. Data are presented as mean ± SEM. ****P < 0.0001, pEGFP vs. *Tbc1d1*-WT vs. *Tbc1d1*-R941K (one-way ANOVA with Tuckey correction).

4.4.2 Expression studies with known TBC1D1 interacting small RabGTPases

4.4.2.1 Expression of *Rab8a*-mutants

RAB8A is a prominent downstream target of TBC1D1, which inhibits its activity. To mimic the effect of TBC1D1-deficiency on GLUT4 protein levels in TA-muscle, a constitutively active *Rab8a*-Q67L variant was expressed by IVE-method (3.1.11) and protein abundance was measured with Western Blotting (3.2.4).

After one week, RAB8a expression was 5.75-fold higher than in control muscles, but no effect on GLUT4 content could be detected (Figure 4.23).

To recover GLUT4 content in TA muscle of D1KO mice, muscles were transfected with a dominant negative *Rab8a*-T22N mutant by IVE (3.1.11). Afterwards Rab8 and GLUT4 protein abundance were measured by Western Blot technique (3.2.4).

The expression of *Rab8a*-T22N in transfected muscles was 2.67-fold higher than Rab8 expression in *pEGFP*-transfected muscles. Consequently, GLUT4 content was not increased, but further reduced (Figure 4.23).

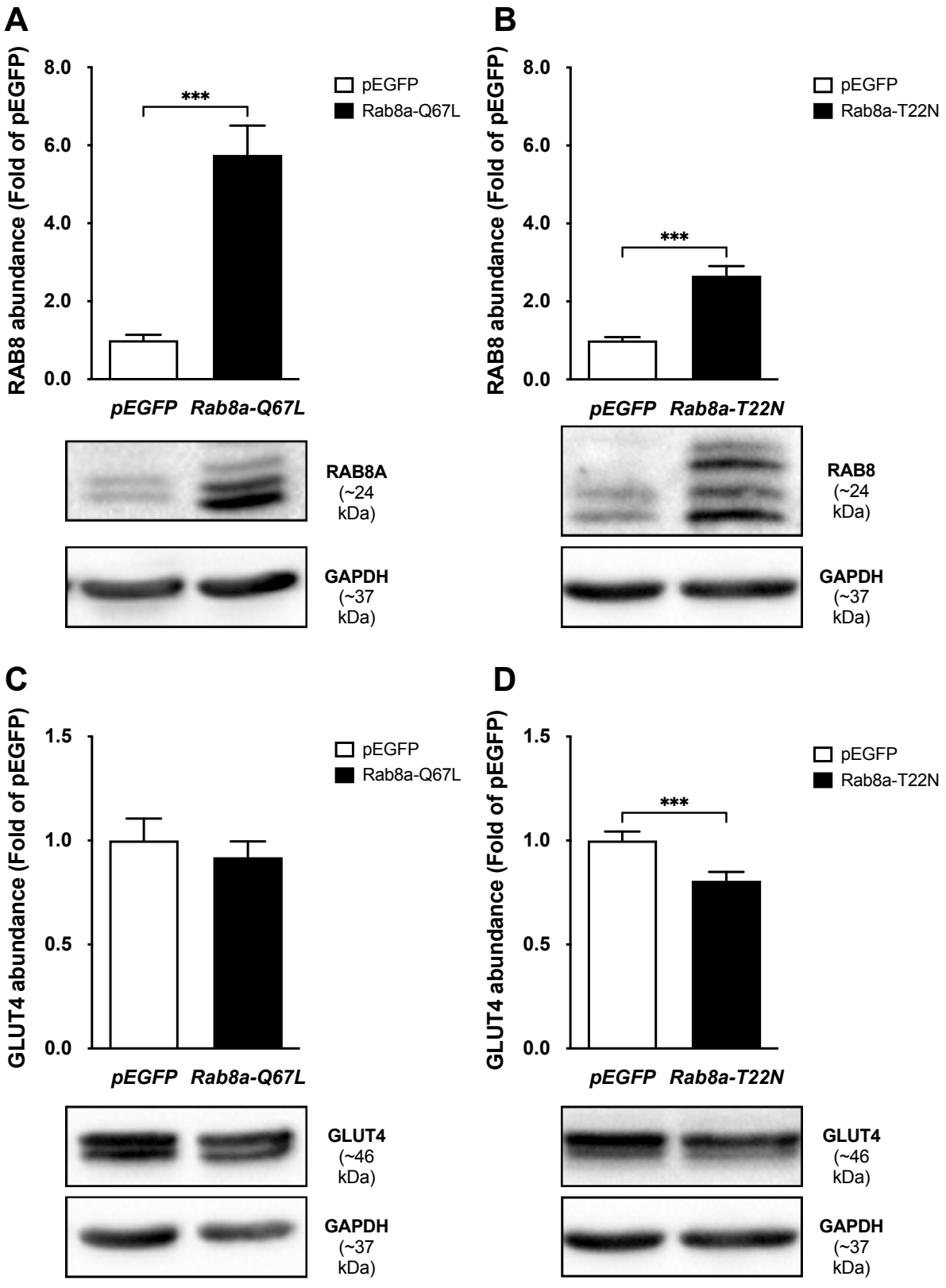

Figure 4.23: Expression of RAB8 and GLUT4 protein in TA muscle of C57BL/6J and D1KO mice after IVE. A and C: Western Blot quantification of RAB8 (A) and GLUT4 (C) protein abundance in TA muscle of C57BL/6J mice after IVE with pcDNA3-vector containing *Rab8a*-Q67L (n = 7) or empty pEGFP-Vector (n = 7) as control. B and D: Western Blot quantification of RAB8 (B) and GLUT4 (D) protein abundance in TA muscle of *Tbc1d1*-deficient (D1KO) mice after IVE with pEGFP-vector containing *Rab8a*-T22N (n = 8) or empty pEGFP-Vector (n = 8) as control. Data are presented as mean ± SEM. ***P < 0.001, pEGFP vs. *Rab8a*-Q67L or *Rab8a*-T22N (Students t-test, paired, two-tailed).

4.4.2.2 Expression of *Rab14*-mutants

Rab14 represents another Rab GTPase that is a substrate for TBC1D1. The aim of this experiment was to express a constitutively active *Rab14*-Q70L in TA muscle of C57BL/6J mice to mimic the effect in reduction of GLUT4 transporter content caused by TBC1D1-deficiency in D1KO mice. Therefore, an expression vector containing the respective gene was transfected into TA-muscle of the mice by IVE-method (3.1.11) and protein abundance of RAB14 and GLUT4 were measured using Western Blot technique (3.2.4).

The expression of RAB14 protein in *Rab14*-Q70L transfected TA muscles was about 169 times higher compared to control muscles which were transfected with an empty *pEGFP*-vector (Figure 4.24A). Constitutively active RAB14 led to a subsequent rise in GLUT4 protein abundance by about 1.7-fold of controls (Figure 4.24C).

As a rescue experiment to recover GLUT4 content in TA muscle of D1KO mice, a dominant negative *Rab14*-S25N mutant was transfected into TA muscle. Afterwards RAB14 and GLUT4 protein abundance were measured by Western Blot technique.

Although, RAB14 expression was 48 times higher in *Rab14*-S25Q transfected muscles than in control muscles, it did not have significant effects on GLUT4 expression (Figure 4.24B, D).

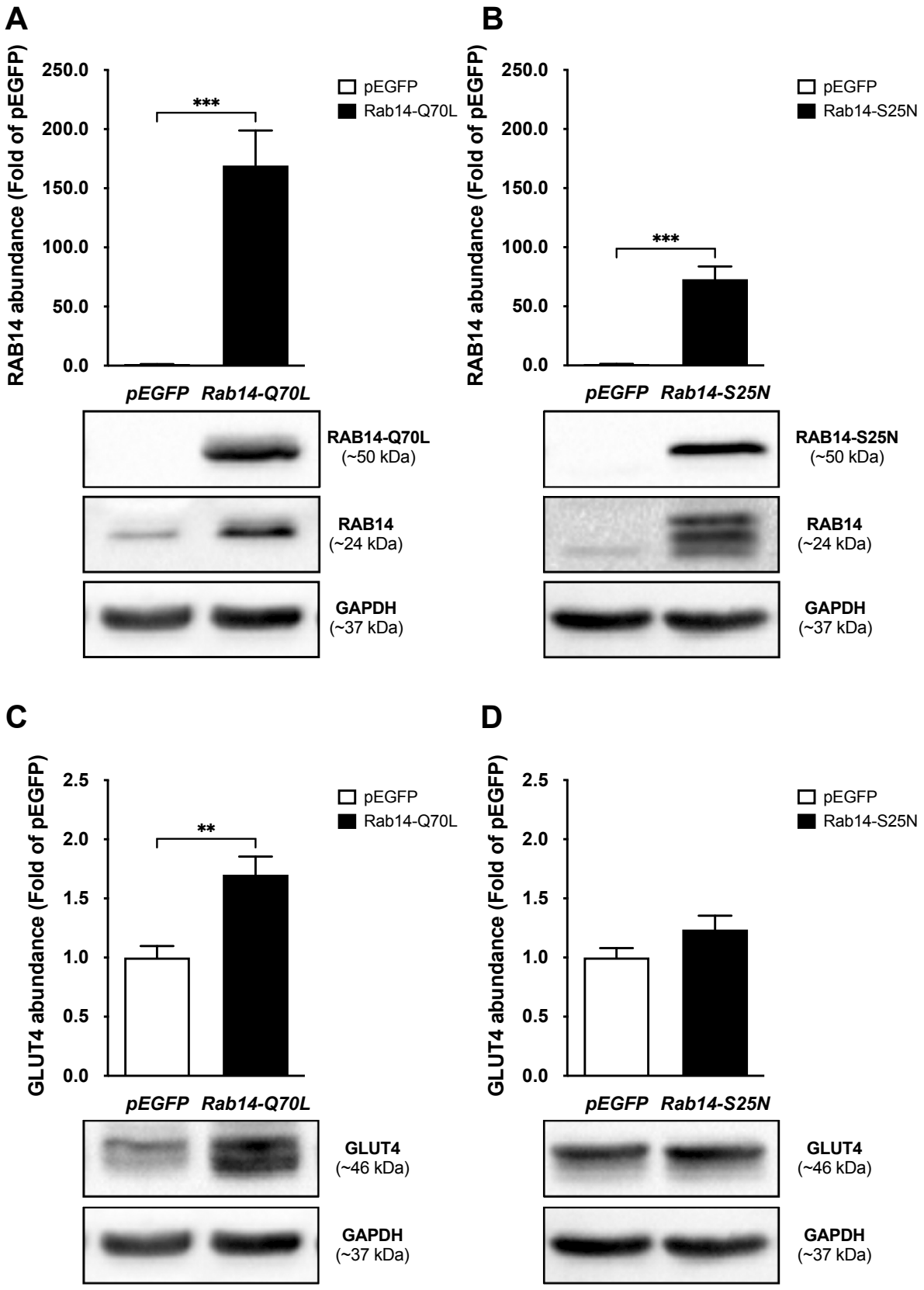

Figure 4.24: Expression of RAB14 and GLUT4 protein in TA muscle of C57BL/6J and D1KO mice after IVE. A and C: Western Blot quantification of RAB14 (A) and GLUT4 (C) protein abundance in TA muscle of C57BL/6J mice after IVE with pEGFP-vector containing *Rab14*-Q70L (n = 8) or empty pEGFP-Vector (n = 8) as control. B and D: Western Blot quantification of RAB14 (B) and GLUT4 (D) protein abundance in TA muscle of *Tbc1d1*-deficient (D1KO) mice after IVE with pEGFP-vector containing *Rab14*-S25N (n = 8) or empty pEGFP-Vector (n = 8) as control. Data are presented as mean ± SEM. **P < 0.01, ***P < 0.001, pEGFP vs. *Rab14*-Q70L or *Rab14*-S25N (Students t-test, paired, two-tailed).

4.4.3 Knockdown of Rab12 as a new TBC1D1 interacting candidate in *EDL* and *Soleus* muscle of C57BL/6J mice

To assess the hypothesis that RAB12 accounts for an increased degradation of GLUT4 during TBC1D1 absence, a knockdown of *Rab12* was conducted in *EDL* and *Soleus* muscle by IVE with siRNA oligonucleotides (3.1.11). One week later, insulin-induced *ex vivo* glucose transport was measured. Furthermore, knockdown was evaluated on mRNA and protein level and GLUT4 protein abundance was looked at in *EDL* and *Soleus* muscle.

Changes in RAB12 expression might have a functional impact on translocation of the glucose transporter to the plasma membrane. To test this, a glucose uptake assay was performed *ex vivo* (3.2.7). No differences in glucose transport could be detected between control and target-siRNA muscles, neither at basal nor at insulin-stimulated state (Figure 4.25A, B).

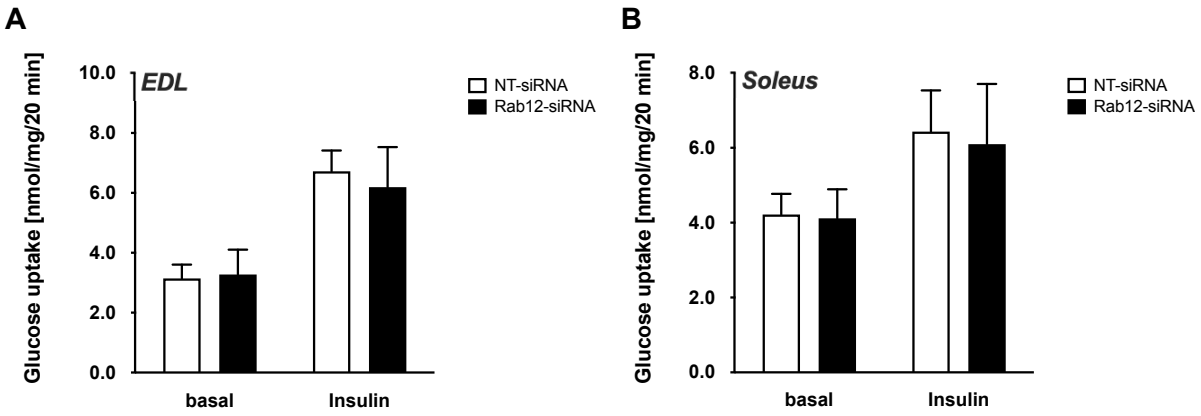

Figure 4.25: Insulin-stimulated *ex vivo* glucose uptake in *EDL* and *Soleus* muscle after *Rab12*-knockdown. Skeletal muscles were isolated and assayed for insulin-induced [^{3}H]-deoxyglucose uptake. *EDL* (A; n = 7-10) and *Soleus* muscle (B; n = 6-9) from C57BL/6J mice one week after IVE with *Rab12*-siRNA. Data are presented as mean ± SEM.

To assess the efficiency of the knockdown, *Rab12* mRNA gene expression was measured by qPCR analysis (3.3.9). *Rab12* mRNA expression was reduced by 72.06 % in transfected *EDL* and 89.74 % in *Soleus* muscle (Figure 4.26) compared to muscles transfected with non-target siRNA oligonucleotides.

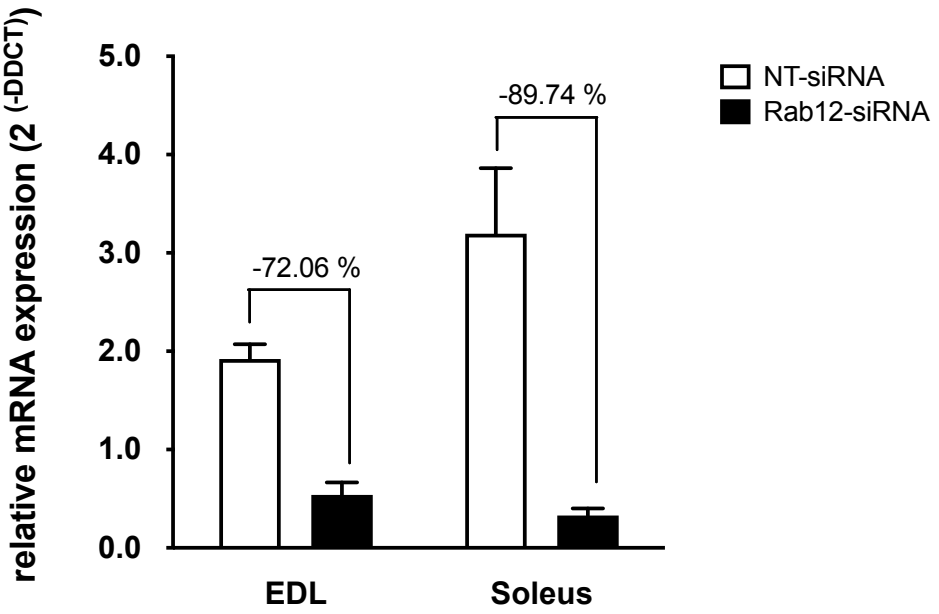

Figure 4.26: Gene expression of *Rab12* after knockdown in *EDL* and *Soleus* muscle with siRNA oligonucleotides.
Relative mRNA expression of *Rab12* (n = 2) in relation to 36B4 as housekeeper in *EDL* and *Soleus* muscle of C57BL/6J mice after IVE with *Rab12*-siRNA. Data are presented as mean ± SEM.

In line with this, RAB12 protein abundance was decreased by about two third after the knockdown in *EDL* and ~80 % in *Soleus* muscle (Figure 4.27A). GLUT4 protein was unchanged after treatment with *Rab12*-siRNA compared to controls (Figure 4.27B).

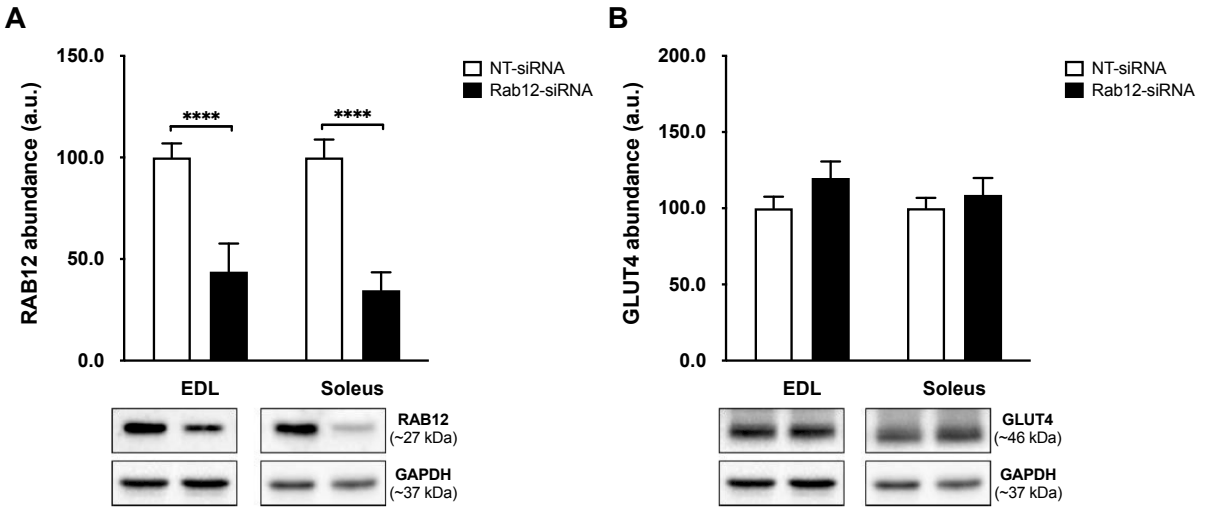

Figure 4.27: Protein abundance of *Rab12* after knockdown in *EDL* and *Soleus* muscle with siRNA.
Western Blot quantification of RAB12 (A) and GLUT4 (B) protein abundance (n = 4) in relation to GAPDH in *EDL* and *Soleus* muscle of C57BL/6J mice after IVE with *Rab12*-siRNA. Data are presented as mean ± SEM. ****P < 0.0001, non-target (NT)-siRNA vs. *Rab12*-siRNA (Students t-test with Welch's correction, unpaired, two-tailed).

5 Discussion

5.1 High fat diet feeding attenuates the effect of TBC1D1- and TBC1D4-deficiency in mice

The aim of this project was to study the impact of combined deficiency of the Rab-GTPase activating proteins (RabGAPs) TBC1D1 and TBC1D4 on glucose metabolism under increased fat intake. To address this question, previously described *Tbc1d1*- (D1KO), *Tbc1d4*- (D4KO) and double-deficient (D1/4KO) mice were used [79].

Can RabGAP-deficiency protect mice from diet induced obesity? The NMR measurements revealed that there were no relevant differences in body weight and lean mass among mice of the different genotypes on HFD. D1/4KO mice developed more body fat mass than WT mice in later stages of the experiment. Although not significant in D1KO mice, the data suggest that loss of TBC1D1 seems to account for this effect more than TBC1D4-deficiency. However, partial compensation of the RabGAPs in single knockout mice might explain why the difference is only evident in D1/4KO animals.

The results contradict the expectations based on previous studies with these mice on SD [79], finding a reduction of body weight in TBC1D1-, TBC1D4- and double-deficient mice. Experiments with D1KO mice showed a reduction in body weight also on HFD [91]. In this study, also lean mass and body fat were reduced. Another study analyzed Leptin and *Tbc1d1* double-deficient mice (D1KO-ob/ob) on HFD and reported a decrease in body weight due to *Tbc1d1*-deficiency compared to Leptin-deficient mice resulting from lower body fat and lean mass [97].

The opposing result of this study cannot be explained so far. However, it is noteworthy that the effect in body weight in all the studies was relatively small and not in every case clearly caused by increased body fat content. In humans, a mutation in the TBC1D1 gene leading to an amino acid exchange (R125W) between the PTB-domains of the protein is even associated with a higher risk for familial obesity [98, 99].

The limitations of this study are, that neither food intake nor energy recovery in the gut were measured. It might be that D1/4KO mice eat more than WT animals or are able to resorb more energy containing substrates from their nutrition.

In conclusion, RabGAP-deficiency in mice on C57BL/6J background did not have major impact on body composition under HFD feeding.

Does RabGAP-deficiency affect the ability to clear glucose from the blood?

As previously reported for mice on SD [79, 81], plasma glucose concentrations after 16 hours fasting were lower in D4KO and D1/4KO than in WT mice during this study. Glucose and insulin tolerance were reduced in D4KO and/or D1/4KO mice. These results confirm previous studies with *Tbc1d1*- and *Tbc1d4*-deficient mice on SD, suggesting that TBC1D4 predominantly determines the *in vivo* phenotype of D1/4KO mice in relation to glucose homeostasis and insulin resistance [84]. Consistent with this, a study with human carriers of a nonsense variant of the *TBC1D4* gene reports an impaired glucose tolerance as well as a reduction in fasting plasma glucose in these individuals [100]. In this study, single knockout animals were not affected as severe as double knockouts by their RabGAP deficiency. A possible explanation for this is that the remaining RabGAP might be able to compensate for the function of the other. AICAR tolerance again seems to be determined by TBC1D1. Deficiency of the protein led to lower blood glucose levels in D4KO and D1/4KO than in WT mice during AICAR tolerance test. This, together with the tendency towards an impaired AICAR tolerance of D1KO mice supports the hypothesis that TBC1D1 is the important RabGAP in the AMPK-dependent glucose uptake, since it is still present in TBC1D4-deficient mice. In 2016, Chen *et al*. showed that mice carrying a *Tbc1d1*^{Ser231Ala}-knockin mutation had a reduced AICAR tolerance and impaired AICAR-induced glucose uptake. In addition, GLUT4 content at the plasma membrane after AICAR-stimulation did not increase compared to basal level. Insulin tolerance was not affected by the mutation [92]. In contrast, TBC1D4-deficiency leads to increased basal glucose uptake in isolated white adipocytes despite of the lower GLUT4 abundance in this tissue [86]. This and the proposed function of the RabGAPs in insulin secretion [101-103] could be causal for the decreased postprandial blood glucose concentrations in D4KO and D1/4KO mice.
Taken together, the results support the hypothesis, that TBC1D4 is the predominant RabGAP in insulin-dependent glucose clearance from the blood, while TBC1D1 is crucial for AICAR-regulated glucose clearance.

Why does feeding a high fat diet not worsen the metabolic phenotype of RabGAP-deficient mice?
Previous studies have demonstrated that D1KO, D4KO and D1/4KO mice were unable to use glucose as a major energy fuel in skeletal muscle and adipose tissue because their amount of glucose transporter 4 (GLUT4) was reduced with concomitant RabGAP- deficiency. Therefore, these mice switched their substrate preference from glucose to fat [104]. This switch was associated with elevated hepatic triglycerides and reduced glycogen content [79]. After HFD feeding, no changes in glycogen or triglyceride storage could be detected in the liver. Comparing SD and HFD results, it becomes clear that hepatic triglyceride content in WT mice was increased under HFD conditions, resulting from a higher intake of fatty acids with the diet. In contrast, triglyceride levels of RabGAP deficient mice were comparable between SD and

HFD, probably resulting from the improved ability to use these as energy source. A hepatic glycogen reduction, which was observed in SD-fed mice was not significant in HFD-fed animals. From skeletal muscle and adipose specific GLUT4 knockout mice an increased conversion of glucose to fatty acids was reported [105]. If the RabGAP-deficient mice reproduce this phenotype, a higher availability of fatty acids would possibly inhibit this reaction, resulting in higher glycogen levels in liver of HFD fed mice. Consequently, the effect that was observed in SD mice might be masked in HFD animals. This also comes into play, looking at skeletal muscle, where SD fed mice had increased glycogen content, although glucose uptake into skeletal muscle was severely impaired. This effect is again comparable to results from skeletal muscle specific GLUT4 knockout mice. These mice show a complex counter regulation of increased glycogen synthesis and decreased glycogen breakdown [15]. Unpublished results from our group could also demonstrate an up regulation of glycogen synthase activity in skeletal muscle of D1/4KO mice on SD [106]. Nevertheless, in quadriceps muscle from HFD-fed mice, no alteration in glycogen content could be detected. Maybe the high availability of fat leads to an inhibition of glycogen synthesis. Consistent with the results from SD-fed mice, triglyceride content in muscle was unchanged in RabGAP-deficient mice fed a HFD.

In summary, high fat diet feeding to RabGAP-deficient mice leads to attenuation of their metabolic phenotype probably due to their improved ability to utilize fat as an energy source.

5.2 Contribution of TBC1D1 and TBC1D4 to contraction-induced glucose uptake is muscle specific

TBC1D1 and TBC1D4 both are downstream targets of AMPK [72, 73, 78], to which a key role in contraction-induced glucose uptake in skeletal muscle is attributed [107]. In accordance with that, AICAR-stimulated glucose uptake differed between D1KO and D4KO mice in glycolytic *EDL* and oxidative *Soleus* muscle [79]. In addition, there is evidence that TBC1D1 and TBC1D4 vary in their number of phosphorylation sites targeted by contraction or exercise [42, 73, 108]. However, no study has directly compared the contribution of TBC1D1 and TBC1D4 to contraction-induced glucose uptake in a functional approach.

Therefore, this work aimed to assess the effect of TBC1D1- and TBC1D4-deficiency on glucose transport stimulated by skeletal muscle contraction in an *ex vivo* setting (4.2).

The differences observed depended on the muscle type. Contraction-induced glucose uptake into *EDL* muscle was reduced when TBC1D1 was missing, and this effect was independent of contraction force ($Force_{max}$) or endurance (Time for Half-Capacity) of the muscle.

In *Soleus* muscle, only the combined deficiency of both RabGAPs caused a significant reduction of contraction-induced glucose transport, although the endurance of contraction performance was even improved for D1/4KO muscles. Still contraction-stimulated glucose transport was not blunted in D1/4KO mice.

It was previously reported that TBC1D1-deficiency is accompanied by a GLUT4-deficit in the *EDL* muscle [79, 83, 90] and other muscle types that predominantly express TBC1D1 instead of TBC1D4. Stöckli *et al*. demonstrated in 2015, that this deficit is directly related to TBC1D1 abundance since it can be recovered by TBC1D1 expression in TA muscle [83]. Accordingly, TBC1D4-deficiency causes a reduction in GLUT4 protein abundance in the *Soleus* muscle where it is predominantly expressed [79]. The amount of GLUT4 transporter determines to a large extent the capability of the muscle to take up glucose. Mice that completely lack GLUT4 in the skeletal muscle showed ~ 75 % reduction in basal glucose transport in the *Soleus* [15]. However, the contraction-induced glucose uptake in *Soleus* muscle of D4KO mice was not reduced compared to WT. This contradicts the theory, that GLUT4 is the rate limiting parameter, at least in *Soleus* muscle.

In *EDL*, a combined stimulation with insulin and contraction that aimed to achieve the highest possible recruitment of GLUT4 transporters to the PM, exceeded the result of a single stimulus in WT but not D1/4KO mice. In *Soleus*, neither of the two stimuli was able to alter glucose uptake significantly in D1/4KO mice. A recent publication showed, that GLUT4 is not essential for overload-induced glucose uptake [109]. The study proposes GLUT1, GLUT3, GLUT6, and/or GLUT10 as mediators of this effect. It is possible that the remaining TBC1D1 in *Soleus* of D4KO mice regulates the translocation of a second glucose transporter.

In summary, the deficiency of TBC1D1 causes a reduction in the abundance of GLUT4 in *EDL* muscle. This GLUT4 deficit seems to be the reason for a substantial reduction in contraction-mediated glucose transport. In contrast, knockout of both RabGAPs is necessary to affect glucose transport in response to *Soleus* muscle contraction, despite a GLUT4 deficit in *Soleus* of D4KO mice.

5.3 Contraction-mediated glucose transport is regulated by TBC1D1 and TBC1D4 in a non-redundant and not solely AMPK-dependent manner

In line with previous studies this work underlines that TBC1D1 and TBC1D4 play critical but non-redundant roles skeletal muscle glucose homeostasis [84, 110]. When it comes to muscle contraction-mediated glucose transport the study provides new evidence that both RabGAPs act differently and muscle specific. Still their contribution in relation to their upstream kinase AMPK is not well understood. The AMPK/RabGAP signaling axis has been implicated to play a critical role in this pathway. However, the importance of AMPK in the contraction- and exercise-mediated signaling pathway in the skeletal muscle is being discussed controversially [92, 107, 111]. A number of alternative signaling pathways have been implicated to play a role in this context [30, 38, 47, 112-116].

This study aimed to clarify the contribution of TBC1D1 and TBC1D4 in AMPK-dependent signaling by using novel mouse models that combine muscle-specific AMPKα_2 inactivity (TG) with additional deficiency in either one or both RabGAPs (TG-D1KO, TG-D4KO, TG-D1/4KO).

In accordance with previous studies [57], the inactivation of AMPK in TG mice substantially reduced glucose transport after contraction stimulation in *EDL* and *Soleus* muscle compared to WT. In glycolytic *EDL* muscle of TG-D1KO and TG-D1/4KO mice a further reduction of glucose transport was measured. This was even indicated at basal state although not significant, which agrees with other studies showing that basal glucose transport is strongly correlated with the GLUT4 abundance in skeletal muscle and adipose tissue cells [117-120]. However, this effect cannot, at least not exclusively, be explained by a marked decrease in GLUT4 transporter expression in *EDL* of TG-D1KO and TG-D1/4KO mice, since in *Soleus* muscle, only the absence of both RabGAPs was sufficient to reduce glucose transport in comparison to TG muscles.

Still, in *EDL* of D1/4KO mice there was a significant response to contraction compared to basal glucose transport rates. This means that inactivation of AMPK and RabGAP deficiency are obviously not sufficient to completely abrogate contraction-mediated glucose fluxes.

This hints towards an additional pathway that ensures contraction-stimulated glucose transport by circumventing the canonical AMPK-RabGAP pathway.

In contrast to the glycolytic *EDL*, contraction-stimulated glucose transport into the oxidative *Soleus* muscle of TG-D1/4KO mice did not differ from basal state, indicating that in this muscle the AMPK-RabGAP signaling axis is responsible for 100 % of the effect.

These results hint towards a different relevance of the AMPK-RabGAP pathway depending on the specific muscle type, which is characterized by a specific fiber type composition, since

different fiber types vary in their metabolic properties [121]. Also, the composition of the AMPK subunits differs between these muscle types. It was shown that in *Soleus* muscle the AMPK α_2 subunit exclusively pairs with β_1, whereas in *EDL* it associates with both β_1 and β_2 [122].

In line with the data from *ex vivo* contraction-stimulated glucose uptake, the exercise capacity of mice with APMKα_2 inactivation was impaired, marked by a decreased time to exhaustion and a lower VO_2max on the treadmill. In TG-D1KO and (by trend) in TG-D1/4KO mice the time to exhaustion was further decreased. In contrast, the running capacity of TG-D4KO mice was comparable to TG animals. This indicates a higher relevance for the TBC1D1-AMPK axis for maintaining physical fitness.
According to these results, previous studies examining *Tbc1d1* knockout mice observed an impaired running capacity of these animals [83]. Furthermore, it was demonstrated that the TG mouse model was unable to perform high-intensity exercise but not low-intensity exercise on a treadmill [123]. Unlike in humans, skeletal muscle glycogen stores do not necessarily correlate with exercise endurance in mice [124]. Instead, increased oxidation of glucose from liver glycogen or the oxidation of fatty acids in skeletal muscle may provide an energy source during acute exercise [124, 125]. Muscle-specific AMPK$\alpha_1\alpha_2$ double knockout resulted in an impaired exercise capacity caused by a decreased mitochondrial oxidative capacity and mitochondrial substrate utilization [126]. Recently, Radhakrishnan *et al*. found out, that the improved exercise capacity of cyclophilin-D knockout mice was associated with enhanced glucose uptake via the AMPK-TBC1D1 signaling nexus [127].

Overall, the results from this thesis indicate that at least in glycolytic muscles a stimulation of glucose uptake is possible, independently of AMPKα_2, TBC1D1 and TBC1D4. Glucose uptake into *EDL* muscle of TG-D1/4KO mice increased significantly after contraction.
Previous studies investigating the role of AMPK in contraction-induced glucose uptake have found that *EDL* and *Soleus* muscles of AMPKα_2 kinase-dead and knockout mice did not show AICAR- but contraction-stimulated glucose uptake *ex vivo* [57, 128].
In addition, there are conflicting results about the role of AMPK activation for glucose uptake during muscle exercise. Studies with AMPKβ_1/β_2 double-deficient mice report that contraction-induced glucose transport was severely decreased in skeletal muscle [107] on the other hand deletion of AMPKα_1 and AMPKα_2 had almost no effect [111].
There have been several AMPK-independent mechanisms discussed, that are involved in contraction- or exercise-induced glucose uptake. Most obvious candidates are AMPK-related kinases. Like AMPK itself, they become activated by their upstream kinase LKB1. LKB1 has been demonstrated to play a key role in AICAR and contraction-induced glucose uptake in muscle [116]. Thus, five of its downstream targets that have been mentioned in the context of

glucose homeostasis or contraction-related energy metabolism [38, 129-131] have been tested for differential regulation in TG, TG-D1KO, TG-D4KO and TG-D1/4KO mice by real-time qPCR. The experiment revealed *Nuak1* coding for AMPK-related protein kinase 5 (ARK5) as a promising candidate being upregulated in *gastrocnemius* of TG mice compared to WT animals. However, on protein level this upregulation could not be confirmed. Previous studies have shown that the abundance of ARK5 which is also known as NUAK family SNF1-like kinase 1 (NUAK1) seems to be highest in highly oxidative tissues such as brain, heart and *Soleus* muscle [132]. It can be phosphorylated by muscle contraction, AICAR and insulin [133]. However, it was also shown that its phosphorylation due to contraction or AICAR incubation seems not to be sufficient to activate ARK5. Therefore, an additional mechanism was needed. Although expression of the sucrose nonfermenting AMPK-related kinase (SNARK/NUAK2) was unaltered, it also remains an interesting candidate since it was demonstrated to become activated by AICAR, contraction and exercise in skeletal muscle [38, 134].

Besides, AMPK-related kinases reactive oxygen species (ROS) can induce glucose uptake during very intense electrical stimulation *in vitro*. Incubation of mouse *EDL* muscle with the unspecific ROS scavenger N-acetylcysteine (NAC) could decrease glucose uptake induced by electrical contraction-stimulation in AMPKα_2 kinase-dead and WT muscles to the same extent [36]. However, studies using a milder way of stimulation in the perfused rat hind limb found, that NAC was ineffective in reducing muscle glucose uptake [135]. In addition, in humans NAC did not decrease exercise-induced glucose uptake making an increased participation of ROS *in vivo* unlikely [36].

The Ras-related C3 Botulinum toxin substrate 1 (Rac1), a small Rho-GTPase has been proven to be activated by mechanical stress or stretching of the muscle during contraction [136-138]. Muscle-specific Rac1 knockout mice displayed reduced *ex vivo* contraction- and *in vivo* exercise-stimulated glucose uptake [139]. Interestingly, AMPKα_2 kinase-dead mice with muscle-specific Rac1 knockout exhibited severely impaired contraction-induced glucose uptake *ex vivo*, whereas *in vivo* exercise-stimulated glucose transport was only partially reduced by Rac1 deficiency with no further effect of AMPKα2 inactivation [40].

In contrast to exercise and muscle contraction-mediated glucose transport, AMPK inactivation had no effect on postprandial blood glucose and plasma insulin levels.

After 16 h fasting and 1 h refeeding, the difference in blood glucose (BG) concentrations between TG-D1/4KO and WT mice was much clearer. Here it becomes obvious, that this effect is determined by the lack of TBC1D4, since the BG levels of TG-D4KO mice are also elevated. This has been previously shown in TBC1D4 knockout mice [89] and underlines the importance of TBC1D4 in the insulin-mediated glucose clearance from the blood. In contrast to Xie *et al*., plasma insulin concentrations were not changed in this study.

Postprandial hyperglycemia caused by *Tbc1d4* deficiency has also been observed in humans. A loss-of-function mutation in the *Tbc1d4*-gene of a Greenlandic Inuit population has been described to cause elevated postprandial blood glucose levels and an increased risk for type 2 diabetes. In line with that, a recent publication described suppressed AKT-TBC1D4 signaling in middle-aged obese individuals with type 2 diabetes [140].

The whole-body tolerance to the AMPK activator AICAR was slightly reduced in TG mice compared to WT. Although AMPKα_2 is the predominant catalytic isoform in skeletal muscle [50], its absence is only partially inhibiting glucose clearance from the blood. This has been shown before in AMPKα_2 knockout mice [128]. The TG mice used in this study are muscle and heart specific. This means that AMPK is still functional in adipose cells and liver and might account for the residual AICAR response.
Additional deficiency in *Tbc1d1* tended to cause a further reduction in AICAR tolerance. This again supports the theory that TBC1D1 is important in the AMPK-related glucose clearance from the blood. In contrast, AICAR tolerance of TG-D4KO and (by trend) TG-D1/4KO mice was not impaired. It has been shown, that the presence of liver kinase B1 (LKB1) is essential for AMPK-activation by AICAR [141]. As discussed above, it might be possible that LKB1 supports the activation of other, maybe AMPK-related kinases, that might target TBC1D4.

In summary, this work demonstrates a non-redundant function of TBC1D1 and TBC1D4 in regulation of whole-body glycemia related to exercise and fasting-refeeding. Moreover, it provides new information about their function in contraction-induced glucose transport into skeletal muscle. Whereas TBC1D1 is essential for exercise capacity and contraction-mediated glucose transport into skeletal muscle, TBC1D4 seems to play an important role in the postprandial clearance of glucose.

5.4 GLUT4 protein abundance is regulated by TBC1D1 via its GAP-domain

In kinase-dead AMPKα_2 and RabGAP-deficient mice, the abundance of GLUT4 protein in skeletal muscle is reduced. This effect can be referred to their RabGAP-deficiency, since it does not occur in TG mice and has also been described in D1KO, D4KO and D1/4KO mice with functional AMPK [79]. There it was also demonstrated that the GLUT4-deficit develops after translation of the gene. Although the current study found a significant reduction in the GLUT4 coding *Scl2a4* gene in *gastrocnemius* muscle of TG-D1/4KO mice, it was demonstrated before, that expression of TBC1D1 in TA muscle of WT and D1KO mice via *in vivo* electrotransfection (IVE) was sufficient to increase GLUT4 protein abundance [83]. The functional domain, however, that accounts for the regulation of GLUT4, was still unknown. Thus, this study focused on the functional GAP- and PTB-Domain of TBC1D1. As proven by Stöckli *et al.* before [83], the expression of wildtype *Tbc1d1* (*Tbc1d1*-WT) in TA muscle of D1KO mice using the IVE method led to an increase in GLUT4 protein after one week. This underlines that TBC1D1 protein itself is sufficient to rescue the GLUT4 deficit in TA muscle of D1KO mice regulating GLUT4 protein abundance. Expressing a TBC1D1 mutant with an inactive PTB-Domain (*Tbc1d1*-R125W), GLUT4 levels achieved similar amounts as after *Tbc1d1*-WT transfection. In humans the R125W mutant was linked to a higher risk for familial obesity in women [98, 99]. However, based on the presented results, the N-terminal PTB domain is not essential in the regulation of GLUT4 abundance.

In contrast, the expression of another mutant, *Tbc1d1*-R941K had no significant impact on GLUT4 protein levels. This mutation leads to an inactivation of the GAP-activity of the protein [80]. Thus, it can be concluded that TBC1D1 needs its GAP-Domain to regulate GLUT4 protein abundance. If it is missing, GLUT4 content is drastically reduced.

In line with these results for TBC1D1 Chie *et al.* reported in 2016 that the GAP-activity of TBC1D4 maintains GLUT4 abundance in a cell/tissue specific manner and that its inactivation causes lysosomal degradation of GLUT4 [89].

In the literature several targets of TBC1D1 GAP-activity have been identified. Silencing of RAB8A and RAB14 inhibited insulin-stimulated GLUT4 translocation in L6 myotubes and rescued the intracellular retention of GLUT4 at basal state that was impaired by TBC1D1 knockdown [61].

Moreover, *Rab8a* has previously been shown to play a role in insulin-regulated GLUT4 trafficking in C2C12 cells [142].

In the absence of TBC1D1 monomeric Rab-GTPases downstream of TBC1D1 are considered to be more active, since deactivation by their RabGAP is missing. However, expressing a constitutively active *Rab8a*-Q67L mutant in C57BL/6J mice did not mimic the effect of TBC1D1-deficiency regarding muscular GLUT4 levels. The dominant-negative *Rab8a*-T22N

mutant was transfected into D1KO muscles to rescue the GLUT4 protein deficit. Surprisingly, GLUT4 abundance was further reduced. Since RAB8A is playing a key role in the translocation of GLUT4 storing vesicles to the plasma membrane [28, 61, 142], it is possible, that this process is disturbed leading to increased degradation of GLUT4.

RAB14 was implicated to play a role in GLUT4 trafficking especially in skeletal muscle. It is also known to be a target of TBC1D1 and TBC1D4 [61].
Expression of the constitutively active *Rab14*-Q70L mutant in TA muscle of C57BL/6J mice caused a significant increase in GLUT4 protein abundance compared to control muscles, whereas expression of the dominant negative *Rab14*-S25N mutant in TA muscles of D1KO mice did not affect GLUT4 protein abundance.
Taken together, RAB14 cannot be the wanted interaction partner of TBC1D1 responsible for increased GLUT4 degradation. Studies in 3T3-L1 adipocytes with *Rab14*-mutants could show, that wild-type and constitutively active *Rab14*-Q70L-mutant but not inactive *Rab14*-S25N-mutant were extensively co-expressed with GLUT4 and IRAP in early endosomal compartments [143]. Thus, it is possible, that it leads the sorting of GLUT4 more towards recycling processes, which inhibits degradation of the glucose transporter.

RAB12 is a previously unknown *in vitro* target of TBC1D1. It is playing a role in autophagy processes since it was shown to control the degradation of transferrin receptor (TfR) and to regulate autophagy through controlling PAT4 (proton/amino acid transporter 4) trafficking from recycling endosomes to lysosomes [144-146]. Unpublished data of our group could show that RAB12 is also a potent interaction partner increasing its GTP-hydrolysis activity when TBC1D1 is present. Thus, it is a possible candidate to increase GLUT4 degradation processes by constant activation in case of TBC1D1 loss.
The knockdown was conducted with siRNA oligonucleotides since there were no mutants available. *EDL* and *Soleus* muscle were transfected to reduce the amount of siRNA oligonucleotides used and to facilitate the measurement of *ex vivo* glucose uptake as functional readout. Although the knockdown was very efficient on mRNA level and the protein amount was at least reduced by two third, no changes could be detected in GLUT4 protein abundance or insulin-stimulated glucose transport. Thus, *Rab12* can be excluded as possible mediator of TBC1D1 regulated GLUT4 protein abundance.

6 Outlook

To find the mechanism behind the residual contraction-mediated glucose transport in *EDL* of TG-D1/4KO mice, further investigation is necessary. Expression of other AMPK-related kinases and should be evaluated on protein level. Their activation following muscle contraction can be assessed by their subsequent phosphorylation status. Our group recently concentrated on Rac1, which was pharmacologically inhibited in *EDL* muscle of RabGAP (and AMPKα_2) inactive mice following muscle contraction. The treatment with the inhibitor NSC23766 completely abolished contraction-mediated glucose transport into D1/4KO and TG-D1/4KO muscles, demonstrating that TBC1D1, TBC1D4 and Rac1 operate in concert downstream of AMPK to regulate GLUT4 translocation.

Regarding the tissue-specific GLUT4 transporter deficit accompanying RapGAP deficiency, it would be interesting to continue the IVE-studies with further Rab-GTPases that are targeted by TBC1D1 and/or TBC1D4. Besides RAB8A and RAB14 that were already tested, RAB2A, 8B and 10 and, more recently, RAB13 and 28 are known to be a target of both RabGAPs [34].

7 Literature

1. IDF, *IDF Diabetes Atlas, 9th edn.* 2019, International Diabetes Federation: Brussels, Belgium.
2. IDF, *IDF Diabetes Atlas - Eighth Edition*. 2017, International Diabetes Federation: Brussels, Belgium.
3. Groop, L. and F. Pociot, *Genetics of diabetes--are we missing the genes or the disease?* Molecular and cellular endocrinology, 2014. **382**(1): p. 726-739.
4. Ahlqvist, E., et al., *Novel subgroups of adult-onset diabetes and their association with outcomes: a data-driven cluster analysis of six variables.* The Lancet Diabetes & Endocrinology, 2018. **6**(5): p. 361-369.
5. Zaharia, O.P., et al., *Risk of diabetes-associated diseases in subgroups of patients with recent-onset diabetes: a 5-year follow-up study.* Lancet Diabetes Endocrinol, 2019. **7**(9): p. 684-694.
6. American-Diabetes-Association, *2. Classification and Diagnosis of Diabetes.* Diabetes Care, 2017. **40**(Supplement 1): p. S11-S24.
7. Liston, A., J.A. Todd, and V. Lagou, *Beta-Cell Fragility As a Common Underlying Risk Factor in Type 1 and Type 2 Diabetes.* Trends in molecular medicine, 2017. **23**(2): p. 181-194.
8. Kwak, S.H. and K.S. Park, *Recent progress in genetic and epigenetic research on type 2 diabetes.* Experimental & molecular medicine, 2016. **48**.
9. WHO, *Global Report on Diabetes*. 2016, World Health Organization (WHO): Geneva, Swiss.
10. Muoio, D.M. and C.B. Newgard, *Mechanisms of disease:Molecular and metabolic mechanisms of insulin resistance and beta-cell failure in type 2 diabetes.* Nature reviews. Molecular cell biology, 2008. **9**(3): p. 193-205.
11. Di Meo, S., S. Iossa, and P. Venditti, *Improvement of obesity-linked skeletal muscle insulin resistance by strength and endurance training.* The Journal of endocrinology, 2017. **234**(3).
12. Chadt, A., et al., *Molecular links between Obesity and Diabetes: "Diabesity"*, in *Endotext*, K.R. Feingold, et al., Editors. 2000: South Dartmouth (MA).
13. Björnholm, M., et al., *Insulin receptor substrate-1 phosphorylation and phosphatidylinositol 3-kinase activity in skeletal muscle from NIDDM subjects after in vivo insulin stimulation.* Diabetes, 1997.
14. Goodyear, L.J., et al., *Insulin receptor phosphorylation, insulin receptor substrate-1 phosphorylation, and phosphatidylinositol 3-kinase activity are decreased in intact skeletal muscle strips from obese subjects.* The Journal of clinical investigation, 1995. **95**(5): p. 2195-2204.
15. Kim, Y.B., et al., *Muscle-specific deletion of the Glut4 glucose transporter alters multiple regulatory steps in glycogen metabolism.* Mol Cell Biol, 2005. **25**(21): p. 9713-23.
16. Bogan, J.S., *Regulation of Glucose Transporter Translocation in Health and Diabetes.* Annual Review of Biochemistry, 2012. **81**(1): p. 507-532.
17. Roach, P.J., et al., *Glycogen and its metabolism: some new developments and old themes.* Biochemical Journal, 2012. **441**: p. 763-787.
18. Garvey, W.T., et al., *Evidence for defects in the trafficking and translocation of GLUT4 glucose transporters in skeletal muscle as a cause of human insulin resistance.* The Journal of clinical investigation, 1998. **101**(11): p. 2377-2386.
19. Adams, J.M., 2nd, et al., *Ceramide content is increased in skeletal muscle from obese insulin-resistant humans.* Diabetes, 2004. **53**(1): p. 25-31.
20. Goodpaster, B.H. and D.E. Kelley, *Skeletal muscle triglyceride: marker or mediator of obesity-induced insulin resistance in type 2 diabetes mellitus?* Curr Diab Rep, 2002. **2**(3): p. 216-22.

21. Krssak, M., et al., *Intramyocellular lipid concentrations are correlated with insulin sensitivity in humans: a 1H NMR spectroscopy study.* Diabetologia, 1999. **42**(1): p. 113-6.
22. Morino, K., K.F. Petersen, and G.I. Shulman, *Molecular mechanisms of insulin resistance in humans and their potential links with mitochondrial dysfunction.* Diabetes, 2006. **55 Suppl 2**: p. S9-S15.
23. Cooney, G.J., et al., *Muscle long-chain acyl CoA esters and insulin resistance.* Ann N Y Acad Sci, 2002. **967**: p. 196-207.
24. Bostrom, P., et al., *The SNARE protein SNAP23 and the SNARE-interacting protein Munc18c in human skeletal muscle are implicated in insulin resistance/type 2 diabetes.* Diabetes, 2010. **59**(8): p. 1870-8.
25. Jaldin-Fincati, J.R., et al., *Update on GLUT4 Vesicle Traffic: A Cornerstone of Insulin Action.* Trends in endocrinology and metabolism: TEM, 2017. **28**(8): p. 597-611.
26. Foley, K., S. Boguslavsky, and A. Klip, *Endocytosis, recycling, and regulated exocytosis of glucose transporter 4.* Biochemistry, 2011. **50**(15): p. 3048-61.
27. Douen, A.G., et al., *Exercise induces recruitment of the "insulin-responsive glucose transporter". Evidence for distinct intracellular insulin- and exercise-recruitable transporter pools in skeletal muscle.* The Journal of biological chemistry, 1990. **265**(23): p. 13427-13430.
28. Sun, Y., et al., *Myosin Va mediates Rab8A-regulated GLUT4 vesicle exocytosis in insulin-stimulated muscle cells.* Molecular Biology of the Cell, 2014. **25**(7): p. 1159-1170.
29. DeFronzo, R.A., et al., *The effect of insulin on the disposal of intravenous glucose. Results from indirect calorimetry and hepatic and femoral venous catheterization.* Diabetes, 1981. **30**(12): p. 1000-7.
30. Sylow, L., et al., *Rac1 Is a Novel Regulator of Contraction-Stimulated Glucose Uptake in Skeletal Muscle.* Diabetes, 2013. **62**(4): p. 1139-1151.
31. Sylow, L., et al., *Akt and Rac1 signaling are jointly required for insulin-stimulated glucose uptake in skeletal muscle and downregulated in insulin resistance.* Cellular Signalling, 2014. **26**(2): p. 323-331.
32. JeBailey, L., et al., *Ceramide- and oxidant-induced insulin resistance involve loss of insulin-dependent Rac-activation and actin remodeling in muscle cells.* Diabetes, 2007. **56**(2): p. 394-403.
33. Mafakheri, S., et al., *AKT and AMP-activated protein kinase regulate TBC1D1 through phosphorylation and its interaction with the cytosolic tail of insulin-regulated aminopeptidase IRAP.* J Biol Chem, 2018. **293**(46): p. 17853-17862.
34. Mafakheri, S., A. Chadt, and H. Al-Hasani, *Regulation of RabGAPs involved in insulin action.* Biochem Soc Trans, 2018. **46**(3): p. 683-690.
35. Eickelschulte, S., et al., *AKT/AMPK-mediated phosphorylation of TBC1D4 disrupts the interaction with insulin-regulated aminopeptidase.* J Biol Chem, 2021. **296**: p. 100637.
36. Merry, T.L., et al., *N-Acetylcysteine infusion does not affect glucose disposal during prolonged moderate-intensity exercise in humans.* The Journal of physiology, 2010. **588**(Pt 9): p. 1623-1634.
37. Witczak, C.A., et al., *CaMKII regulates contraction- but not insulin-induced glucose uptake in mouse skeletal muscle.* American Journal of Physiology - Endocrinology And Metabolism, 2010. **298**(6).
38. Koh, H.-J., et al., *Sucrose nonfermenting AMPK-related kinase (SNARK) mediates contraction-stimulated glucose transport in mouse skeletal muscle.* Proceedings of the National Academy of Sciences, 2010. **107**(35): p. 15541-15546.
39. Jensen, T.E., et al., *Contraction-stimulated glucose transport in muscle is controlled by AMPK and mechanical stress but not sarcoplasmatic reticulum Ca2+ release.* Molecular Metabolism, 2014. **3**(7): p. 742-753.
40. Sylow, L., et al., *Rac1 and Ampk Account for the Majority of Muscle Glucose Uptake Stimulated by Ex Vivo Contraction but not in Vivo Exercise.* Diabetes, 2017. **66**(6).
41. Richter, E.A. and M. Hargreaves, *Exercise, GLUT4, and skeletal muscle glucose uptake.* Physiol Rev, 2013. **93**(3): p. 993-1017.

42. Espelage, L., H. Al-Hasani, and A. Chadt, *RabGAPs in skeletal muscle function and exercise.* J Mol Endocrinol, 2020. **64**(1): p. R1-R19.
43. Jensen, T.E., et al., *Is contraction-stimulated glucose transport feedforward regulated by Ca2+?* Experimental physiology, 2014. **99**(12): p. 1562-1568.
44. Kane, S. and G.E. Lienhard, *Calmodulin binds to the Rab GTPase activating protein required for insulin-stimulated GLUT4 translocation.* Biochemical and biophysical research communications, 2005. **335**(1): p. 175-180.
45. Sylow, L., et al., *Rac1 – a novel regulator of contraction‐stimulated glucose uptake in skeletal muscle.* Experimental Physiology, 2014. **99**(12): p. 1574-1580.
46. Toyoda, T., et al., *Myo1c Regulates Glucose Uptake in Mouse Skeletal Muscle.* Journal of Biological Chemistry, 2011. **286**(6): p. 4133-4140.
47. Merry, T.L., et al., *Skeletal muscle glucose uptake during contraction is regulated by nitric oxide and ROS independently of AMPK.* American Journal of Physiology - Endocrinology and Metabolism, 2010. **298**(3).
48. Ross, R.M., et al., *Local nitric oxide synthase inhibition reduces skeletal muscle glucose uptake but not capillary blood flow during in situ muscle contraction in rats.* Diabetes, 2007. **56**(12): p. 2885-2892.
49. Pinter, K., et al., *Localisation of AMPK γ subunits in cardiac and skeletal muscles.* Journal of muscle research and cell motility, 2013. **34**(5-6): p. 369-378.
50. Kjøbsted, R., et al., *AMPK in skeletal muscle function and metabolism.* The FASEB Journal, 2017.
51. Treebak, J.T., et al., *A-769662 activates AMPK beta1-containing complexes but induces glucose uptake through a PI3-kinase-dependent pathway in mouse skeletal muscle.* American journal of physiology. Cell physiology, 2009. **297**(4): p. 52.
52. Xiao, B., et al., *Structure of mammalian AMPK and its regulation by ADP.* Nature, 2011. **472**(7342): p. 230-233.
53. Suter, M., et al., *Dissecting the role of 5'-AMP for allosteric stimulation, activation, and deactivation of AMP-activated protein kinase.* The Journal of biological chemistry, 2006. **281**(43): p. 32207-32216.
54. Corton, J.M., et al., *5-aminoimidazole-4-carboxamide ribonucleoside. A specific method for activating AMP-activated protein kinase in intact cells?* European journal of biochemistry, 1995. **229**(2): p. 558-565.
55. Sanders, M.J., et al., *Defining the mechanism of activation of AMP-activated protein kinase by the small molecule A-769662, a member of the thienopyridone family.* The Journal of biological chemistry, 2007. **282**(45): p. 32539-32548.
56. Göransson, O., et al., *Mechanism of action of A-769662, a valuable tool for activation of AMP-activated protein kinase.* The Journal of biological chemistry, 2007. **282**(45): p. 32549-32560.
57. Mu, J., et al., *A role for AMP-activated protein kinase in contraction- and hypoxia-regulated glucose transport in skeletal muscle.* Mol Cell, 2001. **7**(5): p. 1085-94.
58. Holmes, B.F., et al., *AMP kinase is not required for the GLUT4 response to exercise and denervation in skeletal muscle.* American journal of physiology. Endocrinology and metabolism, 2004. **287**(4): p. 43.
59. Hutagalung, A.H. and P.J. Novick, *Role of Rab GTPases in Membrane Traffic and Cell Physiology.* Physiological Reviews, 2011. **91**(1): p. 119-149.
60. Brewer, P.D., et al., *Rab14 limits the sorting of Glut4 from endosomes into insulin-sensitive regulated secretory compartments in adipocytes.* The Biochemical journal, 2016. **473**(10): p. 1315-1327.
61. Ishikura, S. and A. Klip, *Muscle cells engage Rab8A and myosin Vb in insulin-dependent GLUT4 translocation.* Am J Physiol Cell Physiol, 2008. **295**(4): p. C1016-25.
62. Zhou, Z., et al., *Rab28 is a TBC1D1/TBC1D4 substrate involved in GLUT4 trafficking.* FEBS letters, 2017. **591**(1): p. 88-96.
63. Lamb, C.A., A. Longatti, and S.A. Tooze, *Rabs and GAPs in starvation-induced autophagy.* Small GTPases, 2016. **7**(4): p. 265-269.

64. Longatti, A., et al., *TBC1D14 regulates autophagosome formation via Rab11- and ULK1-positive recycling endosomes.* The Journal of Cell Biology, 2012. **197**(5): p. 659-675.
65. Matsui, T. and M. Fukuda, *Rab12 regulates mTORC1 activity and autophagy through controlling the degradation of amino-acid transporter PAT4.* EMBO reports, 2013. **14**(5): p. 450-457.
66. Matsui, T., K. Noguchi, and M. Fukuda, *Dennd3 Functions as a Guanine Nucleotide Exchange Factor for Small GTPase Rab12 in Mouse Embryonic Fibroblasts.* Journal of Biological Chemistry, 2014. **289**(20): p. 13986-13995.
67. Matsui, T., T. Itoh, and M. Fukuda, *Small GTPase Rab12 regulates constitutive degradation of transferrin receptor.* Traffic (Copenhagen, Denmark), 2011. **12**(10): p. 1432-1443.
68. Amagai, Y., et al., *Rabin8 suppresses autophagosome formation independently of its guanine nucleotide-exchange activity towards Rab8.* Journal of biochemistry, 2015. **158**(2): p. 139-153.
69. An, D., et al., *TBC1D1 regulates insulin- and contraction-induced glucose transport in mouse skeletal muscle.* Diabetes, 2010. **59**(6): p. 1358-1365.
70. Roach, W.G., et al., *Substrate specificity and effect on GLUT4 translocation of the Rab GTPase-activating protein Tbc1d1.* The Biochemical journal, 2007. **403**(2): p. 353-358.
71. Chen, S., et al., *Complementary regulation of TBC1D1 and AS160 by growth factors, insulin and AMPK activators.* Biochem J, 2008. **409**(2): p. 449-59.
72. Pehmøller, C., et al., *Genetic disruption of AMPK signaling abolishes both contraction- and insulin-stimulated TBC1D1 phosphorylation and 14-3-3 binding in mouse skeletal muscle.* American Journal of Physiology - Endocrinology and Metabolism, 2009. **297**(3).
73. Vichaiwong, K., et al., *Contraction regulates site-specific phosphorylation of TBC1D1 in skeletal muscle.* The Biochemical journal, 2010. **431**(2): p. 311-320.
74. Jessen, N., et al., *Exercise increases TBC1D1 phosphorylation in human skeletal muscle.* American Journal of Physiology - Endocrinology and Metabolism, 2011. **301**(1).
75. Treebak, J.T., et al., *Potential role of TBC1D4 in enhanced post-exercise insulin action in human skeletal muscle.* Diabetologia, 2009. **52**(5): p. 891-900.
76. Ducommun, S., et al., *Thr649Ala-AS160 knock-in mutation does not impair contraction/AICAR-induced glucose transport in mouse muscle.* American Journal of Physiology - Endocrinology and Metabolism, 2012. **302**(9).
77. Geraghty, K.M., et al., *Regulation of multisite phosphorylation and 14-3-3 binding of AS160 in response to IGF-1, EGF, PMA and AICAR.* The Biochemical journal, 2007. **407**(2): p. 231-241.
78. Treebak, J.T., et al., *Identification of a novel phosphorylation site on TBC1D4 regulated by AMP-activated protein kinase in skeletal muscle.* American Journal of Physiology - Cell Physiology, 2010. **298**(2).
79. Chadt, A., et al., *"Deletion of both Rab-GTPase-activating proteins TBC1D1 and TBC1D4 in mice eliminates insulin- and AICAR-stimulated glucose transport [corrected].* Diabetes, 2015. **64**(3): p. 746-59.
80. Chadt, A., et al., *Tbc1d1 mutation in lean mouse strain confers leanness and protects from diet-induced obesity.* Nature Genetics, 2008. **40**(11): p. 1354-1359.
81. Wang, H., et al., *AS160 deficiency causes whole-body insulin resistance via composite effects in multiple tissues.* Biochemical Journal, 2013. **449**(2): p. 479-489.
82. Szekeres, F., et al., *The Rab-GTPase-activating protein TBC1D1 regulates skeletal muscle glucose metabolism.* American journal of physiology. Endocrinology and metabolism, 2012. **303**(4): p. 33.
83. Stockli, J., et al., *The RabGAP TBC1D1 plays a central role in exercise-regulated glucose metabolism in skeletal muscle.* Diabetes, 2015. **64**(6): p. 1914-22.
84. Hargett, S.R., N.N. Walker, and S.R. Keller, *Rab GAPs AS160 and Tbc1d1 play nonredundant roles in the regulation of glucose and energy homeostasis in mice.* Am J Physiol Endocrinol Metab, 2016. **310**(4): p. E276-88.

85. Cartee, G.D., *Roles of TBC1D1 and TBC1D4 in insulin- and exercise-stimulated glucose transport of skeletal muscle.* Diabetologia, 2015. **58**(1): p. 19-30.
86. Lansey, M.N., et al., *Deletion of Rab GAP AS160 modifies glucose uptake and GLUT4 translocation in primary skeletal muscles and adipocytes and impairs glucose homeostasis.* American journal of physiology. Endocrinology and metabolism, 2012. **303**(10): p. 86.
87. Stermann, T., et al., *Deletion of the RabGAP TBC1D1 leads to enhanced insulin secretion and fatty acid oxidation in islets from male mice.* Endocrinology, 2018.
88. Szekeres, F., et al., *The Rab-GTPase-activating protein TBC1D1 regulates skeletal muscle glucose metabolism.* American Journal of …, 2012.
89. Xie, B., et al., *The Inactivation of RabGAP Function of AS160 Promotes Lysosomal Degradation of GLUT4 and Causes Postprandial Hyperglycemia and Hyperinsulinemia.* Diabetes, 2016. **65**(11): p. 3327-3340.
90. Hargett, S.R., et al., *Deletion of the Rab GAP Tbc1d1 modifies glucose, lipid, and energy homeostasis in mice.* American Journal of Physiology - Endocrinology and Metabolism, 2015. **309**(3).
91. Dokas, J., et al., *Conventional knockout of Tbc1d1 in mice impairs insulin- and AICAR-stimulated glucose uptake in skeletal muscle.* Endocrinology, 2013. **154**(10): p. 3502-3514.
92. Chen, Q., et al., *A Tbc1d1Ser231Ala-knockin mutation partially impairs AICAR- but not exercise-induced muscle glucose uptake in mice.* Diabetologia, 2016. **60**(2): p. 336-345.
93. Laemmli, U.K., *Cleavage of structural proteins during the assembly of the head of bacteriophage T4.* Nature, 1970. **227**(5259): p. 680-685.
94. Passonneau, J.V. and V.R. Lauderdale, *A comparison of three methods of glycogen measurement in tissues.* Anal Biochem, 1974. **60**(2): p. 405-12.
95. Livak, K.J. and T.D. Schmittgen, *Analysis of relative gene expression data using real-time quantitative PCR and the 2(-Delta Delta C(T)) Method.* Methods, 2001. **25**(4): p. 402-8.
96. Pan, X., et al., *TBC-domain GAPs for Rab GTPases accelerate GTP hydrolysis by a dual-finger mechanism.* Nature, 2006. **442**(7100): p. 303-306.
97. Dokas, J., et al., *Tbc1d1 deletion suppresses obesity in leptin-deficient mice.* Int J Obes (Lond), 2016. **40**(8): p. 1242-9.
98. Stone, S., et al., *TBC1D1 is a candidate for a severe obesity gene and evidence for a gene/gene interaction in obesity predisposition.* Human Molecular Genetics, 2006. **15**(18): p. 2709-2720.
99. Meyre, D., et al., *R125W coding variant in TBC1D1 confers risk for familial obesity and contributes to linkage on chromosome 4p14 in the French population.* Hum Mol Genet, 2008. **17**(12): p. 1798-802.
100. Moltke, I., et al., *A common Greenlandic TBC1D4 variant confers muscle insulin resistance and type 2 diabetes.* Nature, 2014. **512**(7513): p. 190-193.
101. Rutti, S., et al., *Expression, phosphorylation and function of the Rab-GTPase activating protein TBC1D1 in pancreatic beta-cells.* FEBS Lett, 2014. **588**(1): p. 15-20.
102. Bouzakri, K., et al., *Rab GTPase-activating protein AS160 is a major downstream effector of protein kinase B/Akt signaling in pancreatic beta-cells.* Diabetes, 2008. **57**(5): p. 1195-204.
103. Stermann, T., et al., *Deletion of the RabGAP TBC1D1 Leads to Enhanced Insulin Secretion and Fatty Acid Oxidation in Islets From Male Mice.* Endocrinology, 2018. **159**(4): p. 1748-1761.
104. Benninghoff, T., et al., *The RabGAPs TBC1D1 and TBC1D4 Control Uptake of Long-Chain Fatty Acids Into Skeletal Muscle via Fatty Acid Transporter SLC27A4/FATP4.* Diabetes, 2020. **69**(11): p. 2281-2293.
105. Kotani, K., et al., *GLUT4 glucose transporter deficiency increases hepatic lipid production and peripheral lipid utilization.* Journal of Clinical Investigation, 2004. **114**(11): p. 1666-1675.

106. Toska, L.M., *Investigation of glycogen metabolism in a mouse model of impaired glucose homeostasis*, in *Institut für Stoffwechselphysiologie*. 2015, Heinrich-Heine Universität: Düsseldorf. p. 1-57.
107. O'Neill, H.M., et al., *AMP-activated protein kinase (AMPK) beta1beta2 muscle null mice reveal an essential role for AMPK in maintaining mitochondrial content and glucose uptake during exercise.* Proceedings of the National Academy of Sciences of the United States of America, 2011. **108**(38): p. 16092-16097.
108. Treebak, J.T., et al., *Identification of a novel phosphorylation site on TBC1D4 regulated by AMP-activated protein kinase in skeletal muscle.* American Journal of Physiology-Cell Physiology, 2010. **298**(2).
109. McMillin, S.L., et al., *GLUT4 Is Not Necessary for Overload-Induced Glucose Uptake or Hypertrophic Growth in Mouse Skeletal Muscle.* Diabetes, 2017. **66**(6): p. 1491-1500.
110. Whitfield, J., et al., *Ablating the protein TBC1D1 impairs contraction-induced sarcolemmal glucose transporter 4 redistribution but not insulin-mediated responses in rats.* Journal of Biological Chemistry, 2017. **292**(40): p. 16653-16664.
111. Lantier, L., et al., *AMPK controls exercise endurance, mitochondrial oxidative capacity, and skeletal muscle integrity.* The FASEB Journal, 2014. **28**(7): p. 3211-3224.
112. Ihlemann, J., et al., *Effect of tension on contraction-induced glucose transport in rat skeletal muscle.* The American journal of physiology, 1999. **277**(2 Pt 1): p. 14.
113. Wright, D.C., et al., *Contraction- and hypoxia-stimulated glucose transport is mediated by a Ca2+-dependent mechanism in slow-twitch rat soleus muscle.* American journal of physiology. Endocrinology and metabolism, 2005. **288**(6): p. 6.
114. Deng, B., et al., *PKC and Rab13 mediate Ca2+ signal-regulated GLUT4 traffic.* Biochemical and biophysical research communications, 2018. **495**(2): p. 1956-1963.
115. Kleinert, M., et al., *Mammalian target of rapamycin complex 2 regulates muscle glucose uptake during exercise in mice.* The Journal of Physiology, 2017. **595**(14): p. 4845-4855.
116. Jeppesen, J., et al., *LKB1 Regulates Lipid Oxidation During Exercise Independently of AMPK.* Diabetes, 2013. **62**(5): p. 1490-1499.
117. Al-Hasani, H., D.R. Yver, and S.W. Cushman, *Overexpression of the glucose transporter GLUT4 in adipose cells interferes with insulin-stimulated translocation.* FEBS letters, 1999. **460**(2): p. 338-342.
118. Zisman, A., et al., *Targeted disruption of the glucose transporter 4 selectively in muscle causes insulin resistance and glucose intolerance.* Nature medicine, 2000. **6**(8): p. 924-928.
119. Abel, E.D., et al., *Adipose-selective targeting of the GLUT4 gene impairs insulin action in muscle and liver.* Nature, 2001. **409**(6821): p. 729-733.
120. Ren, J.M., et al., *Overexpression of Glut4 protein in muscle increases basal and insulin-stimulated whole body glucose disposal in conscious mice.* The Journal of clinical investigation, 1995. **95**(1): p. 429-432.
121. Medler, S., *Mixing it up: the biological significance of hybrid skeletal muscle fibers.* J Exp Biol, 2019. **222**(Pt 23).
122. Chen, Z., et al., *Expression of the AMP-activated protein kinase beta1 and beta2 subunits in skeletal muscle.* FEBS Lett, 1999. **460**(2): p. 343-8.
123. Miura, S., et al., *Alpha2-AMPK activity is not essential for an increase in fatty acid oxidation during low-intensity exercise.* Am J Physiol Endocrinol Metab, 2009. **296**(1): p. E47-55.
124. Pederson, B.A., et al., *Mice with elevated muscle glycogen stores do not have improved exercise performance.* Biochem Biophys Res Commun, 2005. **331**(2): p. 491-6.
125. Pederson, B.A., et al., *Glucose metabolism in mice lacking muscle glycogen synthase.* Diabetes, 2005. **54**(12): p. 3466-73.
126. Lantier, L., et al., *AMPK controls exercise endurance, mitochondrial oxidative capacity, and skeletal muscle integrity.* FASEB J, 2014. **28**(7): p. 3211-24.

127. Radhakrishnan, J., et al., *Improved exercise capacity in cyclophilin-D knockout mice associated with enhanced oxygen utilization efficiency and augmented glucose uptake via AMPK-TBC1D1 signaling nexus.* FASEB J, 2019. **33**(10): p. 11443-11457.
128. Jorgensen, S.B., et al., *Knockout of the alpha2 but not alpha1 5'-AMP-activated protein kinase isoform abolishes 5-aminoimidazole-4-carboxamide-1-beta-4-ribofuranosidebut not contraction-induced glucose uptake in skeletal muscle.* J Biol Chem, 2004. **279**(2): p. 1070-9.
129. Fisher, J.S., et al., *Muscle contractions, AICAR, and insulin cause phosphorylation of an AMPK-related kinase.* Am J Physiol Endocrinol Metab, 2005. **289**(6): p. E986-92.
130. Nixon, M., et al., *Skeletal muscle salt inducible kinase 1 promotes insulin resistance in obesity.* Molecular metabolism, 2016. **5**(1): p. 34-46.
131. Säll, J., et al., *Salt-inducible kinase 2 and -3 are downregulated in adipose tissue from obese or insulin-resistant individuals: implications for insulin signalling and glucose uptake in human adipocytes.* Diabetologia, 2017. **60**(2): p. 314-323.
132. Inazuka, F., et al., *Muscle-specific Knock-out of NUAK Family SNF1-like Kinase 1 (NUAK1) Prevents High Fat Diet-induced Glucose Intolerance.* Journal of Biological Chemistry, 2012. **287**(20): p. 16379-16389.
133. Fisher, J.S., et al., *Muscle contractions, AICAR, and insulin cause phosphorylation of an AMPK-related kinase.* Am J Physiol Endocrinol Metab, 2005.
134. Lefebvre, D.L., et al., *Identification and characterization of a novel sucrose-non-fermenting protein kinase/AMP-activated protein kinase-related protein kinase, SNARK.* The Biochemical journal, 2001. **355**(Pt 2): p. 297-305.
135. Merry, T.L., et al., *Local hindlimb antioxidant infusion does not affect muscle glucose uptake during in situ contractions in rat.* Journal of applied physiology (Bethesda, Md. : 1985), 2010. **108**(5): p. 1275-1283.
136. Ito, Y., et al., *Passive stretching produces Akt- and MAPK-dependent augmentations of GLUT4 translocation and glucose uptake in skeletal muscles of mice.* Pflugers Arch, 2006. **451**(6): p. 803-13.
137. Chambers, M.A., et al., *Stretch-stimulated glucose uptake in skeletal muscle is mediated by reactive oxygen species and p38 MAP-kinase.* J Physiol, 2009. **587**(Pt 13): p. 3363-73.
138. Sylow, L., et al., *Stretch-stimulated glucose transport in skeletal muscle is regulated by Rac1.* J Physiol, 2015. **593**(3): p. 645-56.
139. Sylow, L., et al., *Rac1--a novel regulator of contraction-stimulated glucose uptake in skeletal muscle.* Exp Physiol, 2014. **99**(12): p. 1574-80.
140. Larsen, J.K., et al., *Illumination of the Endogenous Insulin-Regulated TBC1D4 Interactome in Human Skeletal Muscle.* Diabetes, 2022. **71**(5): p. 906-920.
141. Hawley, S.A., et al., *Complexes between the LKB1 tumor suppressor, STRAD alpha/beta and MO25 alpha/beta are upstream kinases in the AMP-activated protein kinase cascade.* Journal of biology, 2003. **2**(4): p. 28.
142. Li, H., et al., *Rab8A regulates insulin-stimulated GLUT4 translocation in C2C12 myoblasts.* FEBS letters, 2017.
143. Reed, S.E., et al., *A role for Rab14 in the endocytic trafficking of GLUT4 in 3T3-L1 adipocytes.* J Cell Sci, 2013. **126**(Pt 9): p. 1931-41.
144. Matsui, T., K. Noguchi, and M. Fukuda, *Dennd3 functions as a guanine nucleotide exchange factor for small GTPase Rab12 in mouse embryonic fibroblasts.* J Biol Chem, 2014. **289**(20): p. 13986-95.
145. Matsui, T. and M. Fukuda, *Rab12 regulates mTORC1 activity and autophagy through controlling the degradation of amino-acid transporter PAT4.* EMBO Rep, 2013. **14**(5): p. 450-7.
146. Matsui, T., T. Itoh, and M. Fukuda, *Small GTPase Rab12 regulates constitutive degradation of transferrin receptor.* Traffic, 2011. **12**(10): p. 1432-43.

8 Supplement

8.1 Contribution to manuscripts

Parts of the present thesis are included in the following manuscripts to whom I have contributed significantly:

1) **de Wendt C**, Espelage L, Eickelschulte S, Springer C, Toska L, Scheel A, Bedou AD, Benninghoff T, Cames S, Stermann T, Chadt A, Al-Hasani H (2021). Contraction-Mediated Glucose Transport in Skeletal Muscle Is Regulated by a Framework of AMPK, TBC1D1/4, and Rac1. *Diabetes* 70: 2796-2809

Contribution: Shared first author (de Wendt and Espelage). The main findings of the results with TBC1D1-, TBC1D4- and AMPK-triple-deficient mice are part of this manuscript. The *ex vivo* contraction assays comparing the four and five genotypes, respectively, the *in vivo* tolerance tests, treadmill exercise, the qPCR analysis and most of the western blots were performed in large parts by myself or with the help of collaborators. I analyzed and interpreted the data. For the manuscript, the following figures were adapted from the present thesis: Figure 4.6, Figure 4.7 C-D, Figure 4.9, Figure 4.10, Figure 4.11, Figure 4.12 B, Figure 4.13, Figure 4.14, Figure 4.16, Figure 4.17, Figure 4.18 B, Figure 4.19 A, Figure 4.20.

2) Chadt A, Immisch A, **de Wendt C**, Springer C, Zhou Z, Stermann T, Holman GD, Loffing- Cueni D, Loffing J, Joost HG, Al-Hasani H (2015). Deletion of both Rab-GTPase-activating proteins TBC1D1 and TBC1D4 in mice eliminates insulin- and AICAR-stimulated glucose transport [corrected]. *Diabetes* 64: 746-59.

Contribution: I was involved in conducting *ex vivo* experiments. These included the measurement of insulin- and AICAR-stimulated glucose uptake and AICAR-stimulated fatty acid oxidation in isolated *EDL* and *Soleus* muscles for the generation of Figure 4 A-D and Figure 5 A-B from the manuscript.

3) Kjøbsted R, Chadt A, Jørgensen NO, Kido K, Larsen JK, **de Wendt C**, Al-Hasani H, Wojtaszewski JFP (2019). TBC1D4 Is Necessary for Enhancing Muscle Insulin Sensitivity in Response to AICAR and Contraction. *Diabetes 68*: 1756-1766

Contribution: I helped to perform the *ex vivo* muscle incubations after AICAR stimulation with whole-body *Tbc1d4* knock-out (D4KO) mice.

4) Mafakheri S, Flörke RR, Kanngießer S, Hartwig S, Espelage L, **De Wendt C**, Schönberger T, Hamker N, Lehr S, Chadt A, Al-Hasani H (2018). AKT and AMPK-activated protein kinase regulate TBC1D1 through phosphorlylation and its interaction with cytosolic tail of insulin-regulated aminopeptidase IRAP. *J Biol Chem* 293: 17853-17862

Contribution: I induced an overexpression of IRAP in the TA-muscle of muscle specific *Tbc1d1*-transgenic mice by means of *in vivo* electro transfection.

5) Stermann T, Menzel F, Weidlich C, Jeruschke K, Weiss J, Altenhofen D, Benninghoff T, Pujol A, Bosch F, Rustenbeck I, Ouwens DM, Thoresen GH, **de Wendt C**, Lebek S, Schallschmidt T, Kragl M, Lammert E, Chadt A, Al-Hasani H (2018). Deletion of the RabGAP TBC1D1 Leads to Enhanced Insulin Secretion and Fatty Acid Oxidation in Islets From Male Mice. *Endocrinology* 159: 1748-1761

Contribution: I was mainly involved in conducting the intraperitoneal glucose tolerance tests with D1KO mice. Furthermore, I helped to isolate pancreatic islets from murine pancreas for the measurement of glucose stimulated insulin secretion.

6) Klymenko O, Brecklinghaus T, Dille M, Springer C, **de Wendt C**, Altenhofen D, Binsch C, Knebel B, Scheller J, Hardt C, Herwig R, Chadt A, Pfluger PT, Al-Hasani H, Kabra DG (2020). Histone deacetylase 5 regulates interleukin 6 secretion and insulin action in skeletal muscle. *Mol Metab*. 42: 101062

Contribution: For the *ex vivo* glucose uptake assays, I isolated intact *EDL* and *soleus* muscles from mice and helped to conduct the experiment.

8.2 Tables

8.3 Figures

8.4 Abbreviations

ADP	Adenosine diphosphate
AICAR	5-Aminoimidazole-4-carboxamide ribonucleotide
AMP	Adenosine monophosphate
ATP	Adenosine triphosphate
BCA	bicinchoninic acid
BG	blood glucose
BMI	body mass index
BW	body weight
CBD	calmodulin binding domain
CHO	carbohydrate oxidation
CI	confidence interval
DAG	diacylglycerol
Dennd3	differentially expressed in normal and neoplastic cells domain-containing protein 3
EDL	Extensor digitorum longus
FAO	fatty acid oxidation
FFA	Free fatty acids
GAP	GTPase activating protein
GEF	Guanine nucleotide exchange factor
GLUT1	solute carrier family 2, facilitated glucose transporter member 1
GLUT4	solute carrier family 2, facilitated glucose transporter member 4
GSV	GLUT4 storing vesicles
GWAS	Genome wide association study
h	hour
hTERT-RPE	human telomerase-immortalized retinal pigment epithelial
Hz	Hertz
IR	Insulin receptor
kDa	kilo Dalton
LKB1	liver kinase B1
MCK	muscle creatine kinase
MEFs	mouse embryonic fibroblasts
min	minute
mTORC1	mammalian/mechanistic target of rapamycin complex 1
NO	nitric oxide
NOS	nitric oxide synthase
NT	non target

PAT4	proton-coupled amino-acid transporter 4
PKC	protein kinase C
PM	plasma membrane
PTB	phosphotyrosine-binding
PVDF	polyvinylidene difluoride
qPCR	real-time quantitative polymerase chain reaction
Rab	Ras-related proteins in brain
GAP	GTPase activating protein
RER	respiratory exchange ratio
ROS	reactive oxygen species
RT	room temperature
SD	standard chow diet
SDS-PAGE	sodium dodecyl sulfide polyacrylamide gel electrophoresis
sec	seconds
siRNA	small interfering ribonucleic acid
SNARK	sucrose nonfermenting AMPK-related kinase
TA	Tibialis anterior
TBC1D1	TRE2, Bub2, CDC16 1 domain family member 1
TBC1D4	TRE2, Bub2, CDC16 1 domain family member 4
TfR	Transferin Receptor
TG	tansgenic
VO2max	maximal oxygen (O2) consumption
WAT	white adipose tissue
WT	wildtype

Acknowledgements

First, I want to thank Prof. Dr. Hadi Al-Hasani for providing me with this interesting topic and giving me the chance to prepare my PhD thesis as a member of his working group. He always provided new input to the project and gave me the the opportunity to present the progress of my research at national and international congresses on a regular basis.

I thank Prof. Dr. Eckhard Lammert to supervise my PhD thesis as a second reviewer.

Furthermore, my deepest thanks go to Dr. Alexandra Chadt for her additional supervision of this thesis. She invested much time and energy on this project and supported the present thesis by helping me discussing all the results and planning the next steps. Alexandra introduced me to all the methods involving the handling of experimental animals, like tolerance tests, NMR spectroscopy and the dissection of tissues and isolation of intact skeletal muscles. Furthermore, she taught me, how to perform the *ex vivo* essays and helped me to establish the *ex vivo* contraction method. She also gave great advice on how to prepare scientific abstracts, talks and poster and proofread everything I sent to her very carefully, including this thesis.

I want to thank the animal care takers Peter Herdt, Denise Schauer and Jennifer Schwettmann for breeding, maintenance and taking care of all the experimental animals.

More than grateful, I am for the support of the technicians that helped me during the whole time of this thesis. Namely, these are Angelika Horrighs, Anette Kurowski, Heidrun Podini, Annette Schober, Antonia Osmers, Ilka Römer, Dagmar Grittner, Carina Heitmann, Jürgen Weiß and Kay Jeruschke.
In particular, I want to thank Angelika Horrighs for introducing me to the Western Blotting method and several other lab techniques. Annette Schober showed me how to cultivate and transform *E. coli* bacteria and isolate plasmid DNA and several other methods. Anette Kurowski helped me a lot with all the experiments concerning RNA isolation, qPCR analysis and she and Heidrun Podini helped me with conducting the *ex vivo* experiments.
Angelika, Anette, Heidrun and Ilka did the genotyping of all the experimental mice. Angelika, Anette, Heidrun, Antonia and Carina supported my work by performing countless Western Blotting experiments.
Moreover, I would like to thank each of them for their manifold help and support in the lab.

Many thanks go to all the students for the support during the *ex vivo* experiments and other work. At first, I thank Laura Toska for her help and for conducting many of the Western Blotting experiments. In addition, I would like to thank her and Lina Hellwig for giving me the opportunity to supervise their master theses. Lena Espelage also helped me a lot with the *ex vivo* assays. Furthermore, I want to thank her for continuing the whole project and bringing it to publication.
Dr. Christian Springer taught me how to conduct the treadmill experiments. And from Dr. Tim Benninghoff I was able to learn how to carry out *in vivo* electrotransfection.
Dr. Sandra Lebek, Dr. Torben Stermann and Dr. Delsi Altenhofen helped me with GTT, ATT and ITT experiments.
I also would like to thank all my other present and former colleagues of our institute for the comfortable atmosphere as well as for additional discussion of results during general lab meetings. These include Dr. Ralf Flörke, Dr. Dhiraj Kabra, Dr. Samaneh Eickelschulte, Dr. Tamara Castaneda, Dr. Tanja Schallschmidt, Dr. Delsi Altenhofen, Dr. Sabrina Ralla.
Moreover, I especially thank Dr. Tim Benninghoff, Dr. Christian Binsch, Dr. Christian Springer, Dr. David Barbosa, Dr. Matthias Dille, Dr. Torben Stermann, Dr. Simon Göddeke, Dr. Sven Görgens and Tim Brecklinghaus for creating a special working atmosphere and for spending precious time outside the lab at our regular bowling events.

Most importantly I would like to thank my family for their long-term support during my studies and the long rocky road of preparing this thesis. Special thanks go to Tobias. You were my number one cheer on this Marathon. Thank you for never giving up on me and always encouraging me to keep going. I certainly would never have completed this work without your tenacity. I love you.

Erklärung

Ich versichere an Eides Statt, dass die Dissertation von mir selbständig und ohne unzulässige fremde Hilfe unter Beachtung der „Grundsätze zur Sicherung guter wissenschaftlicher Praxis an der Heinrich-Heine-Universität Düsseldorf“ erstellt worden ist.

Ferner versichere ich, dass die Dissertation bisher keiner anderen Fakultät vorgelegt worden ist.

Mülheim an der Ruhr, den 15.06.2022

Christian de Wendt